Diploma Thesis

Development of algorithms for attitude determination and control of the AsteroidFinder satellite

Mr. cand. mach. Ansgar Heidecker
Matr.-No. 2726436

March 2009

TECHNISCHE UNIVERSITÄT
CAROLO-WILHELMINA
ZU BRAUNSCHWEIG

Deutsches Zentrum
für Luft- und Raumfahrt e.V.
in der Helmholtz-Gemeinschaft

pages: 101
figures: 44
tables: 8

Prof. Dr.-Ing. Peter Vörsmann
Dr.-Ing. Carsten Wiedemann
Technische Universität Braunschweig
Institut für Luft- und Raumfahrtsysteme
Hermann-Blenk-Straße 23, D-38108 Braunschweig
GERMANY

Dr.-Ing. Stephan Theil
Dr.-Ing. Markus Schlotterer
Dipl.-Ing. Marcus Hallmann
Deutsches Zentrum für Luft- und Raumfahrt e.V.
Institut für Raumfahrtsysteme
Navigations- und Regelungssysteme
Robert-Hooke-Straße 7, D-28359 Bremen
GERMANY

Technische Universität Braunschweig

Institut für
Luft- und Raumfahrtsysteme

Prof. Dr.-Ing. Peter Vörsmann

Inst. für Luft- und Raumfahrtsysteme Hermann-Blenk-Str. 23 D-38108 Braunschweig

Unser Zeichen: pv/cw

Name: Prof. Dr.-Ing. Peter Vörsmann
Fon: +49 531 391-9960
Fax: +49 531 391-9966
E-Mail: p.voersmann@tu-bs.de
Net: www.aerospace-systems.de

Datum: 22.10.2008

Diploma Thesis
of Mr. cand. mach. Ansgar Heidecker
Matr.- No. 2726436

Subject:
Development of algorithms for attitude determination and control of the AsteroidFinder satellite

Background

The “AsteroidFinder“ is a compact satellite mission designed by the German Aerospace Centre (DLR). The mission goal is to detect asteroids with orbits that are completely inside the earth’s orbit. These objects are called “Inner Earth Objects”. To fulfill this mission a satellite system is designed that will fly in a low earth orbit and has an optical payload.
Currently the mission is in phase A.
The attitude control system is a critical system of the AsteroidFinder. It is responsible for determining and keeping the attitude. The payload requires a precise attitude control system which has never been achieved in this satellite class before.

Tasks:

The goal of this thesis is the detailed design of the attitude control system. The mission is at the end of phase A and a sensor and actuator configuration has already been chosen. The goal of this thesis is to develop algorithms for attitude determination and control.
In detail, the following task shall be performed:

1. Orientation to the actual project state with help of Phase 0/A documentation
   The main task is to get a detailed knowledge of the mission and actual state of the attitude control system development.

2. Development of a simulation in Matlab/Simulink for attitude control
   For the development of an attitude control system it is important to investigate the behaviour of the complete control loop. A simulation shall be developed to support this development.

3. Development of an attitude determination algorithm
   For the attitude determination algorithm a KALMAN-Filter for the sensor configuration shall be developed. The detailed design of the KALMAN-Filter shall be identified.

4. Test of the attitude determination algorithm with the simulation
   The attitude determination algorithm accuracy shall be tested and validated with respect to the simulation.

5. Development of an attitude control algorithm
   There are high pointing requirements for the AsteroidFinder Mission. The main task of this thesis is to develop two different attitude control algorithms for two different operational modes (inertial pointing, target pointing). To fulfill this task it is important to investigate the control loop and chose a dedicated development procedure for the controller.

6. Performance analyses of the attitude control in the closed loop simulation
   The performance of the attitude control algorithm in the closed loop simulation shall be validated and tested.

At the beginning of the thesis a definition and description of individual work packages has to be carried out (Work Breakdown Structure, Work Package Description), which then have to be merged to a project schedule. The thesis has to be prepared according to the guidelines of the Institute of Aerospace Systems and submitted unbounded in duplicate (original and copy).

The Institute of Aerospace Systems supports the scientific publication of their student's theses with prior permission; nevertheless disposing of the results is only allowed after consultation of the mentoring institutions. Passing on to a third party or publication of this thesis is only allowed after consultation of the mentoring institutions. The thesis remains property of the mentoring institutions.

Time-frame:	6 months
Tutors:	Prof. Dr. Peter Vörsmann, Dr.-Ing. Carsten Wiedemann and project scientists Dr.-Ing. Stephan Theil, Dipl.-Ing. Marcus Hallman, German Aerospace System (DLR), Institute of Space Systems (Bremen)

Issued on:

Submitted on:

Prof. Dr.-Ing. Peter Vörsmann

Eidesstattliche Erklärung - Statutory Declaration

Ich erkläre hiermit an Eides Statt, dass ich die nachfolgende Arbeit selbstständig und nur unter Zuhilfenahme der angegebenen Literatur angefertigt habe.

Herewith i certify that i have written the following thesis by myself and only with the help of the indicated literature.

Ansgar Heidecker

Braunschweig, den 30. März 2009

Abstract

The following diploma thesis is related to the AsteroidFinder/SSB project of the German Aerospace Center (DLR). AsteroidFinder/SSB is a compact satellite that will be used for detecting asteroids with an optical payload (telescope). Especially the objects that are completely inside the Earth orbit are of interest. The task of detecting weak light sources like asteroids places challenging requirements to the Attitude Control System (ACS). Therefore the AsteroidFinder/SSB needs to be stabilised and controlled by an active there axis ACS. A preliminary design was established during Phase 0/A of the project. Based on these results the following diploma thesis focus on the development of the attitude determination and control algorithm. Therefore a simulation environment is programmed and two different KALMAN filters are investigated as attitude determination algorithms. These are the extended KALMAN filter and the unscented KALMAN filter. Afterwards a guidance strategy is derived to reach the main mission goals. It is followed by the development of an attitude control strategy which is based on linear quadric GAUSSIAN control. At the end the algorithm functionality is validated through simulation.

Übersicht

Die vorliegende Diplomarbeit wurde im Rahmen des AsteroidFinder/SSB Projektes des Deutschen Zentrums für Luft- und Raumfahrt e.V. (DLR) erstellt. Der AsteroidFinder/SSB ist ein Kompaktsatellit und soll zur Entdeckung von Asteroiden eingesetzt werden. Hierfür wird ein Teleskop verwendet, welches die Nutzlast des Satelliten ist. Die Aufgabe lichtschwache Objekte, wie Asteroiden, zu entdecken stellt anspruchsvolle Anforderungen an das Lageregelungssystem. Aus diesem Grund wird AsteroidFinder/SSB durch eine aktive dreiachsige Lageregelung stabilisiert. Das vorläufige Design des Lageregelungssystems wurde bereits in den Phasen 0/A des Projektes festgelegt. Aufbauend auf diesen Ergebnissen fokussiert sich die folgende Arbeit auf die Entwicklung der Lagebestimmungs- und Lageregelungsalgorithmen. Dafür wird zunächst eine Simulationsumgebung entwickelt und zwei verschiedene KALMAN Filter untersucht. Die KALMAN Filter sind der Extended und der Unscented KALMAN Filter, welche als Lagebestimmungsalgorithmen in Frage kommen. Anschließend werden verschiede Flugführungsstrategien besprochen, um die Missionsziele zu erreichen. Dies wird gefolgt von der Entwicklung einer Lageregelungsstrategie bei deren Entwicklung Methoden der Linearen Quadratischen Regelung zum Einsatz kommen. Als letztes werden sämtliche Algorithmen durch Simulation validiert.

Anmerkung: Diese Arbeit ist in englischer Sprache abgefasst und enthält eine Zusammenfassung in Deutscher Sprache im Anhang.

Contents

Nomenclature

Greek

Ω	right ascension of ascending node
ω	argument of perigee
α	scaling parameter for sigma point spread in the UT
β	scaling parameter for incorporating signal distribution behavior in the UT
$\underline{\chi}_i$	sigma point
γ	universal gravitational constant
κ	scaling parameter for fine tuning in the UT
λ	scaling parameter of the UT
λ	longitude
μ_E	earth gravitational constant
$\underline{\underline{\nu}}$	Innovation of measurements
$\underline{\omega}_D$	desired angular rate
$\underline{\underline{\Omega}}$	skew-symmetric matrix of the angular rate
ϕ	latitude
$\underline{\underline{\Phi}}$	state transition matrix
$\underline{\underline{\Xi}}$	corresponding matrix of $\underline{\underline{\Omega}}$

Roman

a	semimajor axis
e	eccentricity
I	moment of inertia
i	inclination

m mass of an object

R_{Earth} radius of the Earth

$\underline{\underline{A}}$ state matrix

$\underline{\underline{B}}$ input matrix

$\underline{\underline{C}}$ output matrix

c_i Cholesky factor of a covariance matrix

C_{nm} tesseral/sectoral harmonic coefficients

$\underline{\underline{D}}$ input to output coupling matrix

$\underline{e}$ eigenaxis unit vector

$\underline{\underline{E}}$ disturbance matrix

e integral of an average error

$\underline{F}$ force vector

$\underline{\underline{F}}$ linearised system dynamic matrix

f function of nonlinear system dynamic

$\underline{G}$ gravitational force

$\underline{\underline{H}}$ linearised measurement dynamic matrix

h function of nonlinear measurement dynamic

y altitude

$\underline{\underline{I}}$ Moment of Inertia

$\underline{\underline{I}}_{n\times n}$ unity matrix of the dimension $n \times n$

i counting variable $i \in \natural$

J moment of inertia around a single axis

J quadric cost function

J_n zonal harmonic coefficients

$\underline{\underline{K}}$ KALMAN gain

$\underline{\underline{K}}$ control gain

$\underline{L}$ angular momentum

M mass of a central body

m mass

n indicates a dimension $n \in \natural$

$\underline{\underline{P}}$ covariance matrix

P_{nm} LEGENDRE polynomial function

$\underline{q}$ unit quaternion

$\underline{q}_D$ desired attitude quaternion

$\underline{\underline{Q}}$ covariance matrix of the system model uncertainties

$\underline{\underline{Q}}$ weighting matrix of the system states

$\underline{r}$ radius vector

$\underline{\underline{R}}$ covariance matrix of the measurements

$\underline{\underline{R}}$ weighting matrix of the control input

S_{nm} tesseral/sectoral harmonic coefficients

$\underline{T}_D$ desired torque

t time variable

$\underline{u}$ control input

U gravitational potential

$\underline{v}$ velocity vector

$\underline{v}$ white noise

$\underline{w}$ white noise

W_i^c weights for the covariance P_{yy} in the UT

W_i^m weights for the mean of y in the UT

$\underline{x}$ state vector

$\overline{\underline{y}}$ mean value of $\underline{y}$

$\underline{z}_k$ measurement at time step t_k

$\hat{\underline{\zeta}}_i^-$ expected measurement out of a sigma point set

Abbreviations

μASC	Micro Advanced Stellar Compass
ACS	Attitude Control System
AD	Attitude Determination
AD	Analogue Digital
AF	AsteroidFinder
AMR	Anisotropic Magnetoresistive Effect
AoS	Automatic dependent surveillance - broadcast over Satellite
APA	Absolute Pointing Accuracy
APS	Absolute Pointing Stability
BF	Body Fixed
BIRD	Bi-Spectral-InfraRed Detection
CCD	Charge Coupled Device
CHARM	CH4 Atmospheric Remote Monitoring
CHU	Camera Head Unit
CMG	Control Momentum Gyro
CoG	Centre of Gravity
CSS	Coarse Sun Sensor
DLR	Deutsches Zentrum für Luft- und Raumfahrt e.V. German Aerospace Centre
DTU	Denmarks Technical University
EKF	Extended KALMAN Filter
ESA	European Space Agency
FOG	Fiber Optic Gyro
FSS	Fine Sun Sensor
GG	Gravity Gradient
GPS	Global Positioning System
IEO	Inner Earth Object
IGRF	International Geomagnetic Reference Field
JPL	Jet Propulsion Laboratories
KF	KALMAN Filter
LQG	Linear Quadric Gaussian Control
LQR	Linear Quadric Regulator
MCF	Mechanical Coordinate Frame
MEMS	Micro Electro Mechanical System
MIMO	Multiply Input Multiply Output System
MoI	Moment of Inertia
MPE	Maximum Pointing Error
MT	Magnetic Torquer

MW	Momentum Wheel
NASA	National Aeronautics and Space Administration
NEA	Noise Equivalent Angle
NEO	Near-Earth Objects
ONS	On Board Navigation System
OSIRIS	Optical High Speed Infrared Link System
PD	Proportional Derivative Control
PHA	Potential Hazardous Asteroids
PID	Proportional Integral Derivative Control
PSR	Pointing Stability Rate
RW	Reaction Wheel
SISO	Single Input Single Output
SSB	Standard Satellite Bus
TET	Technologieerprobungsträger
TNO	Toegepast Natuurwetenschappelijk Onderzoek
ToD	True of Date
UKF	Unscented KALMAN Filter
UT	Unscented Transformation
WGS	World Geodetic System
ZARM	Zentrum für angewandte Raumfahrttechnologie und Mikrogravitation (Centre of Applied Space Technology)

Chapter 1

Introduction

This chapter gives an introduction to the AsteroidFinder/SSB mission. It describes the mission goals and its heritage. A special focus is placed on the system requirements and the state of the attitude control system.

1.1 General Overview

The German Aerospace Center (Deutsches Zentrum für Luft- und Raumfahrt e.V. DLR) aims to develop and operate a standard satellite bus (SSB) [11]. It will be suitable for multi-type missions and enable independent and fast access to space for DLR's research institutes. Additionally the project shall establish necessary capabilities and facilities for small satellite development within DLR. DLR's Institute of Space Systems in Bremen (Germany) will supervise the SSB program.

The SSB program is based on the Bi-Spectral-InfraRed-Detection (BIRD) and the TechnologieErprobungsTräger (TET) satellite buses, which were built with contributions from DLR. It uses the experience and expertise gained during these two programs. BIRD was launched in October 2001 and is in its final operation phase today while TET is in development Phase C/D. The SSB is in Phase A/B and will extend the capabilities of these two programs to achieve a more sophisticated system which can be adapted to a broader range of mission requirements.

BIRD, TET and SSB are all compact satellites with an overall mass of approximately 100 kg to 150 kg. The dimensions of each satellite allow a piggy-back launch.

The idea for the SSB was born during the TET development and at the beginning of 2007 a DLR-internal call for proposals was issued to identify possible missions scenarios and payloads. Out of this call three possible primary mission scenarios were identified.

- AsteroidFinder - Search for asteroids with a space borne telescope on a compact satellite
- CHARM - Remote monitoring of methane (CH_4) in the Earth's atmosphere using Differential Absorption Lidar (DIAL) technology
- LiveSat - Life science/interactive pedagogical/technological multi-user payload

During the following Phase 0 a first mission analysis was performed and AsteroidFinder was chosen to be the primary payload of the first SSB.

In February 2008 Phase A was initialized which results in a preliminary design. The first step of Phase A ended in November 2008 with a design review. Due to some design inconsistencies a Delta Phase A was initiated which ended in March 2009. Figure 1.1 shows the preliminary design of AsteroidFinder/SSB at the end of Delta Phase A. In addition to the primary payload two secondary payloads were considered during Phase 0/A as suitable for the AsteroidFinder/SSB mission.

- OSIRIS - Optical high speed infra red link system for low earth orbit satellites
- AoS - Automatic dependent surveillance - broadcast over satellite

During the Phase A Review a recommendation was made that the secondary payload option should not be taken into account any further because the secondary payload was identified as a design driver. Although a secondary payload shall be no design driver it will be considered in this diploma thesis due to educational reasons.

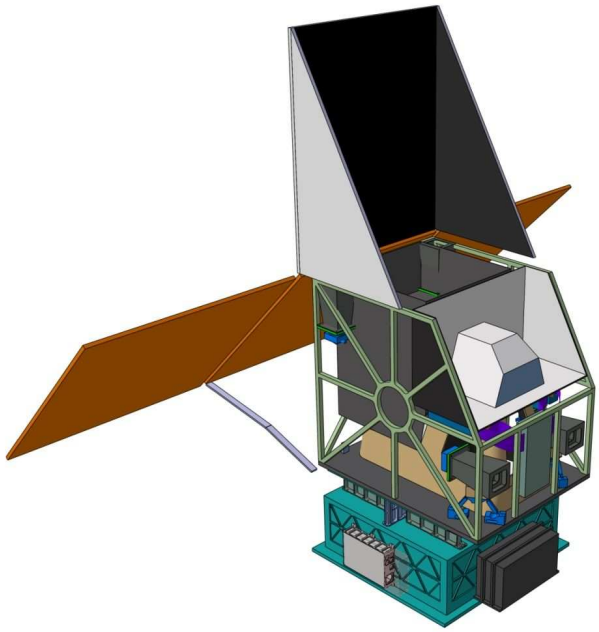

Figure 1.1: AsteroidFinder/SSB design in March 2009 [13]

1.2 Requirements

The requirements for the attitude control system are directly related to the payload activity. Basically there is a handful of requirements that are driving the attitude control system design. These requirements can be tailored down to four error values that should not be exceeded.

To be able to compare different error definitions all values will be given as 3σ boundary values. This assumes that a signal can be described as an expected value μ which is corrupted with white

noise. These signals can be expressed as a GAUSSIAN distribution which can be formulated in a mathematical sense. A GAUSSIAN distribution of the random variable x is described by the distribution function $F(x)$ and its density function $f(t)$ [5]

$$F(x) = \frac{1}{\sigma\sqrt{2\pi}} \int_{-\infty}^{x} \exp\left(-\frac{1}{2} \cdot \left(\frac{t-\mu}{\sigma}\right)^2\right) dt \tag{1.1}$$

$$f(t) = \frac{1}{\sigma\sqrt{2\pi}} \exp\left(-\frac{1}{2} \cdot \left(\frac{t-\mu}{\sigma}\right)^2\right) \tag{1.2}$$

where σ is the standard deviation from the expected value μ. Figure 1.2 shows the normal GAUSSIAN distribution with $\mu = 0$ and $\sigma = 1$. Therefore the different σ boundaries are equal to the values on the x-axis. The $\pm 3\sigma$ boundary values are specifying the interval where 99.73% of all measured values lay inside. The usage of the 3σ boundary is a common approach to describe error characteristic and will be used through the whole thesis.

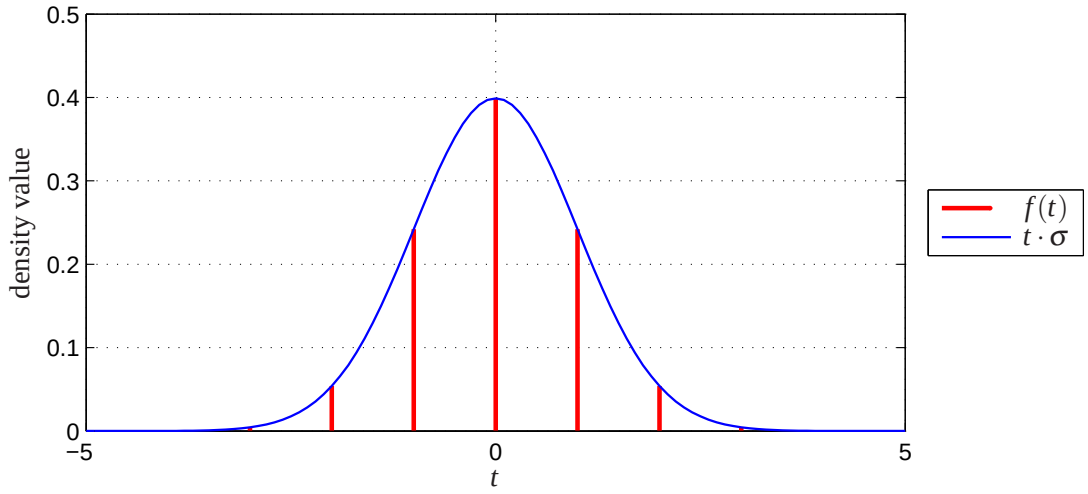

Figure 1.2: Normal GAUSSIAN distribution

1.2.1 AsteroidFinder

The scientific goal of AsteroidFinder is to detect and characterize Near-Earth Objects (NEO). Especially Inner Earth Objects (IEO) orbiting completely inside the Earth's orbit are of interest. Today only about ten IEOs have been found [21], of which two are Potentially Hazardous Asteroids (PHA). An impact of a PHA on the earth could lead to significant environmental damage. The little knowledge of the IEOs is the motivation for the AsteroidFinder payload.

To reach the scientific goal the AsteroidFinder telescope has to be pointed towards a target in inertial space. Each target shall be observed for one minute. Afterwards the telescope shall be reoriented towards a new target and kept there again for one minute. The time to reorient and stabilize the telescope shall not exceed one minute. Beside this first observation strategy there are three other requirements for the attitude control system which are directly related to the

production of an observation image. An image will be produced by a Charged Coupled Device (CCD) array that is fixed at the focal plane of the telescope.

For the CCD are existing three requirements that are relevant for the attitude control system [9].

- During an individual exposure, the modulus of the shift of the imaged field on the focal plane shall be smaller than 0.215 pixel (3σ), see figure 1.3.
- During an equivalent exposure the field rotation about the optical axis shall be within $\pm 2.15 \cdot 10^{-4}$ rad (3σ), see figure 1.4.
- The individual images forming a stacked image shall overlap over an area >95% of the field of view (3σ), see figure 1.5

To understand these terms table 1.1 shall clarify the wording.

Term	**explanation**
Individual exposure	The time during which light is continuously recorded on a photosensitive sensor (within a single shutter cycle).
Individual image	The two-dimensional scene recorded by a photosensitive sensor during an individual exposure.
Stacked image	The two-dimensional scene resulting from registering and stacking two or more individual images.
Equivalent exposure	The time elapsing from the first to the last individual exposure of the individual images forming a stacked image.

Table 1.1: Glossary for the attitude control requirements [9]

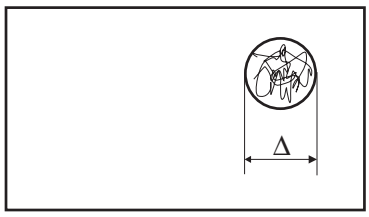

Figure 1.3: AsteroidFinder shift requirement

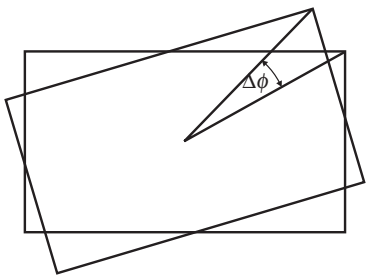

Figure 1.4: AsteroidFinder rotation requirement

Theses requirements are directly related to the CCD design and will undergo some iterations up to the middle of Phase B where they will be fixed. Due to that fact these requirements were

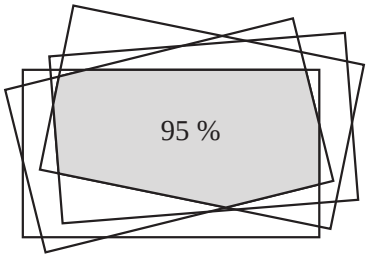

Figure 1.5: AsteroidFinder overlapping requirement

transfered for a first iteration into three error values (3σ) that are relevant for the attitude control system.

- Pointing Stability Rate (PSR) < 7.5”/s
- Absolute Pointing Accuracy (APA) < 120”
- Absolute Pointing Stability (APS) < 100”

The definition of these values can be found in figure 1.6. Where the x-axis describes the time and the y-axis is the deviation from ideal target attitude. The different angle errors are noticed as the horizontal boundaries while the angular rate error is identified as the ascending line.

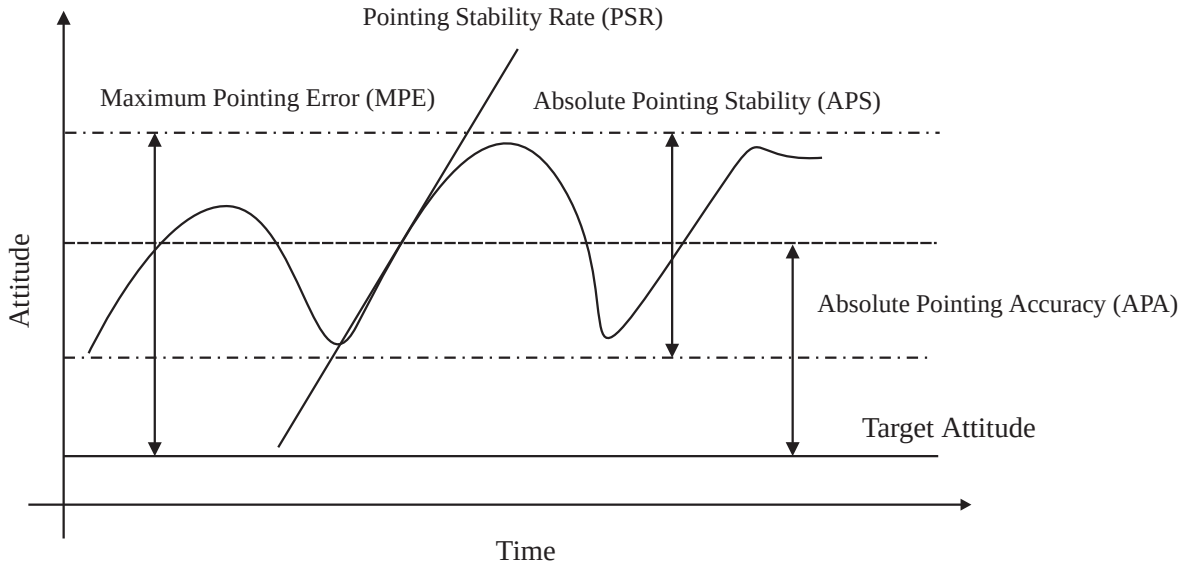

Figure 1.6: Error definition [16]

1.2.2 OSIRIS

As a potential secondary payload OSIRIS has to be taken into account. OSIRISs goal is to establish an optical link between the ground station and the satellite to be able to demonstrate a high data rate transfer. The requirements from this payload can be described in a quite simple way.

- The optical axis of OSIRIS shall be pointed towards a defined ground station as long as it is accessible. The maximum angle deviation between the vector from the satellite to the ground station and the optical axis shall not exceed a value of 20 arc seconds (3σ) during payload activity.

This maximum deviation is not allowed to be exceeded due to the fact that only in such a small range the high data rate link can be established. For the attitude control system this requirement is:

- Maximum Pointing Error (MPE) < 20”

Exactly this stringent MPE was one of the reasons why the Phase A review board recommended not to consider a secondary payload anymore. Nevertheless it will be considered inside the further study for educational purpose.

1.2.3 AoS

The optional secondary payload AoS does not have any driving requirements to the attitude control system. The fact that it is in principal only a receiver which receives broadcasts signals and can be oriented anywhere does not lead to an attitude control requirement. Therefore the AoS payload is no more addressed inside the following chapters.

1.2.4 Requirements for Attitude Determination

It should be mentioned that the requirements are only valid for the attitude control but not for the attitude determination. Therefore some attitude determination requirements have to be defined. A good starting value for a possible set of attitude determination requirements is that they should be ten times better than the attitude control requirements.

$$AD-PSR = \frac{7.5''/s}{10} = 0.75''/s \tag{1.3}$$

$$AD-APA = \frac{120''}{10} = 12'' \tag{1.4}$$

$$AD-APS = \frac{100''}{10} = 10'' \tag{1.5}$$

$$AD-MPE = \frac{20''}{10} = 2'' \tag{1.6}$$

1.3 State of the Attitude Control System

Driven by the requirements of the previews section a first design was established which is heavily based on BIRD and TET. According to this the following hardware configuration was chosen within Phase 0/A [11], [15], [16].

- Attitude Determination Hardware
  - 1x 4π Coarse Sun Sensor by Antrix Ltd., India
  - 4x Miniaturizes Fine Sun Sensor by TNO, Netherlands
  - 2x AMR-digital Magnetometer by ZARM-Technik AG, Germany
  - 4x μFORS 6-U Gyroscope by Litef GmbH, Germany
  - 1x μAdvancedStellarCamera (1x DPU, 4x Heads) by DTU, Denmark
  - 2x Phoenix GPS-Receiver by DLR
- Attitude Control Hardware
  - 4x Reaction Wheel 90 by Astro- & Feinwerktechnik GmbH, Germany
  - 3x MagneticTorquer 10-2 by ZARM-Technik AG, Germany

It was realized during Phase A that the BIRD and TET attitude controller is not able to fulfill the requirements. Especially the control algorithms were not able provide a suitable control for AsteroidFinder/SSB. Regarding to this new control algorithms have to be defined. The definition and development of these algorithms and their verification is the main topic of this diploma thesis.

The primary driving requirement is the pointing stability rate while the secondary driving requirement is the maximum pointing error. The task to develop an attitude control system that is able to fulfill these requirements with the previous hardware is an interesting and challenging task.

Chapter 2

Simulator Models

This chapter presents the mathematical models that are used in the Attitude Control System Simulator. It starts with a brief overview of the simulator structure and the underlying attitude dynamics. The focus is placed on the description of common sensors and actuators. At the end a basic modeling structure of the space environment is given.

2.1 Simulator Overview

The whole task of algorithm development and testing is done with the help of a simulator environment. This simulator is developed inside Matlab/Simulink . Matlab/Simulink is a well known and tested environment to analysis mathematical and engineering problems. An additional favor of this environment is that it is able to interact with a lot of others programming languages e.g. C, C++, FORTRAN and ADA. Another advantage is the ability to communicate with a real time simulation system provided by the company dSpace. This system allows to execute simulated models in real time which is helpful for algorithm design. A so called dSpace System is available at the DLR and will be used for the future development process of AsteroidFinder's attitude control system. During this diploma thesis a basic algorithm structure is developed which shall be able to be merged with the real time simulation system. Regarding to this Matlab/Simulink is the right environment for further algorithm development.

The basic structure of the attitude system simulator is shown in figure 2.1. The overall framework is oriented toward a control loop. The starting point is the attitude dynamics at the center of figure 2.1. From there some transformations have to be performed that are used in the other blocks. The next block are the simulated sensors which are producing the measurements. Behind the sensors follows the attitude determination and the guidance algorithms, which deliver the desired and the estimated attitude state to the comparator. The comparator determines the attitude error and forwards it to the attitude control algorithm. This algorithm derives control commands for the actuators that are acting on the satellite.

Due to the fact that the satellite is a real world system in space there are external disturbances acting on the satellite. These external disturbances are modeled and added as additional torques and forces into the satellite dynamics.

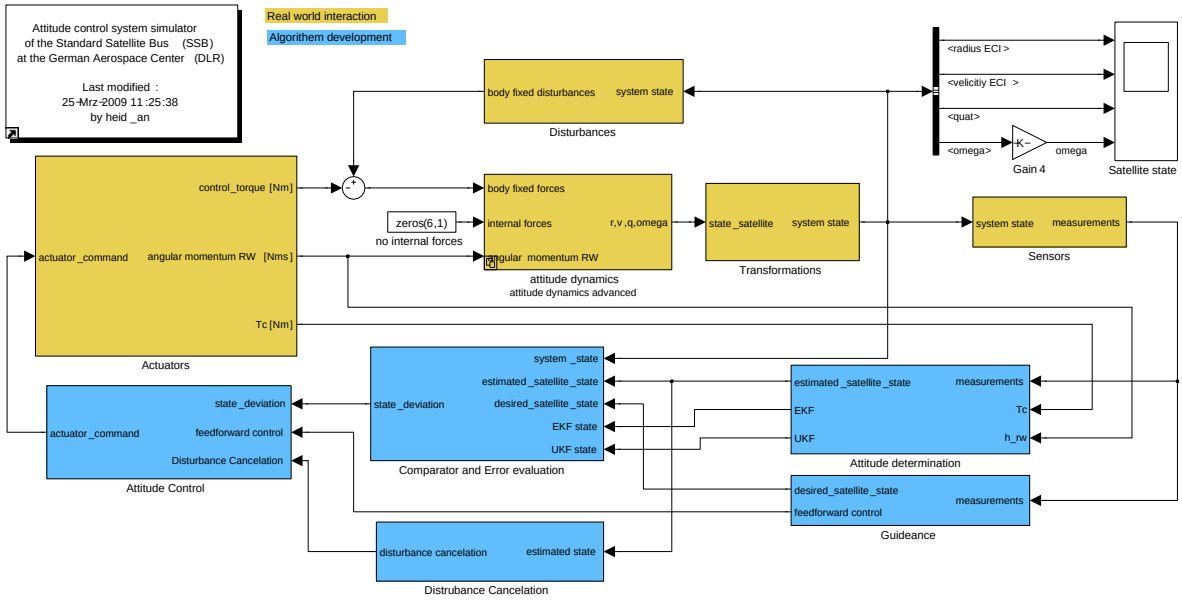

Figure 2.1: Attitude determination and control system simulator overview

2.1.1 Simulink Block Library

During the development of the simulator it was realized that the standard Matlab/Simulink block sets could not be used to describe the mathematical background in a clear way. Regarding to this a new Simulink library was developed which is related especially to satellite dynamics. The library itself includes e.g. quaternion algebra, satellite dynamic models, sensors and actuators and space environment.

2.1.2 Preconditions

To be able to test and to verify designed algorithms the simulator has to be used with a precise defined set of preconditions. These conditions are directly related to defined mission scenarios which are inputs form the mission analysis team [34]. Right now there is an orbit envelope defined in which the standard satellite bus shall be able to work.

These conditions with respect to AsteroidFinder/SSB's attitude control system are:

- semimajor axis $a = R_{Earth} + (650 \ldots 850)$ km, with the Earth radius R_{Earth}
- eccentricity $e = 0$
- inclination $i = 97.99 \ldots 98.82\,\text{deg}$
- argument of perigee $\omega = undefined$ (due to $e = 0$)
- right ascension of ascending node $\Omega = 6{:}00 \ldots 12{:}00$ h (sun synchronous)
- Mass $m = 100 \ldots 150$ kg
- Moment of Inertia $I = 4 \ldots 6\ \text{kgm}^3$

The intention for this envelope is driven by the fact that a launch to a low earth orbit (LEO) is cheaper than to a higher orbit altitude. The choice for a sun synchronous orbit (SSO) is driven by the requirements of the primary payload. The fact that many launches deliver satellites to SSOs and piggy back launches are available is another reason.

In addition to this envelope there is a set of coordinate frames defined that will be applied during the algorithm development. The definition of each coordinate frame can be found in [12]. The most important frames are summarized in the Appendix and shall be mentioned here.

- Mechanical Coordinate Frame (MCF) - this frame will be used as a body fixed frame
- Principal Axis Frame (BF) - inside this frame the moment of inertia tensor is diagonal therefore it can be used to solve the dynamic equation
- True of Date Frame (ToD) - is an earth centered inertial frame which is used to determine inertial values
- World Geodetic Coordinate System (WGS84) - is an earth fixed frame that is used to determine e.g. the ground station coordinates.

2.2 Attitude Dynamics

The core of the simulator are the attitude dynamics which are shown in figure 2.2. This block allows to simulate the behavior of a satellite with respect to the acting torques and forces. It is important to use a suitable dynamic model to ensure that the algorithm design which is based on this simulation can fulfill the requirements for the real world. As an input this block needs the

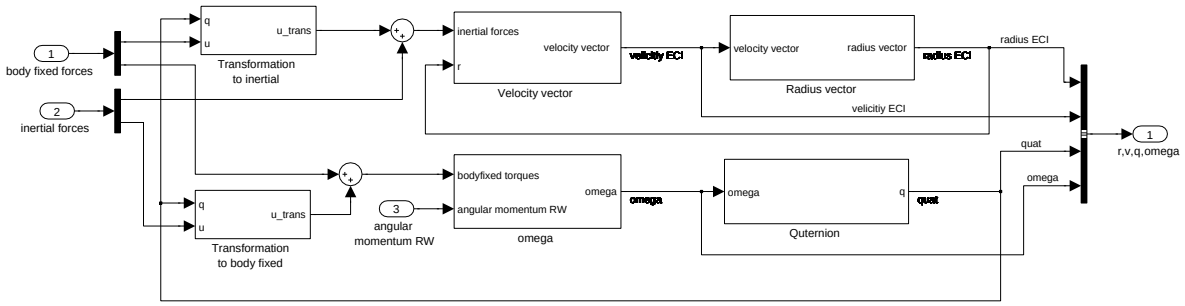

Figure 2.2: Simulink block diagram of attitude dynamics

body fixed forces, the inertial forces and the angular momentum vector of all reaction wheels. It outputs a state vector which contains the radius vector and the velocity vector in an earth centered inertial frame. The second part of the state vector consists of a unit quaternion which is used to describe the attitude and the angular rates of the satellite in body fixed coordinates.

To understand the equations behind this simulation block it is useful to distinguish between the movement of a satellite around the earth and the motion of a rigid body around its center of mass.

2.2.1 Equation of Motion of a Satellite

To determine an equation for the satellites movement around a central body (Earth) there have to be made the following three assumptions [4].

- The gravitational field of the central body is spherical-symmetrical. This assumes that the gravitational force points everywhere to the central's body center of mass.
- There are no other forces.
- The satellite mass is much more smaller than the mass of the central body.

With these assumption NEWTONs second law can be applied to a satellite orbiting a central body.

$$\begin{aligned} \underline{G} &= \frac{d}{dt}(m \cdot \underline{v}) \\ &= m\ddot{\underline{r}} \end{aligned} \tag{2.1}$$

The satellite mass is identified by m and $\underline{r}$ defines the radius vector from the central body's center of gravity (CoG) to the satellites CoG. The gravitational force $\underline{G}$ is described by NEWTON's law of universal gravitation.

$$\underline{G} = -\frac{\gamma M m}{r^2} \cdot \frac{\underline{r}}{r} \tag{2.2}$$

The universal gravitational constant γ and the mass of the central body M are normally combined to one value

$$\mu_E = \gamma \cdot M = 3.986 \cdot 10^{14} \frac{\mathrm{m}^3}{\mathrm{s}^2} \tag{2.3}$$

which is here the gravitational constant of the Earth.

By the combination of equation 2.1 and 2.2 the satellite equation of motion can be derived.

$$\dot{\underline{v}} = -\frac{\mu_E}{r^3} \cdot \underline{r} \tag{2.4}$$

$$\dot{\underline{r}} = \underline{v} \tag{2.5}$$

These two equations are the basis for the simulation. They can be integrated numerically to obtain a velocity and a radius vector.

After the derivation of these equations the assumptions which were made at the beginning can be retracted piecewise. At first the assumption of no other forces can be retracted by adding adding a second term [3] that represents other forces.

$$\dot{\underline{v}} = -\frac{\mu}{r^3} \cdot \underline{r} + \frac{\underline{F}}{m} \tag{2.6}$$

Here $\underline{F}$ is the combination of all inertial forces that are acting on the satellite e.g. atmospheric drag. All forces can be transformed into inertial forces which makes it possible to address them in a proper way inside the dynamics. The adding of the second term results out of the fact that the sum of all forces is equal to the mass multiplied with its acceleration which is equal to NEWTON's second law.

$$m \cdot \underline{\ddot{r}} = \sum \underline{F} \tag{2.7}$$

The second assumption of a spherical symmetrical gravitational field can be retracted by redefining the gravitational potential U not as a sphere but with the help of an appropriate spherical harmonic expansion [8], [3].

$$U = -\frac{\mu}{r} + B(r,\theta,\phi) \tag{2.8}$$

$$\begin{aligned} B(r,\theta,\phi) = \frac{\mu}{r}\Big(&\sum_{n=2}^{\infty}\left(\frac{R_E}{r}\right)^n J_n P_{n0}\cos(\theta)\ldots \\ &\ldots+\sum_{m=1}^{n}\left(\frac{R_E}{r}\right)^n (C_{nm}\cos(m\theta)+S_{nm}\sin(m\theta))P_{nm}\cos(\theta)\Big) \end{aligned} \tag{2.9}$$

Here J_n are zonal harmonic coefficients, P_{nm} are LEGENDRE polynomials, and C_{nm} and S_{nm} are tesseral harmonic coefficients for $n \neq m$ and sectoral harmonic coefficients for $n = m$. In the dynamic equation the gravitational potential is represented up to the sixth order this allows to use the attitude dynamic block not only for attitude simulation but for a rough orbit evolution, too.

Now it is possible to rewrite equation 2.6.

$$\underline{\dot{v}} = \nabla U + \frac{F}{m} \tag{2.10}$$

The last assumption that the mass of the satellite is much smaller than the mass of the central body is still used due to the fact that their effect is negligible. The full equation of motion is now defined by 2.5 and 2.10 and is used in the simulator core.

2.2.2 Motion of a Rigid Body

One of the most important variables to describe the attitude dynamics is the angular momentum $\underline{L}$. It is defined as follows.

$$\underline{L} = \int_m \underline{r} \times \underline{v}\, dm \tag{2.11}$$

Where $\underline{r}$ is the position vector of a point mass and $\underline{v}$ is the velocity vector of this mass. The mass itself is indicated by m. Due to the fact that the velocity is the cross product of the angular

velocity $\underline{\omega}$ and the position vector the angular momentum vector can be rewritten.

$$\begin{aligned} \underline{L} &= \int_m \underline{r} \times (\underline{\omega} \times \underline{r})\, dm && (2.12) \\ &= \int_m [\underline{r}\times]\,[-\underline{r}\times]\,\underline{\omega}\, dm \\ &= \int_m \begin{pmatrix} y^2+z^2 & -xy & -xz \\ -yx & x^2+z^2 & -yz \\ -zx & -zy & x^2+y^2 \end{pmatrix} \underline{\omega}\, dm && (2.13) \end{aligned}$$

The term $[\underline{u}\times]$ denotes the corresponding matrix expression of the crossproduct.

$$[\underline{u}\times] = \begin{bmatrix} 0 & -u_z & u_y \\ u_z & 0 & -u_x \\ -u_y & u_x & 0 \end{bmatrix}$$

If the angular velocity is equal for all point masses the integral of equation 2.13 can be solved.

$$\underline{L} = \underline{\underline{I}}\,\underline{\omega} \qquad (2.14)$$

$\underline{\underline{I}}$ indicates the Moment of Inertia (MoI) which is a constant value that just depends on the geometric characteristic and the mass distribution.

Now the derivative over time of the angular momentum can be obtained in three different ways. The first one is to use equation 2.14 and apply the product rule to it.

$$\begin{aligned} \frac{d}{dt}\underline{L} &= \frac{d}{dt}\underline{\underline{I}} \cdot \underline{\omega} + \underline{\underline{I}} \cdot \frac{d}{dt}\underline{\omega} \\ \dot{\underline{L}} &= \underline{\underline{I}}\,\dot{\underline{\omega}} && (2.15) \end{aligned}$$

The second one is to use equation 2.11 which leads to a relation between the angular momentum and the applied torques $\underline{T}$ through NEWTON's second law and describes the angular momentum in an inertial frame.

$$\begin{aligned} \dot{\underline{L}} &= \int_m \dot{\underline{r}} \times \underline{v} + \underline{r} \times \dot{\underline{v}}\, dm \\ &= \int_m \underline{r} \times \dot{\underline{v}}\, dm \\ &= \int_m \underline{r} \times d\underline{F} = \underline{T} && (2.16) \end{aligned}$$

The third option rewrites equation 2.16 toward a body fixed frame. This is used in attitude control due to the fact that the Moment of Inertia tensor stays constant inside the body fixed frame [42], [30].

$$\dot{\underline{L}} = T - \underline{\omega} \times \underline{L} \qquad (2.17)$$

$\underline{\omega}$ is the angular rate in the body fixed frame. In the next step the derived equations are written for a satellite system with reaction wheels. At first the overall angular momentum $\underline{L}$ now consists out of two parts. The first one is the satellites angular momentum $\underline{L}_{sat}$ and the second one is the reaction wheels angular momentum $\underline{L}_{rw}$.

$$\underline{L} = \underline{L}_{sat} + \underline{L}_{rw} \tag{2.18}$$

$$\dot{\underline{L}} = \dot{\underline{L}}_{sat} + \dot{\underline{L}}_{rw} \tag{2.19}$$

By substituting equations 2.18 and 2.19 inside 2.17. The following equation can be obtained

$$\dot{\underline{L}}_{sat} + \dot{\underline{L}}_{rw} = T - \underline{\omega}_{sat} \times (\underline{L}_{sat} + \underline{L}_{rw}) \tag{2.20}$$

where $\underline{\omega}_{sat}$ is the satellite's angular rate in the body fixed frame. The derivative of the satellite angular momentum can be rewritten with equation 2.15.

$$\underline{\underline{I}}_{sat}\, \dot{\underline{\omega}}_{sat} + \dot{\underline{L}}_{rw} = T - \underline{\omega}_{sat} \times (\underline{L}_{sat} + \underline{L}_{rw}) \tag{2.21}$$

After some mathematical rearrangements of 2.21 the following equation can be obtained.

$$\dot{\underline{\omega}}_{sat} = \underline{\underline{I}}_{sat}^{-1} \left(\underline{T}_d - \underline{\omega}_{sat} \times \underline{L}_{sat} - \underline{\omega}_{sat} \times \underline{L}_{rw} - \dot{\underline{L}}_{rw} \right) \tag{2.22}$$

This equation completely describes the relation between the angular acceleration of the satellite and the torques that are acting on it. In an undisturbed environment the torque $\underline{T}$ would be zero therefore all torques that are acting are disturbance torques $\underline{T}_d$.

In addition to this relation the attitude itself has to be described by another equation. Any attitude of an ridged body can be described by a $[3 \times 3]$ direct cosine matrix $\underline{\underline{M}}$. Such a matrix rotate any three dimensional vector $\underline{u}$.

$$\underline{u}_1 = \underline{\underline{M}} \cdot \underline{u}_0 \tag{2.23}$$

The representation of a rotation by a direct cosine matrix is widely used and can be found in many textbooks[30], [41]. A better representation for attitude control is a unit quaternion. Quaternions q are hyper complex numbers with three imaginary parts i, j, k and can be used for attitude representation [42], [43].

$$q \equiv q_4 + iq_1 + jq_2 + kq_3 \tag{2.24}$$

$$i^2 = j^2 = k^2 = -1 \tag{2.25}$$

For attitude representation a quaternion is usually written as a four dimensional vector

$$\underline{q} = [q_1\ q_2\ q_3\ q_4]^T \tag{2.26}$$

which has the EUKLIDIAN length one.

$$\sqrt{q_1^2+q_2^2+q_3^2+q_4^2}=1 \tag{2.27}$$

EULER had shown that each point on a unit sphere can be rotated by one single rotation around a single axis to every other point on the unit sphere [23]. The axis of rotation can be described by a unit vector $\underline{e}$ and the rotation by an angle θ. Quaternions are directly related toward this representation by a clear definition.

$$\begin{aligned} q_1 &= e_x \sin\frac{\theta}{2} \\ q_2 &= e_y \sin\frac{\theta}{2} \\ q_3 &= e_z \sin\frac{\theta}{2} \\ q_4 &= \cos\frac{\theta}{2} \end{aligned} \tag{2.28}$$

The favor of quaternions is that they allow a global attitude description without singularities. Additional they have a single redundancy due to the fact that one component can be calculated out of the three remaining values (see equation 2.27). To be able to transform a quaternion into a direct cosine matrix the following definition has to be used [42], [33].

$$\underline{\underline{M}} = \begin{bmatrix} q_1^2-q_2^2-q_3^2+q_4^2 & 2(q_1q_2+q_3q_4) & 2(q_1q_3-q_2q_4) \\ 2(q_1q_2-q_3q_4) & -q_1^2+q_2^2-q_3^2+q_4^2 & 2(q_2q_3+q_1q_4) \\ 2(q_1q_3+q_2q_4) & 2(q_2q_3-q_1q_4) & -q_1^2-q_2^2+q_3^2+q_4^2 \end{bmatrix} \tag{2.29}$$

If there are several successive rotations the classical approach is to multiply the direct cosine matrices with each other. The same procedure can be applied toward quaternions. For example consider a direct cosine matrix $\underline{\underline{M}}_b^a$ which rotates a vector from a frame b to a frame a with two rotations.

$$\underline{\underline{M}}_b^a = \underline{\underline{M}}_c^a \cdot \underline{\underline{M}}_b^c \tag{2.30}$$

In the quaternion algebra this formulation is written in the following way.

$$\underline{q}_c^a = \underline{q}_b^c \cdot \underline{q}_c^a \tag{2.31}$$

It can be seen that the multiplying order had changed. This is the result of the quaternion algebra [42]. To be able to perform the multiplication in the same way as the direct cosine matrices a new operator $\otimes$ is introduced [33].

$$\underline{q}_c^a = \underline{q}_c^a \otimes \underline{q}_b^c \tag{2.32}$$

This operator defines a matrix with which the following quaternion can be multiplied.

$$\underline{q}\otimes = \begin{bmatrix} q_4 & q_3 & -q_2 & q_1 \\ -q_3 & q_4 & q_1 & q_2 \\ q_2 & -q_1 & q_4 & q_3 \\ -q_1 & -q_2 & -q_3 & q_4 \end{bmatrix} \tag{2.33}$$

Inside the following chapters this new operator is used to enable a consistence between the direct cosine multiplication an the quaternion multiplication.

In addition to the quaternion description the time evolution of a quaternion is needed. This is describe by a well known differential equation [42]

$$\dot{\underline{q}} = \frac{1}{2}\,\underline{\underline{\Omega}}\,\underline{q} \tag{2.34}$$

$$= \frac{1}{2}\,\underline{\underline{\Xi}}\,\underline{\omega} \tag{2.35}$$

with

$$\underline{\underline{\Omega}} = \begin{pmatrix} -[\underline{\omega}\times] & \underline{\omega} \\ -\underline{\omega}^T & 0 \end{pmatrix} \tag{2.36}$$

$$\underline{\underline{\Xi}} = \begin{pmatrix} q_4\, I_{3\times 3} + -[q_{123}\times] \\ -\underline{q}_{123}^T \end{pmatrix} \tag{2.37}$$

This equation connects the angular rate $\underline{\omega}$ with the attitude description and is used inside the attitude dynamic block.

2.3 Sensor models

2.3.1 Gyroscope

2.3.1.1 Measurement Principal

An angular rate gyro is used to measure the angular rate of the satellite. There are different principals to measure the angular rate. One is to use a constant spinning mass which is fixed to the satellite and monitor its angular displacement with respect to the satellites structure. This is a classical gyro compass which is not used anymore in modern satellite systems. Another option is to use optical gyroscopes. Such an angular rate sensor can be realised as a fiber optic gyro (FOG) or a ring laser gyro utilizing the Sagnac effect. To uses this effect two optical waves are fed into opposite direction of a closed optical path e.g. circular coils (see figure 2.4). At occurrence of inertial rotation a phase shift Δ can be observed. When the two waves are brought to interference at a given point the phase shift can be seen as intensity variation measured by a photo detector. The AsteroidFinder/SSB mission will use four fiber optic gyros. A third option

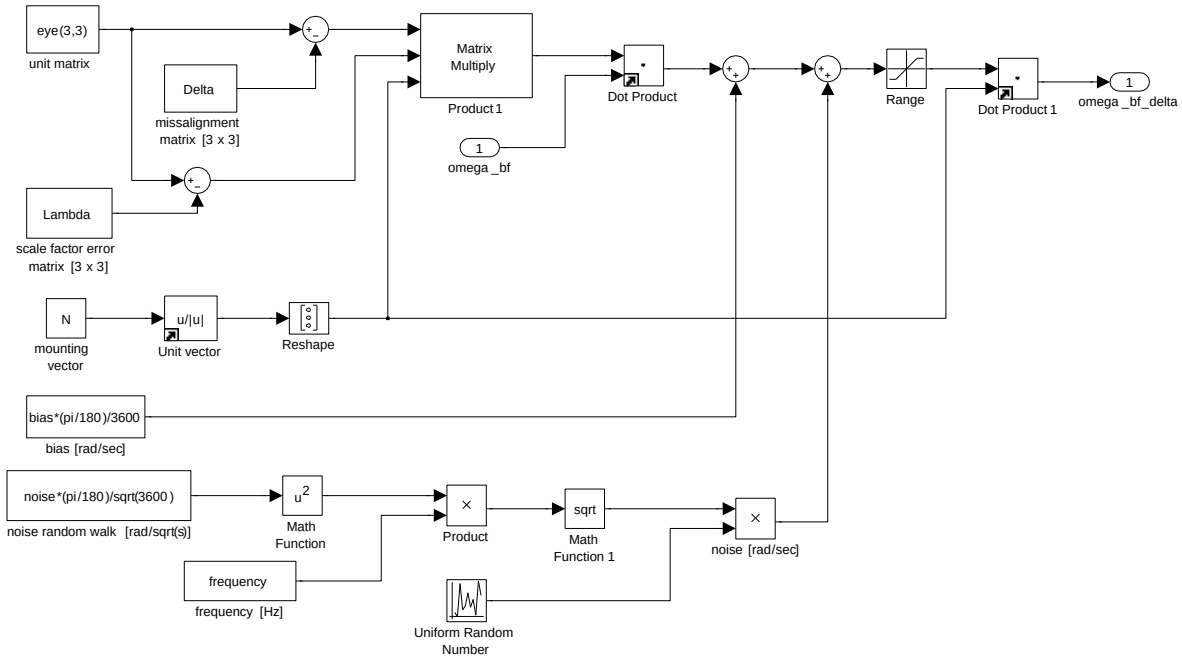

Figure 2.3: Simulink model of a gyroscope

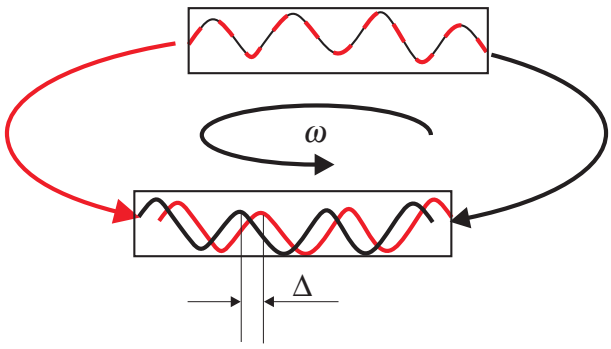

Figure 2.4: Sagnac effect inside a fiber optic gyroscope

is to use rate sensors which are based on a Micro-Electro-Mechanical-System (MEMS). One principle of such a MEMS gyro is to measure a Coriolis acceleration of a vibrating mass and transform it to a angular rate. The advantage of such sensors is that they are very cheap but in the same case they are not very precise regarding to fiber optic gyros. Due to this they are quiet seldom used in satellite projects but their development is still under process.

2.3.1.2 Mathematical Model

The goal of a mathematical model is to simulate as good as possible the real measured value. The relation between the real angular rate vector $\underline{\omega}^{bf}$ in body fixed coordinates and a single measurement ω^{gyro} can be described as

$$\omega^{gyro} = \underline{N}_{\Delta}^{bf} \cdot \underline{\omega}^{bf} + \beta^{gyro} + \eta^{gyro} \tag{2.38}$$

$$\underline{N}_{\Delta}^{bf} = (I_{[3\times3]} - \underline{\underline{\Delta}})\,(I_{[3\times3]} - \underline{\underline{\Delta}})\,\underline{N}^{bf} \tag{2.39}$$

where β^{gyro} is gyro bias, η^{gyro} is white noise driving the angular random walk. $\underline{N}_{\Delta}^{bf}$ is the disturbed mounting vector of the gyroscope which is related to the undisturbed mounting vector $\underline{N}^{bf}$ through a nonorthogonal small angle misalignment matrix $I_{[3\times3]} - \underline{\underline{\Delta}}$ and the diagonal scale factor error matrix $I_{[3\times3]} - \underline{\underline{\Delta}}$. This equation can be used for all different rate gyros cause it is very general.

To simulate the real measurement the values of equation 2.38 and 2.39 have to be chosen and the measurement has to be calculated. In the next step the disturbed angular rate $\underline{\omega}_{\Delta}^{bf}$ of the body is determined by inverting the equation with the assumption of no misalignment, noise or bias error. This leads directly to the following equation.

$$\underline{\omega}_{\Delta}^{bf} = \underline{N}^{bf} \cdot \omega^{gyro} \tag{2.40}$$

These equations reflect the behavior of a gyroscope in a good way and is used in the further simulation. The block diagram of the gyroscope model, based on this equations, is shown in figure 2.3. In addition to the equations above the measurements is limited by an upper an lower bound which is the case for a real sensor.

Regarding to the producer specifications white noise is quite often expressed as a random walk. It has to be transformed to the suitable covariance that can be used in equation 2.38. This can be achieved by

$$\eta^{gyro}(t) = \sqrt{\eta_{rw}^2 \cdot f} \cdot \gamma(t) \tag{2.41}$$

where η_{rw} is the power spectral density, specified in $rad/\sqrt{sec}$ for a random walk. The time is indicated by t and f is the frequency of the samples while γ is a uniformly distributed random number.

The realisation of the mathematical model inside a simulink block diagram is shown in figure 2.3.

2.3.1.3 Litef μFORS-6U

The AsteroidFinder mission will use four rate gyros in a tetragon arrangement. At least three rate gyros are used to determine the angular rate about the three axis and the fourth in a tetragon arrangement is used to have a singular point failure redundancy. The preferred rate gyros are the μFORS-6U [22] from Litef GmbH, Germany. The values for this rate gyro fitting to the mathematical model are listed in table 2.1.

Name	Value
Range	$\pm$ 1000 °/s
Scale factor error	$\leq$ 0.6% (3σ)
Bias	$\leq 9^\circ$/h (3σ)
Noise (random walk)	$\leq 0.15^\circ/\sqrt{h}$
Misalignment	$\pm$ 5 mrad max.

Table 2.1: Rate gyro characteristic μFORS-6U, Litef GmbH

2.3.2 Magnetometer

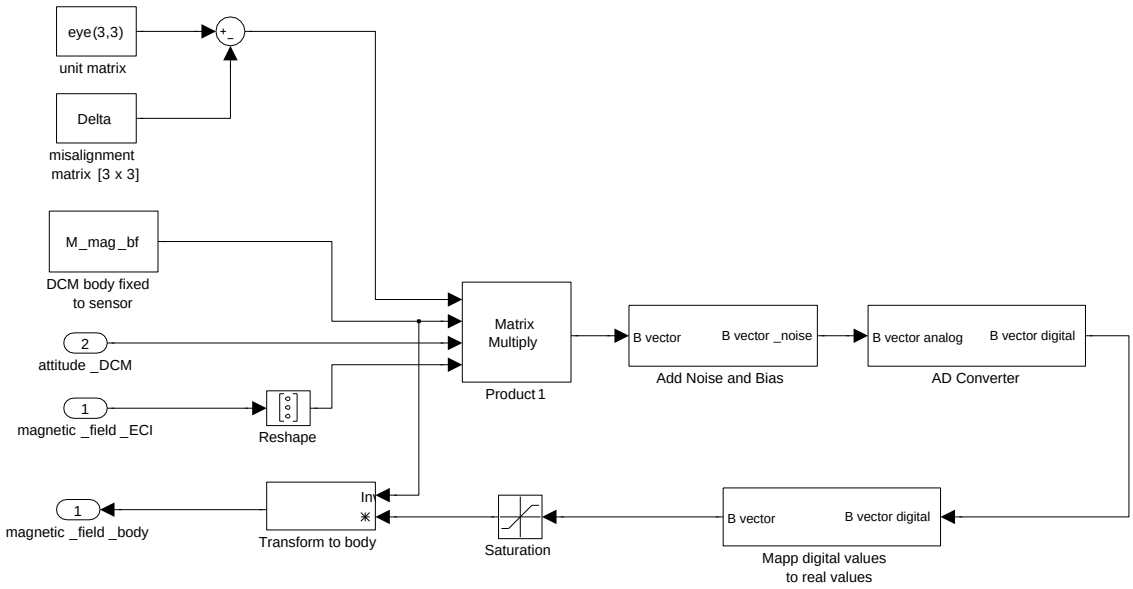

Figure 2.5: Simulink model of a digital magnetometer

2.3.2.1 Measurement Principal

Magnetometers are common sensors on satellite systems as they are reliable and cost efficient sensors that measure the magnetic field vector. Mainly there are two different principals to measure the magnetic field vector. The first one is called Fluxgate. A Fluxgate magnetometer consists of a small, magnetical susceptible, core wrapped by two coils of wire. An alternating

electrical current is passed through one coil to drive the core through an alternating cycle of magnetic saturation. This constantly changing field induces an electrical current in the second coil which can be measured by a detector. In a magnetical neutral background both currents (input, output) will match. If the core is exposed to a magnetic field the component along the core induces a current inside the coils. Due to this fact the input and the induced current will be out of step. The step size is depending on the magnetic field strength and can be used to measure the magnetic field.

The second principal uses the anisotropic magneto resistive (AMR) effect. The effect uses the property of ferromagnetic material to change its internal electromagnetic resistor under the influence of an external magnetic field. The resistor value change can be measured and interpreted as a change in the external magnetic field.

The preferred magnetometer for the AsteroidFinder mission is a digital AMR magnetometer.

2.3.2.2 Mathematical Model

An error model which describes the behavior of a three axis magnetometer is set up nearly in the same way as it is used for the gyroscopes. The magnetometer model is based on the following equation.

$$\underline{B}^{mag} = (I_{[3\times3]} - \underline{\underline{\Delta}})\, \underline{\underline{M}}^{mag}_{bf}\, \underline{\underline{M}}^{bf}_{eci}\, \underline{B}^{eci} + \underline{\beta}^{mag} + \underline{\eta}^{mag} \tag{2.42}$$

Where $\underline{B}^{mag}$ is the measured vector by the magnetometer in sensor coordinates, $\underline{B}^{eci}$ is the magnetic field vector in inertial coordinates, $\underline{\underline{M}}^{mag}_{bf}$ is the direct cosine matrix which transforms the vector from body fix into sensor coordinates, $\underline{\underline{M}}^{bf}_{eci}$ transforms the vector from inertial to body fix coordinates and is the actual attitude matrix, $\underline{\beta}^{mag}$ is the the bias and $\underline{\eta}^{mag}$ is the white noise of the sensor. $(I_{[3\times3]} - \underline{\underline{\Delta}})$ is again a nonorthogonal small angle misalignment matrix.

For the simulation the values in equation 2.42 have to be chosen and the parts of the equation have to be inverted. This leads to

$$\underline{B}^{bf}_{\Delta} = \left(\underline{\underline{M}}^{mag}_{bf}\right)^{-1} \underline{B}^{mag} \tag{2.43}$$

with the disturbed measured magnetic field vector $\underline{B}^{bf}_{\Delta}$. This is the basic principal with which the magnetometer can be simulated.

Due to the fact that a digital magnetometer will be used on the AsteroidFinder mission an analogue to digital conversion is included in the simulated measurement vector $\underline{B}^{mag}$. The simulink block model of such a magnetometer is shown in figure 2.5.

2.3.2.3 ZARM Technik AMR digital magnetometer

The preferred magnetometer for the AsteroidFinder mission is the AMR digital magnetometer [27] of the ZARM Technik AG. The relevant characteristic of this magnetometer can be found in table 2.2.

Name	Value
Measurement Range	$\pm$ 250 μT
Resolution / Noise	16 bit / < 10 nT
Accuracy	1% of full scale
Linearity	$\pm$ 100 μT
Axial Alignment	< 1.5°

Table 2.2: Magnetometer characteristic AMR, ZARM Technik AG

2.3.3 Sun Sensor

2.3.3.1 Measurement Principal

Sun sensors are used to determine the direction of the sun. All sun sensors are based on the principal that a surface has to be illuminated. This surface is often a solar cell and produces a current which can be measured.

One principal is to use a so called truncated pyramid, where five solar cells are arranged on each surface of the pyramid. The relation between current I which is produced by the solar cell and the incident sun angle θ is given by the cosine law.

$$I(\theta) = I(0)\, cos\theta \tag{2.44}$$

Due to the five available current measurements it is possible to determine the direction of the sun. One truncated pyramid has a hemispheric field of view. Therefore two of them would be enough to get spheric view.

Another construction principal is to use solar cells on every side of the satellite (cube). Each side is illuminated in a different way and the cosine law can be applied in the same way as before. These both principals are used for coarse sun sensors.

The third principal is used especially for fine sun sensors. Here a slit mask with underlying solar cell or a CCD array is used. Depending on the sun angle different regions are illuminated and the direction can be calculated in a much more precise way than before.

For the AsteroidFinder a coarse sun sensor working on the cube principal and a fine sun sensor will be used.

2.3.3.2 Mathematical Model of a Coarse Sun Sensor

The coarse sun sensor of the AsteroidFinder/SSB will have a spherical field of view. It consists out of four small sensor heads which have solar cells on three of its side. Figure 2.6 shows the principal construction of the sensor. The four heads are arranged in such a way that two solar cell sides (gray) are pointing in the same direction of the overall satellite cube. For the simulation it is assumed that there is no redundancy in the design because it is not needed for the algorithm development. Each solar cell generates a current I that can be measured. The mathematical description to simulate it follows the cosine law.

$$I(\theta) = I(\theta = 0) \cdot \cos(\theta) + \eta^{sol} \tag{2.45}$$

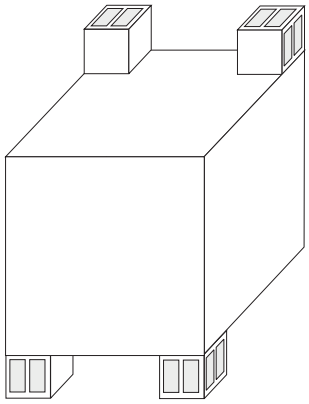

Figure 2.6: 4π sun sensor

Where η^{sol} is white noise regarding to the current and the cosine term is expressed as:

$$\cos\theta = \frac{\underline{S}^{bf} \cdot \underline{N}^{bf}}{|\underline{S}^{bf}| \cdot |\underline{N}^{bf}|} \tag{2.46}$$

$$\underline{N}_{\Delta}^{bf} = (I_{[3\times 3]} - \underline{\underline{\Delta}})\underline{N}^{bf} \tag{2.47}$$

where $\underline{S}_{bf}$ indicates the sun vector in body fixed coordinates and $\underline{N}$ is the surface normal of the solar cell. The misalignment of one cell is addressed by $\underline{\underline{\Delta}}$. One solar cell itself is measuring an analogue current that has to be converted into a digital value I_d.

$$I(\theta) \mathrel{\hat{=}} I_d(\theta) \tag{2.48}$$

If all values of all six surfaces $(\pm x, \pm y, \pm z)$ are converted the measured sun vector $\underline{S}_{\Delta}^{bf}$ in sensor coordinates can be determined by the subtraction of the opposition values and its normalisation.

$$\underline{I}_d = \begin{pmatrix} I_{d,x} - I_{d,-x} \\ I_{d,y} - I_{d,-y} \\ I_{d,z} - I_{d,-z} \end{pmatrix} \tag{2.49}$$

$$\underline{S}_{\Delta}^{bf} = \frac{\underline{I}_d}{|\underline{I}_d|} \tag{2.50}$$

The simulink realisation of the single solar cell of such a cube sensor can be seen in figure 2.7. In addition to the equations the illumination of the solar cell is check by a comparison of the dot product in equation 2.46 with zero. If it is smaller than zero the simulation produces a zero which is equivalent to a shadowed solar cell.

2.3.3.3 Antrix 4π SunSensor

As a coarse sun sensor the same sensor as it was used in the BIRD and TET program will be used for the AsteroidFinder/SSB mission. This sensor is the 4π SunSensor [32] form Antrix Ltd., India. Its main characteristic is listed in table 2.3.

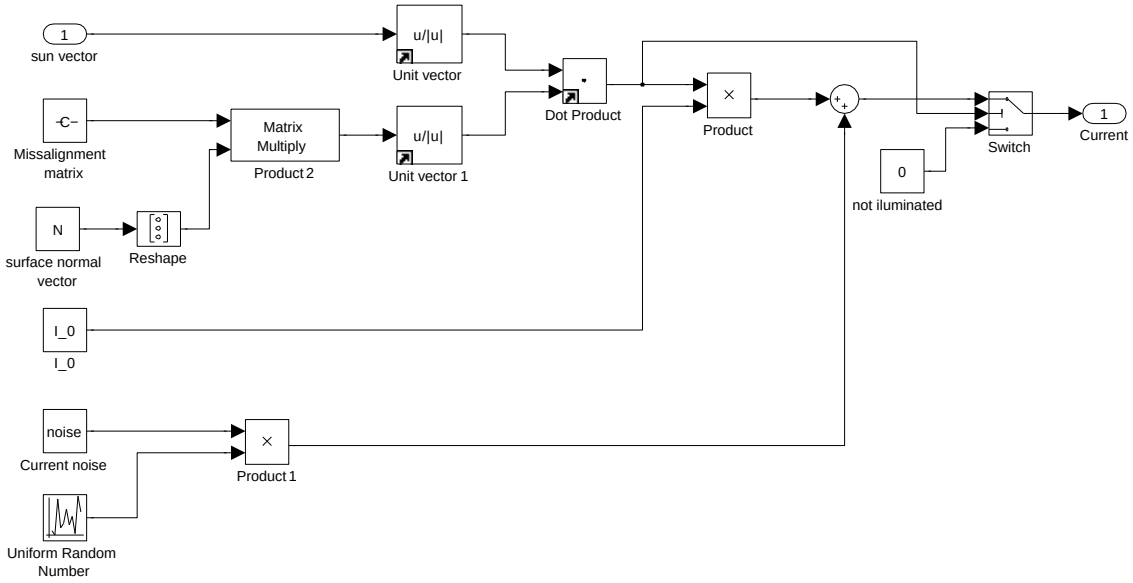

Figure 2.7: Simulink model of one solar cell for the coarse sun sensor

Name	Value
Field of View	4π steradian
	(combined FOV of four sensor heads)
Null Accuracy	$\pm$ 5°
Output	Analog 4.5 $\pm$ 0.5 V
Detector	Solar Cell
Size	55 x 42 x 29 (each sensor head)
Mass	0.05 kg

Table 2.3: Characteristic of Antrix 4π SunSensor, India

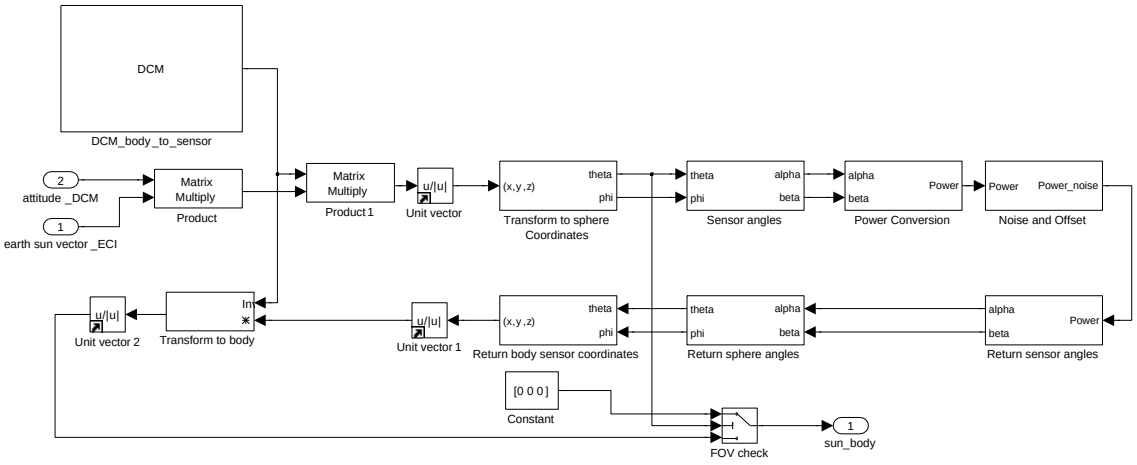

Figure 2.8: Simulink model of a fine sun sensor

2.3.3.4 Mathematical Model of a Fine Sun Sensor

In addition to the coarse sun sensor AsteroidFinder/SSB will have four additional fine sun sensors to determine the sun direction in a more precise way. The fine sun sensor model describes a two axis slit sun sensor that is measuring the two angles α and β.

To be able to simulated the sensor the sun vector $\underline{S}^{bf}$ in body fixed coordinates has to be expressed in spherical coordinates [5]. Where the $arctan_2$ function is used to determine the right quadrant of the solution

$$\theta = \arccos S^{bf}_{z,\Delta} \tag{2.51}$$

$$\phi = \arctan_2 \frac{S^{bf}_{y,\Delta}}{S^{bf}_{x,\Delta}} \tag{2.52}$$

and $\underline{S}^{bf}_{\Delta}$ is the sun vector in sensor frame and includes a structural misalignment $\underline{\underline{\Delta}}$.

$$\underline{S}^{bf}_{\Delta} = (I_{[3\times3]} - \underline{\underline{\Delta}})\, \underline{\underline{M}}^{bf}_{eci}\, \underline{S}^{eci} \tag{2.53}$$

At this point a field of view check is implemented. If the field of view is expressed as a cone angle it just has to be checked if $\theta >$ FOV and therefore the sun is no more visible to the sensor. In the next step the two spherical angles are converted into the measured angles [42].

$$\tan\alpha = \tan\theta \cdot \sin\phi \tag{2.54}$$

$$\tan\beta = \tan\theta \cdot \cos\phi \tag{2.55}$$

Now the two angles can be transformed to a current value with help of the cosine law and noise η^{sol} and bias β^{sol} can be added.

$$I_\alpha = I_{max} \cdot \cos\alpha + \beta^{sol} + \eta^{sol} \tag{2.56}$$

$$I_\beta = I_{max} \cdot \cos\beta + \beta^{sol} + \eta^{sol} \tag{2.57}$$

Afterwards an analogue to digital conversion is performed and the whole calculation is inverted. Figure 2.8 shows the simulink model that is related to the fine sun sensor equations.

2.3.3.5 TNO miniFSS

The AsteroidFinder/SSB mission requires the knowledge of the sun vector to avoid an exposure of the telescope to the sun. The coarse sun sensor is not able to deliver the sun vector in such a precise way that a save operation can be ensured. Therefore four additional fine sun sensors from TNO [36] are added. The main characteristic of this miniaturised fine sun sensor (MiniFSS) is listen in table 2.4.

Name	Value
Envelope dimensions	46 x 45 x 17 mm^3
Mass	< 60 grams
Field of view	128° x 128°
Accuracy	with ground calibration 0.3° (3σ) in whole FOV
	without ground calibration < 2° (3σ) in whole FOV
Power	miniFSS is passiv

Table 2.4: Characteristic of miniFSS by TNO, Netherlands

2.3.4 Star Camera

2.3.4.1 Measurement Principal

For high accuracy attitude determination magnetic field, sun vector or earth vector measurements are not sufficient enough. Due to that fact a third reference has to be observed. It is common to do this by observing the stellar background with a star camera. A star camera/star tracker is observing the stars and taking pictures of it. These pictures are processed to identify the brightest points on each picture and determine their relative distance between each other. At the end these distance information is compared to an on board star catalogue to identify the exact attitude of the satellite.

Star cameras are able to determine the attitude and the rotation of the satellite without further information. For high precision star cameras it is common to combine them with a navigation system to deliver the satellite velocity with respect to the earth to cancel out effects of abberation [33], [28].

2.3.4.2 Mathematical Model

The detailed description of a star camera would include a complete star catalogue and a lot of image processing techniques. Such a simulation would go far behind this diploma thesis. In the following the star camera effects shall be described in a more simple way that can be used inside the simulation. A star camera is able to deliver an attitude quaternion which describes the rotation between an inertial and the body fixed frame. This signal is corrupted by white noise and bias. For the simulation of the star camera the real quaternion $\underline{q}_{eci}^{bf}$ will be multiplied by a noisy $\underline{q}_{\eta}$ and a bias $\underline{q}_{\beta}$ quaternion. Beside the quaternion the angular rate $\underline{\omega}_{\Delta}^{bf}$ is measured which is simulated by a simple addition of noise $\underline{\eta}$ and bias $\underline{\beta}$ to the original angular rate.

$$\underline{q}_{eci,\Delta}^{bf} = \underline{q}_{\eta} \otimes \underline{q}_{\beta} \otimes \underline{q}_{eci}^{bf} \tag{2.58}$$

$$\underline{\omega}_{\Delta}^{bf} = \underline{\omega}^{bf} + \underline{\beta}^{bf} + \underline{\eta}^{bf} \tag{2.59}$$

Another possibility to calculate the angular rate would be to take the quaternion derivative. The problem with that simulation would be a delay inside the attitude determination. Due to the fact that a star camera often includes an internal propagator for the angular rate it seems to be more realistic to simulated the angular rate beside the quaternion.

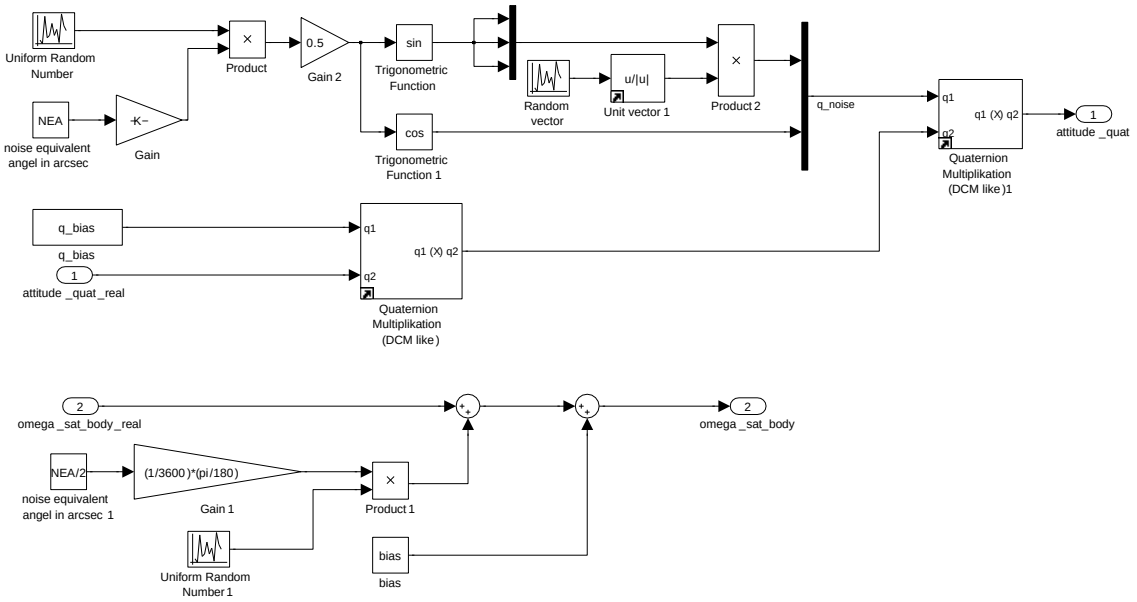

Figure 2.9: Simulink block model of a star camera

The noise of a star camera is often defined by a noise equivalent angle (NEA) which has to be converted into the noise quaternion. For the simulation this is done by the definition of equation 2.28.

$$
\begin{aligned}
q_{\eta,1} &= e_x \sin\frac{NEA}{2} \\
q_{\eta,2} &= e_y \sin\frac{NEA}{2} \\
q_{\eta,3} &= e_z \sin\frac{NEA}{2} \\
q_{\eta,4} &= \cos\frac{NEA}{2}
\end{aligned}
$$

For the simulation the NEA is a simulated as random number of the NEA range and the vector $\underline{e}$ is a random unit vector. Due to the fact that there is a relation between the NEA and the determination of the angular rate the noise of the angular rate is set to a half NEA angle.

The realisation of these equation is shown in the simulink block diagram in figure 2.9.

2.3.4.3 DTU μAdvanced Stellar Compass

The preferred star camera for the AsteroidFinder/SSB mission is the μAdvanced Stellar Compass (μASC) [29]. Its producer is the Denmark's Technical University (DTU). The μASC is the design line for the TET mission and shall therefore be reused. The main characteristic of these star camera are listed in table 2.5.

Name	value
Camera head units (CHU)	4
Field of View single CHU	18.4° x 12.4°
Single image accuracy (NEA)	3” pitch and yaw 24”roll (3σ)

Table 2.5: Characteristic of μAdvanced Stellar Compass, DTU

2.4 Actuator Models

2.4.1 Reaction Wheel

Reaction Wheels (RW) are a quite common system on satellites [41]. They exist in many different versions e.g as momentum wheels (MW), reaction wheels or control momentum gyros (CMG). Basically they are all related to the same principal of conversion of angular momentum.

Every wheel is in principal a symmetrically rotating mass where its rotating axis is connected to the satellite structure. Due to the rotation of the mass the wheel produces a torque when the mass is accelerated about its axis of rotation. While the wheel is rotating it includes an initial constant angular momentum vector $\underline{L}_{rw}$. This angular momentum vector can be transfered from the reaction wheels to the satellite and backwards without changing the overall angular momentum. This is the principal of conversion of angular momentum and can directly be used for attitude control.

The SSB is a three axis stabilized satellite that will have four reaction wheels arranged in a tetrahedron [16]. Three wheels are essential for a three axis attitude control and the fourth one is needed for redundancy.

2.4.1.1 Mathematical Model

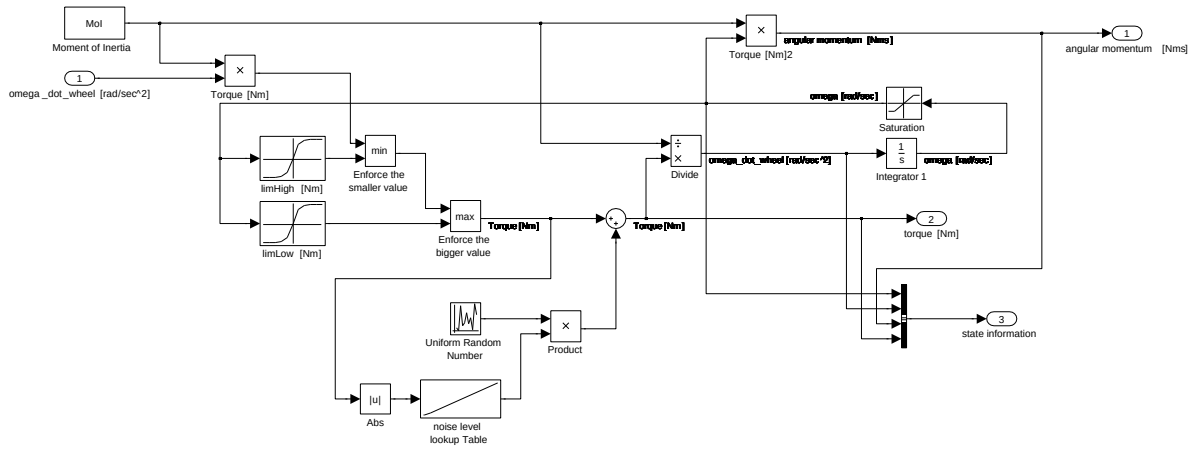

Figure 2.10: Simulink model of a reaction wheel

The mathematical model of a single reaction wheel is realized in a quite simple way.

$$T_{rw} = J_{rw}\dot{\omega}_{rw} + \eta_{rw}(\omega) \tag{2.60}$$

Where T is the torque that is acting on the satellite, J is the moment of inertia of the wheel around its spinning axis and $\dot{\omega}$ is the angular acceleration that is commanded to the reaction wheel. The disturbing noise that is included in every reaction wheel can be expressed as a white noise $\eta(\omega)$ that depends on the actual wheel speed.

In addition to the disturbing noise there exists a maximum wheel speed which defines the maximum angular momentum limit of a reaction wheel. These two boundaries are check inside the model for the angular momentum as well as for the angular rate.

The noise level $\eta_{rw}(\omega)$ is simulated with a lookup table that allows to specify the noise level at each angular rate. If an angular rate is not addressed in the lookup data its noise level is linear interpolated. Figure 2.10 shows the simulink model of these equations.

2.4.1.2 Tetragon Arrangement

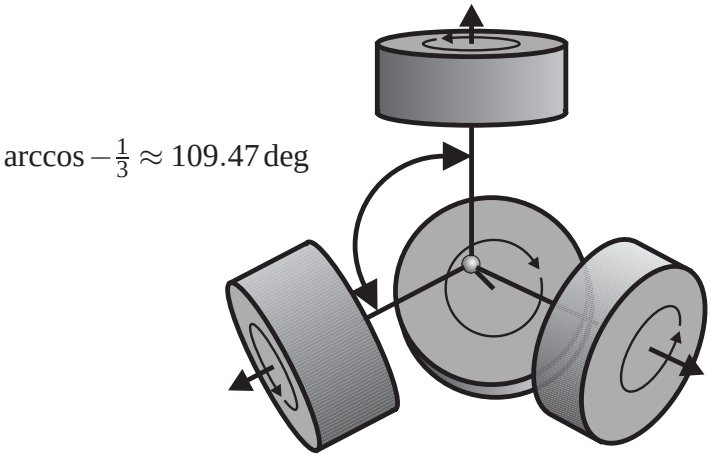

Figure 2.11: Tetragon arrangement of reaction wheels

The above equation can be used to describe every single reaction wheel that is used on a satellite. Due to the fact that the AsteroidFinder/SSB will use four reaction wheels the summed torque and angular momentum have to be calculated. The transformation from the four reaction wheels toward the satellite vectors is clearly defined through the mounting matrix $\underline{\underline{N}}_{rw}^{bf}$.

$$\underline{L}_c^{bf} = \underline{\underline{N}}_{rw}^{bf}\,\underline{L}^{rw} \tag{2.61}$$

$$\underline{T}_c^{bf} = \underline{\underline{N}}_{rw}^{bf}\,\underline{T}^{rw} \tag{2.62}$$

The columns of $\underline{\underline{N}}_{rw}^{bf}$ define the four vectors of each reaction wheel in satellite body fixed coordinates. The matrix itself has therefore the dimension $[3 \times 4]$ and includes the mounting information of the reaction wheels. The torque and angular momentum information of every wheel forms the four dimensional vectors $\underline{L}^{rw}$ and $\underline{T}^{rw}$. Finally the results are the two three dimensional vectors $\underline{L}^{bf}$ and $\underline{T}^{bf}$ that can be forwarded to the dynamic equation.

During the control task the matrix $\underline{\underline{N}}_{rw}^{bf}$ has to be inverted to allocate the three dimensional torque command to the four reaction wheels. There are several principals how to to this "momentum management" the simplest approach is to use the a pseudo inverse formulation of $\underline{\underline{N}}_{rw}^{bf}$ [33].

$$\underline{\underline{N}}_{bf}^{rw} = \underline{\underline{N}}_{rw}^{bf\,T} \cdot \left(\underline{\underline{N}}_{rw}^{bf} \, \underline{\underline{N}}_{rw}^{bf\,T} \right) \tag{2.63}$$

This is a simple approach and will be applied for the further development.

2.4.1.3 Astro- & Feinwerktechnik RW90

For the AsteroidFinder/SSB mission four reaction wheels of the type RW90 [1] are foreseen. These reaction wheels were already used for the BIRD and TET program and shall be reused. The characteristic of the RW90 is listed in table

Name	**value**
Angular momentum	0.36 Nms @ 7800 rpm
Nominal rotation speep	6000 rpm
Max. rotation speed	ca. 7820 rpm
Resolution	0.12 rpm
Speed deviation - rms. value	0.26 rpm
Speed deviation - max. value	$\pm$ 0.96 rpm
Nominal torque (max. commendable)	0.015 Nm
Torque deviation - rms value	$< 2 \cdot 10^{-5}$ Nm
Torque deviation - max. value	$< 6 \cdot 10^{-5}$ Nm
Mass	$<$ 0.9 kg
Moment of inertia (rotating mass)	$4.5 \cdot 10^{-4}$ kgm^2

Table 2.6: Astro- & Feinwerktechnik GmbH RW90

2.4.2 Magnetic Coils

Magnetic attitude stabilization and control is one of the oldest principals that is used on satellites. The basic principal is to produce a magnetic field vector inside the satellite. Due to the interaction of the satellite magnetic field vector with the Earth magnetic field vector a torque is produced and the satellite is rotated.

On former satellites the magnetic field vector was quite often produced by a permanent magnet which had a constant magnetic field vector. This technique was especially used in combination with gravity gradient stabilization. Today the magnetic field vector on board of a satellite is produced by electromagnetic coils. There exist two different systems. One is using an electrical wire that is wound around a frame the other and more efficient system is using a torque rod. Here the electrical wire is wound around an inner core with a specific permeability. The inner core allows to reach a higher dipole moment without consuming more electrical power as it would be the case for coils without an inner core.

2.4.2.1 Mathematical Model

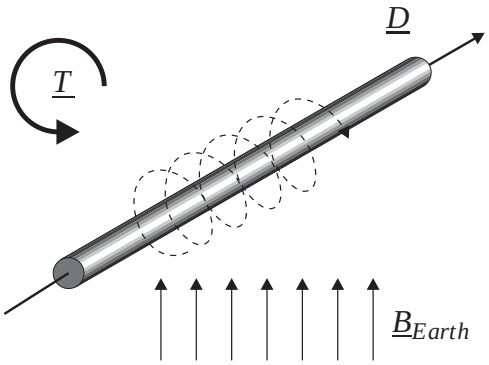

Figure 2.12: Magnetic Torquer principal

The basic mathematical description of a magnetic coils does not relay on its design. Therefore it can be performed in a quite simple way.

$$\underline{T}^{bf} = \underline{D}^{bf} \times \underline{B}^{bf}_{Earth} \tag{2.64}$$

Here $\underline{B}_{Earth}$ is the magnetic field vector of the earth in body fixed coordinates and $\underline{D}^{bf}$ is the magnetic dipole of the coil. The resulting torque $\underline{T}^{bf}$ is the cross product of both vectors. This principal is shown in figure 2.12.

2.4.2.2 ZARM Technik AG MT10-2

The AsteroidFinder/SSB comprises a set of three internally redundant magnetic torquers (MT) which are operated in cold redundancy. The desired magnetic torquers are the MT10-2 of the ZARM Technik AG, Germany [26]. Their main characteristic is mentioned in the table 2.7.

Name	Value
Number of coils	2
Linear dipole moment	10 Am^2
Saturation moment	> 12 Am^2
Linear voltage	10 V
Linear power	1 W
Mass	0.35 kg
Length	330.0 mm
Diameter	17 mm

Table 2.7: ZARM Technik AG MT10-2

2.5 Space Environment

2.5.1 Gravity Gradient

One relevant disturbing torque results off a non uniformed satellite's mass distribution. The gravity force is acting on each mass element of the satellite. The sum of all forces with respect to the center of gravity produces a Gravity Gradient torque (GG). If the mass is distributed equally over the whole satellite there would be no torque due to the fact that all forces are compensated by an opposition force. The torque $\underline{T}_{gg}^{bf}$ that is generated by this effect can be described with

$$\underline{T}_{gg}^{bf} = \frac{3\mu}{|\underline{r}^{bf}|^3}\left(\frac{\underline{r}^{bf}}{|\underline{r}^{bf}|} \times \left(\underline{\underline{I}}_{sat} \cdot \frac{\underline{r}^{bf}}{|\underline{r}^{bf}|}\right)\right) \tag{2.65}$$

where $\underline{r}^{bf}$ is the radius vector of the satellite from the central body's center of gravity to the satellites's center of gravity. The satellite's mass distribution is reflected by the Moment of Inertia $\underline{\underline{I}}_{sat}$ and the central body is identified by its gravity constant μ.

For the description of the gravity gradient torque a spherical gravity field can be assumed [42]. This assumption results in the constant gravity constant. The incorporation of higher order terms is not useful for the simulation of a small satellite and shall therefore be omitted.

For a small satellite the higher order terms of the gravity field are much more influencing the orbit dynamics than the attitude dynamics therefore the description of equation 2.65 is valid [41] and implemented in the simulator. It's implementation can be seen in figure 2.13.

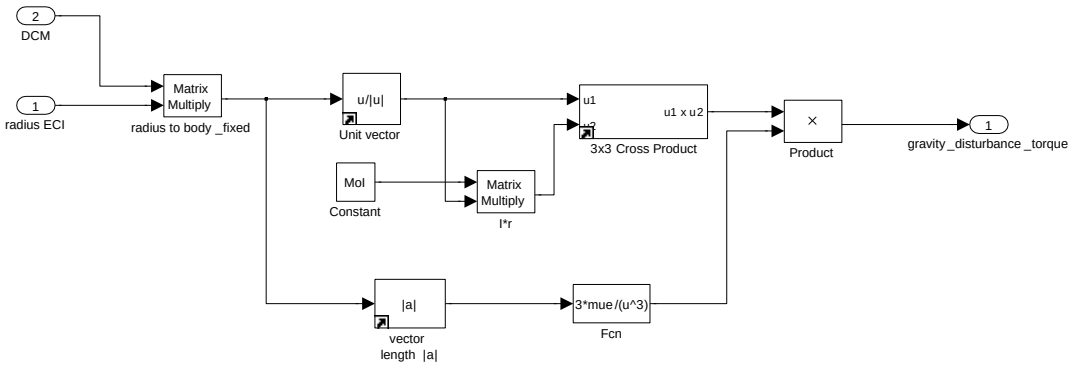

Figure 2.13: Implementation of gravity gradient disturbances

In a worst case scenario the gravity gradient disturbing torque of the AsteroidFinder/SSB was estimated to $\pm 10^{-6}$ Nm [16], which can be reflected by the equation above.

2.5.2 Magnetic Field

Another disturbing torque is the result of the interaction between the magnetic field of the Earth and the residual satellite's magnetic field. On the one hand this effect can be used to control

the attitude and on the other hand it is a disturbing torque which has to be addressed. The interaction formula itself is the same as equation 2.64.

$$\underline{T}^{bf} = \underline{D}^{bf} \times \underline{B}^{bf}_{Earth}$$

where $\underline{T}^{bf}_{mag}$ is the disturbing torque, $\underline{D}^{bf}$ is the residual magnetic dipolemoment of the satellite and $\underline{B}^{bf}_{Earth}$ indicates the magnetic field of the earth.

The calculation of the earth magnetic field vector is done by a precompiled routine that uses the data of the International Geomagnetic Reference Field (IGRF) this routine calculates the magnetic field vector in dependence to the position of the satellite and the actual date.

The IGRF is a available in the 10th generation which is implemented by a set of coefficients. Inside the routine the magnetic field is described with a spherical harmonic expansion. The mathematical background therefore is the same as it is used for the gravitational potential which was explained before.

An expected wost case magnetic torque for the AsteroidFinder/SSB mission is $4.5 \cdot 10^{-5}$ Nm [16] and can be simulated by the above equation.

2.5.3 Solar Radiation

The solar radiation is a another sort of disturbances that does not only generate a torque but a force too. This results of the interaction of the solar radiation with the surface of the satellite. Each surface which is hit by the solar radiation generates a force and a torque. To simulate this effect the satellite itself was split up into small triangles as seen in figure 2.14 and the force and torque for every visible segment is calculated. The calculation for one surface element *i* is

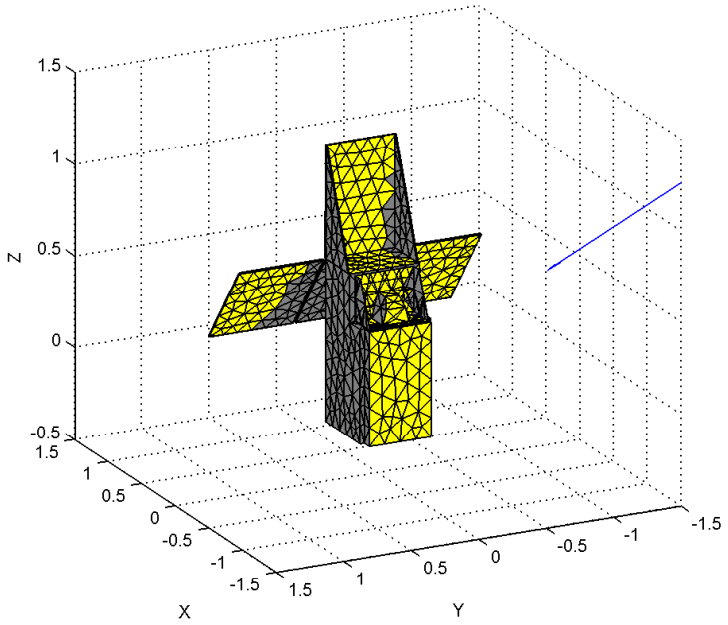

Figure 2.14: Illumination of the AsteroidFinder/SSB

described by [42]

$$\underline{F_i} = -P\left[(1-C_s)\underline{S}+2(C_s\cos\theta+\frac{1}{3}C_d)\underline{N}\right]\cos\theta\, A_i \tag{2.66}$$

where $\underline{F}$ is the acting force, P is the solar constant, $\underline{N}$ the surface normal unit vector and A_i the area of the element. The variables C_s is the spectral reflection coefficient while C_d is the diffuse reflection coefficient. These coefficient allow to define the material of the satellite. In the simplest simulation configuration these coefficients are equal for each surface element.

The overall force and torque of the solar radiation is therefor

$$\underline{F_{sol}} = \sum_{i=1}^{n}\underline{F_i} \tag{2.67}$$

$$\underline{T_{sol}} = \sum_{i=1}^{n}\underline{r_i}\times\underline{F_i} \tag{2.68}$$

where n defines the number of elements and $\underline{r_i}$ is the distance vector from the satellite's center of gravity to the surface center of the element.

Due to the fact that an online calculation of the solar radiation force and torque would consume much to much computing power a lookup table is precalculated.

Therefore the satellite model is observed from many different directions and the normed forces and torques are calculated. They are normed toward the solar constant P which leads the freedom of adjusting it to the proper solar activity without recalculating the look up table. For the simulation a small lookup table generation module was written in Matlab which can read a mesh file and generates a lookup table for different viewing directions. Between the different directions a linear interpolation scheme was implemented.

For the AsteroidFinder/SSB mission the worst case disturbance solar torque is expected to be $3.28\cdot10^{-6}$ Nm [16].

2.5.4 Atmosphere

The last relevant disturbance which will be simulated in the AsteroidFinder/SSB simulator is the aerodynamic force and torque. The characteristic of the aerodynamics can be treated in nearly the same way as it is done with the solar radiation [42].

Where the main formula of the surface force is adapted to

$$\underline{F_i} = -P\left[(1-C_s)\underline{V}+2(C_s\cos\theta+\frac{1}{3}C_d)\underline{N}\right]\cos\theta\, A_i \tag{2.69}$$

$$P = \frac{1}{2}\rho V^2\cdot C_D \tag{2.70}$$

$$C_s = 0 \tag{2.71}$$

$$C_d = 0 \tag{2.72}$$

and the solar pressure P is exchanged by the dynamic pressured including the drag coefficient C_D. The velocity of the satellite with respect to the atmosphere is described by V and the density of the atmosphere is indicated by ρ. By setting the coefficient C_s and C_d to zero the same module can be used to determine a lookup table for the aerodynamics as for the solar radiation.

In a straight forward manner the sum of all forces and torques can be found.

$$\underline{F}_{aero} = \sum_{i=1}^{n} \underline{F}_i \tag{2.73}$$

$$\underline{T}_{aero} = \sum_{i=1}^{n} \underline{r}_i \times \underline{F}_i \tag{2.74}$$

The worst case disturbance torque for AsteroidFinder/SSB was estimated to $6.33 \cdot 10^{-5}$ Nm [16] and is reflected inside this model in a sufficient way.

Chapter 3

Attitude Determination

This chapter describes the algorithm of attitude determination. The focus is placed on two different KALMAN filtering techniques. The extended KALMAN filter (EKF) and the unscented KALMAN filter (UKF) are compared.

3.1 Extended KALMAN Filter

One widely spread attitude estimator is an extended KALMAN filter (EKF). Originally it was developed during in the late 1950s by Rudolf Emil Kálmán a hungarian mathematician who was working at the Research Institute for Advanced Studies in Baltimore (United States). R. Kálmán provided in his paper [20] an approach to predict the behavior of a linear system in an optimal way by combining measurements with a linear system model and removing any white noise completely. The credit of R. Kálmán was the definition of a real time algorithm that allows the optimal prediction of linear system dynamics while including available measurements. His algorithm became popular through its use in NASA's Apollo program and is found today in many technical applications. Although R. Kálmán was only focusing on linear systems the filter was soon extended to nonlinear system which is done by a linearisation around a certain operation point. The following shall point out the main principals of the continues extended KALMAN filter which have to be understood to use such a filter inside a satellite system as an attitude estimator. For more details about KALMAN filtering the reader is referred to [10] and [31] where a broader range of filtering techniques is presented.

3.1.1 Algorithm

The EKF is starting with any nonlinear system dynamics of the form

$$\dot{\underline{x}} = f(\underline{x}(t),\underline{u}(t)) + \underline{w}(t) \tag{3.1}$$

$$\underline{z}_k = h(\underline{x}_k) + \underline{v}_k \tag{3.2}$$

where f is indicating the nonlinear system dynamics with the system state $\underline{x}$ and the control input $\underline{u}$. It is assumed that this function is corrupted by white noise $\underline{w}$. The measurements at

time step $_k$ are identified by $\underline{z}_k$ while h represents the nonlinear measurement dynamic. As well as the state the measurements are assumed to be corrupted by white noise $\underline{v}_k$.

The goal is now to estimate the state $\underline{x}_{k+1}$ in an optimal way. Therefore the knowledge of the old state $\underline{x}_k$ and the measurements $\underline{z}_{k+1}$ are used.

To understand the EKF algorithm consider a starting point $\underline{x}_0$ which has a covariance matrix $\underline{\underline{P}}$. The covariance matrix is representing the expected variance in the variable $\underline{x}$.

To optimal estimate the actual state at time step $k+1$ the EKF is first propagating the old state,

$$\hat{\underline{x}}_{k+1}^{-} = \int_{t_k}^{t_k+\Delta t} f(\hat{\underline{x}}_k, \underline{u}_k) dt \tag{3.3}$$

which can be done by a direct integration of the nonlinear system dynamics. The upper minus sign on the left side of the equations is indicating the propagation step while the ˆ indicates an estimation. After this propagation the expected measurement $\hat{\underline{z}}_{k+1}$ can be calculated directly.

$$\hat{\underline{z}}_{k+1} = h(\hat{\underline{x}}_{k+1}) \tag{3.4}$$

Due to the fact that the two equations 3.1 and 3.2 are nonlinear the next task is to linearise them around the new operating point $\hat{\underline{x}}_{k+1}^{-}$.

$$\underline{\underline{F}}(t) \approx \left.\frac{\partial f(\underline{x}, \underline{u})}{\partial \underline{x}}\right|_{\underline{x}=\hat{\underline{x}}(t)} \tag{3.5}$$

$$\underline{\underline{H}}_{k+1} \approx \left.\frac{\partial h(\underline{x})}{\partial \underline{x}}\right|_{\underline{x}=\hat{\underline{x}}_{k+1}^{-}} \tag{3.6}$$

This has to be done to apply them inside the EKF. In addition to the linearisation the system dynamic will be discretised to be able to be used in a real world system. This is achieved by the standard state transition matrix $\underline{\underline{\Phi}}$ [24].

$$\underline{\underline{\Phi}}_k = = \underline{\underline{\Phi}}(t_{k+1}, t_k) = e^{\underline{\underline{F}} \cdot (t_{k+1} - t_k)} = e^{\underline{\underline{F}} \cdot \Delta t} \tag{3.7}$$

which is used in the further development.

The next step in the EKF is to propagate the covariance matrix $\underline{\underline{P}}$ up to the desired time step.

$$\underline{\underline{P}}_{k+1}^{-} = \underline{\underline{\Phi}}_k \underline{\underline{P}}_k \underline{\underline{\Phi}}_k^{\,T} + \underline{\underline{Q}} \tag{3.8}$$

At this point another covariance matrix $\underline{\underline{Q}}$ is added to the propagation which reflects the uncertainties inside the system model. The covariance matrix $\underline{\underline{Q}}$ has to be defined by the user. After the system state covariance is propageted the KALMAN gain can be calculated

$$\underline{\underline{K}}_{k+1} = \underline{\underline{P}}_{k+1}^{-} \underline{\underline{H}}_{k+1} \left(\underline{\underline{H}}_{k+1} \underline{\underline{P}}_{k+1}^{-} \underline{\underline{H}}_{k+1}^{\,T} + \underline{\underline{R}} \right)^{-1} \tag{3.9}$$

which is named after R.E. Kálmán. The uncertainties of the measurements are incorporated inside the KALMAN gain by the addition of $\underline{\underline{R}}$. This is the covariance matrix of the measurements and has to be defined by the user. With the knowledge of the KALMAN gain the propagated state and covariance can be corrected which is indicated by the upper plus sign.

$$\underline{\hat{x}}_{k+1}^{+} = \underline{\hat{x}}_{k+1}^{-} + \underline{\underline{K}}_{k+1}\left(\underline{z}_{k+1} - \underline{\hat{z}}_{k+1}^{-}\right) \tag{3.10}$$

$$\underline{\underline{P}}_{k+1}^{+} = \left(\underline{\underline{I}} - \underline{\underline{K}}_{k+1}\,\underline{\underline{H}}_{k+1}\right)\underline{\underline{P}}_{k+1}^{-} \tag{3.11}$$

The equations 3.3 to 3.11 are forming the continues extended KALMAN filter which will be investigated as an attitude estimator. With this last equation the algorithm is closed and can be recalculated with the last estimates as the new starting values

$$\begin{aligned} \underline{\hat{x}}_k &\equiv \underline{\hat{x}}_{k+1}^{+} \\ \underline{\underline{P}}_k &\equiv \underline{\underline{P}}_{k+1}^{+} \end{aligned}$$

By applying this algorithm to a systems where new measurements are available at discrete times the EKF will estimated the system state in an optimal way regarding to white noise disturbances.

With the definition of the EKF there are three remaining parameters that are used to “tune” the filter. To adjust the steady state behavior of the filter the covariance matrices of the system $\underline{\underline{Q}}$ and of the measurements $\underline{\underline{R}}$ can be chosen. Normally both matrices are chosen to be diagonal which is equal to defining the variance of each system state and each measurement. The smaller one variance is the more the system model or the sensor is trusted inside the filter. By “tuning” $\underline{\underline{Q}}$ and $\underline{\underline{R}}$ the steady state performance of the EKF is adjusted.

The third remaining parameter is the covariance $\underline{\underline{P}}_0$ of the initial state this covariance is used to tune the settling time of the EKF. Where the main diagonal defines the variance of the initial system state.

When these parameters are chosen the filter is completed and can be initialised by an initial state $\underline{x}_0$

3.1.2 Implementation

For the implementation of the EKF it is necessary to choose a state vector $\underline{x}$ which describes the state of the satellite. A state vector of a satellite which can describe the dynamic around its center of gravity should include at least the actual attitude $\underline{q}$ and the angular rate $\underline{\omega}_{sat}$. During the development of the EKF it appeared to be useful to add a third component into the state vector which are the disturbance torques $\underline{T}_d$. Therefore the full state vector is defined as

$$\underline{x} = [q_1\ q_2\ q_3\ q_4\ \omega_{sat,x}\ \omega_{sat,y}\ \omega_{sat,z}\ T_{d,x}\ T_{d,y}\ T_{d,z}]^T \tag{3.12}$$

which will be used in the EKF. Regarding to the state vector the non linear system model $f(\underline{x})$ can be expressed with the standard attitude dynamics equations of chapter 2.2.

$$\begin{aligned} \dot{\underline{q}} &= \frac{1}{2}\,\underline{\underline{\Omega}}\,\underline{q} = \frac{1}{2}\underline{\omega}\otimes\underline{q} \\ \dot{\underline{\omega}}_{sat} &= \underline{\underline{I}}_{sat}^{-1}\left(\underline{T}_d - \underline{\omega}_{sat}\times\underline{L}_{sat} - \underline{\omega}_{sat}\times\underline{L}_{rw} - \dot{\underline{L}}_{rw}\right) \end{aligned}$$

It should be mentioned that the quaternion derivative can be written in terms of a quaternion multiplication if the angular rate is assumed as a four dimensional vector with a zero as fourth component. In addition to these equations the disturbance torque is assumed to be constant.

$$\dot{\underline{T}}_d = \underline{0} \tag{3.13}$$

This assumption is quite stringent and can only be made due to the reason that the disturbances are slowly varying and therefore nearly constant. Problems with this assumption could arise due to the fact that the disturbance torque is not independent from the attitude (e.g. aerodynamic drag). This could lead especially during maneuvers to a wrong attitude determination. Therefore the settling time of the KALMAN filter should be much shorter than the maneuver time.

The equations above are used for the nonlinear propagation part of the EKF but they are not used for the linearised attitude dynamics. Therefor an error state vector $\Delta\underline{x}$ will be used which estimates only the error of the state and not the full state. The idea of an error state vector estimation is presented in [35] and [2] and is adapted for this filter structure. After the error is estimated it is removed from the full state and the error is reset to zero for the next calculation loop. The error state vector will be defined as

$$\Delta\underline{x} = [\Delta\underline{q}\ \Delta\underline{\omega}_{sat}\ \Delta\underline{T}_d] \tag{3.14}$$

where

$$\underline{q} = \Delta\underline{q}\otimes\hat{\underline{q}} \tag{3.15}$$

$$\underline{\omega}_{sat} = \hat{\underline{\omega}}_{sat} + \Delta\underline{\omega}_{sat} \tag{3.16}$$

$$\underline{T}_d = \hat{\underline{T}}_d + \Delta\underline{T}_d \tag{3.17}$$

and $\Delta\underline{q}$ is near to $[0\ 0\ 0\ 1]^T$ while $\Delta\underline{\omega}$ and $\Delta\underline{T}_d$ are near to zero. The values $\hat{\underline{q}}$,$\hat{\underline{\omega}}_{sat}$ and $\hat{\underline{T}}_d$ are indicating the current propagated estimate.

By applying such a definition it has to be mentioned that the update of the quaternion part of the full state vector can not be done in the conventional way. The quaternion update has to be performed by a quaternion multiplication while the estimated errors are removed from the last full state vector.

$$\hat{\underline{q}}^{+} = \Delta\underline{q}^{-1}\otimes\hat{\underline{q}} \tag{3.18}$$

$$\hat{\underline{\omega}}_{sat}^{+} = \hat{\underline{\omega}}_{sat} - \Delta\underline{\omega}_{sat} \tag{3.19}$$

$$\hat{\underline{T}}_d^{+} = \hat{\underline{T}}_d - \Delta\underline{T}_d \tag{3.20}$$

The main task is now to find the Jacobian matrix $\underline{\underline{F}}$ for the nonlinear system dynamics of the error state vector. The starting point is the equation for the system dynamic of the error state vector.

$$\Delta\dot{\underline{x}} = f(\Delta\underline{x}) \tag{3.21}$$

This dynamic equation will be split up into the three parts quaternion, angular rate and disturbance torque. The first one is the dynamic of the error quaternion $\Delta\underline{q}$. To find the dynamics of the error quaternion the product rule is applied to equation 3.15.

$$\frac{d}{dt}\underline{q} = \frac{d}{dt}\Delta\underline{q}\otimes\hat{\underline{q}}+\Delta\underline{q}\otimes\frac{d}{dt}\hat{\underline{q}} \tag{3.22}$$

Inside this equation the single derivatives can be determined easily. Here all $\underline{\omega}$ are represented as a four dimensional vector with a zero in the fourth dimension.

$$\frac{1}{2}(\hat{\underline{\omega}}_{sat}+\Delta\underline{\omega}_{sat})\otimes\underline{q} = \Delta\dot{\underline{q}}\otimes\hat{\underline{q}}+\Delta\underline{q}\otimes\frac{1}{2}\hat{\underline{\omega}}_{sat}\otimes\hat{\underline{q}} \tag{3.23}$$

By invoking the definition of an inverse quaternion and the error quaternion

$$\hat{\underline{q}}\otimes\hat{\underline{q}}^{-1} = (0,0,0,1)^T \tag{3.24}$$

$$\Delta\underline{q} = \underline{q}\otimes\hat{\underline{q}}^{-1} \tag{3.25}$$

and rearranging equation 3.23 the dynamic of the error quaternion can be found [35], [2].

$$\Delta\dot{\underline{q}} = \frac{1}{2}\left[\hat{\underline{\omega}}_{sat}\otimes\Delta\underline{q}+\Delta\underline{\omega}_{sat}\otimes\Delta\underline{q}-\Delta\underline{q}\otimes\hat{\underline{\omega}}_{sat}\right] \tag{3.26}$$

Equation 3.26 is the full description of the error quaternion dynamics. Due to the fact that the error quaternion will be near the unit quaternion one more simplification is possible. At first the error quaternion will be reduced by one dimension. To carry out such a reduction the forth component of the full error quaternion is defined positive. This is a valid assumption due to the fact that each rotation can be described by a quaternion with a positive fourth component. Therefore the full fourth dimensional error quaternion $\Delta\underline{q}$ and its reduced three dimensional counterpart $\delta\underline{q}$ are described as

$$\Delta\underline{q} = [\delta q_1\ \delta q_2\ \delta q_3\ \sqrt{1-\delta q_1^2-\delta q_2^2-\delta q_3^2}]^T \tag{3.27}$$

$$\delta\underline{q} = [\delta q_1\ \delta q_2\ \delta q_3]^T \tag{3.28}$$

which leads to a reduced state vector. With this definition and the definition of the quaternion multiplication the dynamics of the reduced error quaternion $\delta\underline{q}$ can be written to [7]:

$$\delta\dot{\underline{q}} = \frac{1}{2}(-\Delta\underline{\omega}-2\hat{\underline{\omega}})\times\delta\underline{q}+\Delta\underline{\omega} \tag{3.29}$$

where $\underline{\omega}$ is now indicating the three dimensional angular rates. For the extended KALMAN filter a linearised version of this equation is needed. These version can be found in straight forward manner by calculating its derivatives.

$$\frac{\partial \delta \dot{\underline{q}}}{\partial \delta \underline{q}} = \frac{1}{2}\left[(-\Delta\underline{\omega}_{sat} - 2\hat{\underline{\omega}}_{sat})\times\right] \tag{3.30}$$

$$\frac{\partial \delta \dot{\underline{q}}}{\partial \Delta\underline{\omega}_{sat}} = \frac{1}{2}\left([\delta\underline{q}\times] + I_{3\times 3}\right) \tag{3.31}$$

$$\frac{\partial \delta \dot{\underline{q}}}{\partial \Delta\underline{T}_d} = 0_{3\times 3} \tag{3.32}$$

Now the error quaternion dynamic and the linearisation is fully described. In a next step the error angular rate will be investigated. Recalling the attitude dynamics the angular rate dynamics without reaction wheels is written as:

$$\dot{\underline{\omega}}_{sat} = \underline{\underline{I}}_{sat}^{-1}\left[\underline{T}_d - \underline{\omega}_{sat}\times\underline{\underline{I}}_{sat}\,\underline{\omega}_{sat}\right] \tag{3.33}$$

With substituting the definition 3.16 of the angular rate inside equation 3.33 it can be rearranged. In the following the index $_{sat}$ is skipped due to better readability.

$$\begin{aligned}
\dot{\underline{\omega}} &= \underline{\underline{I}}^{-1}\left[\underline{T}_d + \Delta\underline{T}_d - (\hat{\underline{\omega}} + \Delta\underline{\omega})\times\underline{\underline{I}}\,(\hat{\underline{\omega}} + \Delta\underline{\omega})\right] \\
&= \underline{\underline{I}}^{-1}\left[\underline{T}_d + \Delta\underline{T}_d - \hat{\underline{\omega}}\times\underline{\underline{I}}\,\hat{\underline{\omega}} - \hat{\underline{\omega}}\times\underline{\underline{I}}\,\Delta\underline{\omega} - \Delta\underline{\omega}\times\underline{\underline{I}}\hat{\underline{\omega}} - \Delta\underline{\omega}\times\underline{\underline{I}}\Delta\underline{\omega}\right] \\
&= \underline{\underline{I}}^{-1}\left[\underline{T}_d - \hat{\underline{\omega}}\times\underline{\underline{I}}\,\hat{\underline{\omega}}\right] + \dots \\
&\quad \dots\underline{\underline{I}}^{-1}\left[\Delta\underline{T}_d - \hat{\underline{\omega}}\times\underline{\underline{I}}\,\Delta\underline{\omega} - \Delta\underline{\omega}\times\underline{\underline{I}}\hat{\underline{\omega}} - \Delta\underline{\omega}\times\underline{\underline{I}}\Delta\underline{\omega}\right]
\end{aligned} \tag{3.34}$$

It is obvious that the first term of the right hand side represents the dynamics of the real angular rate. Therefore the second term has to be the dynamic of the error angular rate [35].

$$\Delta\dot{\underline{\omega}} = \underline{\underline{I}}^{-1}\left[\Delta\underline{T}_d - \underline{\omega}\times\underline{\underline{I}}\,\Delta\underline{\omega} - \Delta\underline{\omega}\times\underline{\underline{I}}\underline{\omega} - \Delta\underline{\omega}\times\underline{\underline{I}}\Delta\underline{\omega}\right] \tag{3.35}$$

The previous equations show that it is simple to find the the angular rate dynamic. The full version of the error angular rate dynamic including reaction wheels can be found in the same way by adding the reaction wheel part.

$$\Delta\dot{\underline{\omega}} = \underline{\underline{I}}^{-1}\left[\Delta\underline{T}_d - \underline{\omega}\times\underline{\underline{I}}\,\Delta\underline{\omega} - \Delta\underline{\omega}\times\underline{\underline{I}}\underline{\omega} - \Delta\underline{\omega}\times\underline{\underline{I}}\Delta\underline{\omega} - \Delta\underline{\omega}\times\underline{L}_{rw}\right] \tag{3.36}$$

Once again the linearised version of the equation has to be determined. Which leads to.

$$\frac{\partial \Delta\dot{\underline{\omega}}}{\partial \delta \underline{q}} = 0_{3\times 3} \tag{3.37}$$

$$\frac{\partial \Delta\dot{\underline{\omega}}}{\partial \Delta\underline{\omega}} = \underline{\underline{I}}^{-1}\left(-[\underline{\omega}\times]\underline{\underline{I}} + [\underline{\underline{I}}\underline{\omega}\times] - [\Delta\underline{\omega}\times]\underline{\underline{I}} + [\underline{\underline{I}}\Delta\underline{\omega}\times] + [\underline{L}_{rw}\times]\right) \tag{3.38}$$

$$\frac{\partial \Delta\dot{\underline{\omega}}}{\partial \Delta\underline{T}_d} = \underline{\underline{I}}^{-1} \tag{3.39}$$

Now the remaining part is the linearised dynamic of the disturbance torques which has a quite trivial solution.

$$\frac{\partial \Delta \dot{\underline{T}}_d}{\partial \delta \underline{q}} = 0_{3\times 3} \tag{3.40}$$

$$\frac{\partial \Delta \dot{\underline{T}}_d}{\partial \Delta \underline{\omega}} = 0_{3\times 3} \tag{3.41}$$

$$\frac{\partial \Delta \dot{\underline{T}}_d}{\partial \Delta \underline{T}_d} = I_{3\times 3} \tag{3.42}$$

Now the linearised state error vector dynamics are fully specified and can be used in the extended KALMAN filter.

$$\underline{\underline{F}} = \begin{pmatrix} \frac{\partial \delta \dot{\underline{q}}}{\partial \delta \underline{q}} & \frac{\partial \delta \dot{\underline{q}}}{\partial \Delta \underline{\omega}} & \frac{\partial \delta \dot{\underline{q}}}{\partial \Delta \underline{T}_d} \\ \frac{\partial \Delta \dot{\underline{\omega}}}{\partial \delta \underline{q}} & \frac{\partial \Delta \dot{\underline{\omega}}}{\partial \Delta \underline{\omega}} & \frac{\partial \Delta \dot{\underline{\omega}}}{\partial \Delta \underline{T}_d} \\ \frac{\partial \Delta \dot{\underline{T}}_d}{\partial \delta \underline{q}} & \frac{\partial \Delta \dot{\underline{T}}_d}{\partial \Delta \underline{\omega}} & \frac{\partial \Delta \dot{\underline{T}}_d}{\partial \Delta \underline{T}_d} \end{pmatrix} \tag{3.43}$$

In addition to the system dynamics the measurement dynamics have to be defined. For a first analysis of the AsteroidFinder mission only the star camera $_{st}$ and the gyroscopes $_{gyro}$ will be taken into account. Where the star camera is able to deliver an attitude quaternion and an angular rate. This will lead to a quite simple but for the further comparison sufficient measurement equations.

$$\begin{aligned} \underline{z} &= h(\underline{x}) \\ h_{st,q}(\underline{x}) &= \underline{q} \\ h_{st,\omega}(\underline{x}) &= \underline{\omega} \\ h_{gyro}(\underline{x}) &= \underline{\omega} \end{aligned}$$

Therefor the measurement model h is simply defined.

$$h(\underline{x}) = \begin{bmatrix} \underline{q} \\ \underline{\omega} \\ \underline{\omega} \end{bmatrix} \tag{3.44}$$

To be able to propagate the covariance in a correct way the measurement equations have to be linearised too.

$$\underline{\underline{H}} = \frac{\partial h}{\partial \delta x} \tag{3.45}$$

$$= \begin{bmatrix} \frac{\partial \underline{q}}{\partial \delta \underline{q}} & \frac{\partial \underline{q}}{\partial \Delta \underline{\omega}} & \frac{\partial \underline{q}}{\partial \Delta \underline{T}_d} \\ \frac{\partial \underline{\omega}}{\partial \Delta \underline{\omega}} & \frac{\partial \underline{\omega}}{\partial \Delta \underline{\omega}} & \frac{\partial \underline{\omega}}{\partial \Delta \underline{T}_d} \\ \frac{\partial \underline{\omega}}{\partial \Delta \underline{\omega}} & \frac{\partial \underline{\omega}}{\partial \Delta \underline{\omega}} & \frac{\partial \underline{\omega}}{\partial \Delta \underline{T}_d} \end{bmatrix} \tag{3.46}$$

This linearisation itself simplifies into the two different parts of the quaternion and the angular rate. The quaternion part can be obtained to

$$\frac{\partial \underline{q}}{\partial \delta \underline{q}} = \frac{1}{2}\left([\underline{q}_{123}\times]; -q_1 \; -q_2 \; -q_3\right) \tag{3.47}$$

$$\frac{\partial \underline{q}}{\partial \Delta \underline{\omega}} = 0_{4\times 3} \tag{3.48}$$

$$\frac{\partial \underline{q}}{\partial \Delta \underline{T}_d} = 0_{4\times 3} \tag{3.49}$$

and the angular rate part to

$$\frac{\partial \underline{\omega}}{\partial \delta \underline{q}} = 0_{3\times 3} \tag{3.50}$$

$$\frac{\partial \underline{\omega}}{\partial \Delta \underline{\omega}} = I_{3\times 3} \tag{3.51}$$

$$\frac{\partial \underline{\omega}}{\partial \Delta \underline{T}_d} = 0_{3\times 3} \tag{3.52}$$

The angular rate part has to be used twice one time for the star camera and another time for the gyroscope.

3.1.3 Tests

To verify the previous developed EKF it will be tested beside an ideal control loop. Therefore the actuators are assumed as ideal with no errors and the deviation which drives the control input is calculated from perfect measurements. Beside this control loop the EKF is loaded with the real measurements and its performance is investigated. This procedure allows the EKF verification without having interferences to the attitude controller.

To test the EKF the remaining free parameters of have to be chosen. These are the full initial state $\underline{x}_0$, the initial covariance $\underline{\underline{P}}_0$ of the reduced error state, the system covariance $\underline{\underline{Q}}$ of the reduced error dynamics and the measurement covariance $\underline{\underline{R}}$.

For further comparison the initial state is initialised by the real value this allows to focus only on the steady state performance of the EKF, which is the relevant performance criteria. The covariance matrices are all chosen to have a diagonal form which assumes a linear independence between the different states and measurements [10]. The diagonal elements are chosen to incorporate the standard deviation σ of each state. Therefore the initial system state covariance is chosen to be

$$\underline{\underline{P}}_0 = \begin{bmatrix} I_{[3\times 3]}\sigma^2_{\delta q_0} & 0 & 0 \\ 0 & I_{[3\times 3]}\sigma^2_{\Delta \omega_0} & 0 \\ 0 & 0 & I_{[3\times 3]}\sigma^2_{\Delta T_{d,0}} \end{bmatrix} \tag{3.53}$$

with the squared standard deviation (variance) on its main diagonal. Here the initial standard deviations are simple assumed to

$$\sigma_{\delta q_0} = 10 \tag{3.54}$$
$$\sigma_{\Delta\omega_0} = 10 \tag{3.55}$$
$$\sigma_{\Delta T_{d,0}} = 10 \tag{3.56}$$

which allows the filter to convergent fast enough to a steady state.

For the fist test the system and measurement covariances are set to the same values on its main diagonals elements.

$$\underline{\underline{Q}} = \begin{bmatrix} I_{[3\times3]}\sigma^2_{\delta q} & 0 & 0 \\ 0 & I_{[3\times3]}\sigma^2_{\Delta\omega} & 0 \\ 0 & 0 & I_{[3\times3]}\sigma^2_{\Delta T_d} \end{bmatrix} \tag{3.57}$$
$$\sigma_{\delta q} = 0.1 \tag{3.58}$$
$$\sigma_{\Delta\omega} = 0.1 \tag{3.59}$$
$$\sigma_{\Delta T_d} = 0.1 \tag{3.60}$$

$$\underline{\underline{R}} = \begin{bmatrix} I_{[4\times3]}\sigma^2_{q_{st}} & 0 & 0 \\ 0 & I_{[3\times3]}\sigma^2_{\omega_{st}} & 0 \\ 0 & 0 & I_{[3\times3]}\sigma^2_{\omega_{gyro}} \end{bmatrix} \tag{3.61}$$
$$\sigma_{q_{st}} = 0.1 \tag{3.62}$$
$$\sigma_{\omega_{st}} = 0.1 \tag{3.63}$$
$$\sigma_{\omega_{gyro}} = 0.1 \tag{3.64}$$

This parameter set is referred as the “untuned” case. To test the actual EKF performance the measurements were simulated with disturbances. Figure 3.1 shows the performance results of the EKF for the untuned case. The x-axis identifies the time in seconds while the upper diagram shows the angular deviation and the lower diagram the angular rate deviation from the real values. The angular deviation is extracted from the deviation between the real and the measured quaternion which is done by a quaternion multiplication. This error quaternion is transformed to an EULER angle set Ψ,Θ,Φ an plotted in the upper diagram in arcseconds. This error representation allows a direct comparison to the requirements of chapter 1.2 which were given in arc seconds. The requirements itself are plotted as the horizontal lines that equals the 3σ values of them.

It is obvious that only the angular rate requirement is the driving one due to the fact that the angular deviation requirement with 10 and 12 arc seconds is already reached in the untuned case.

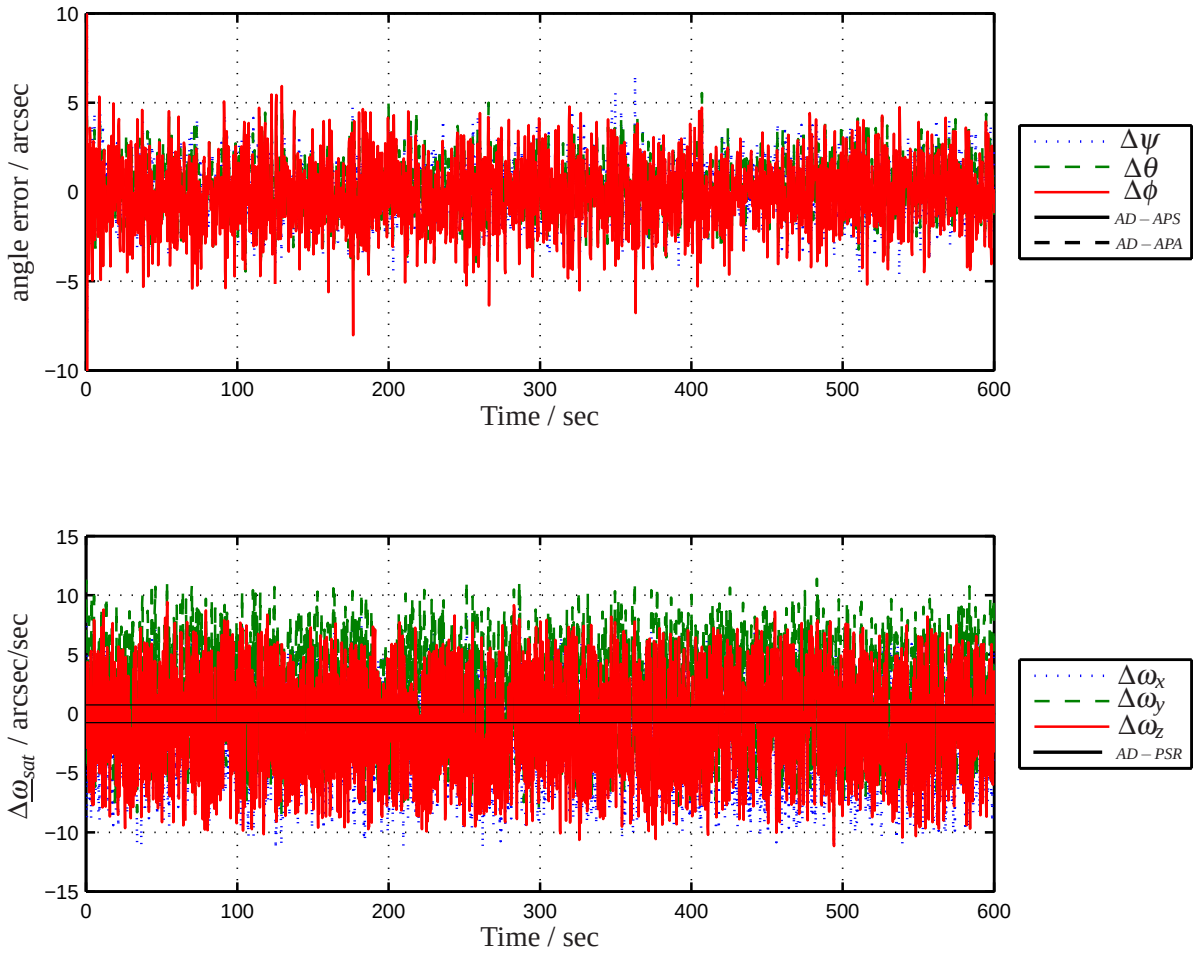

Figure 3.1: Performance of the untuned extended KALMAN filter

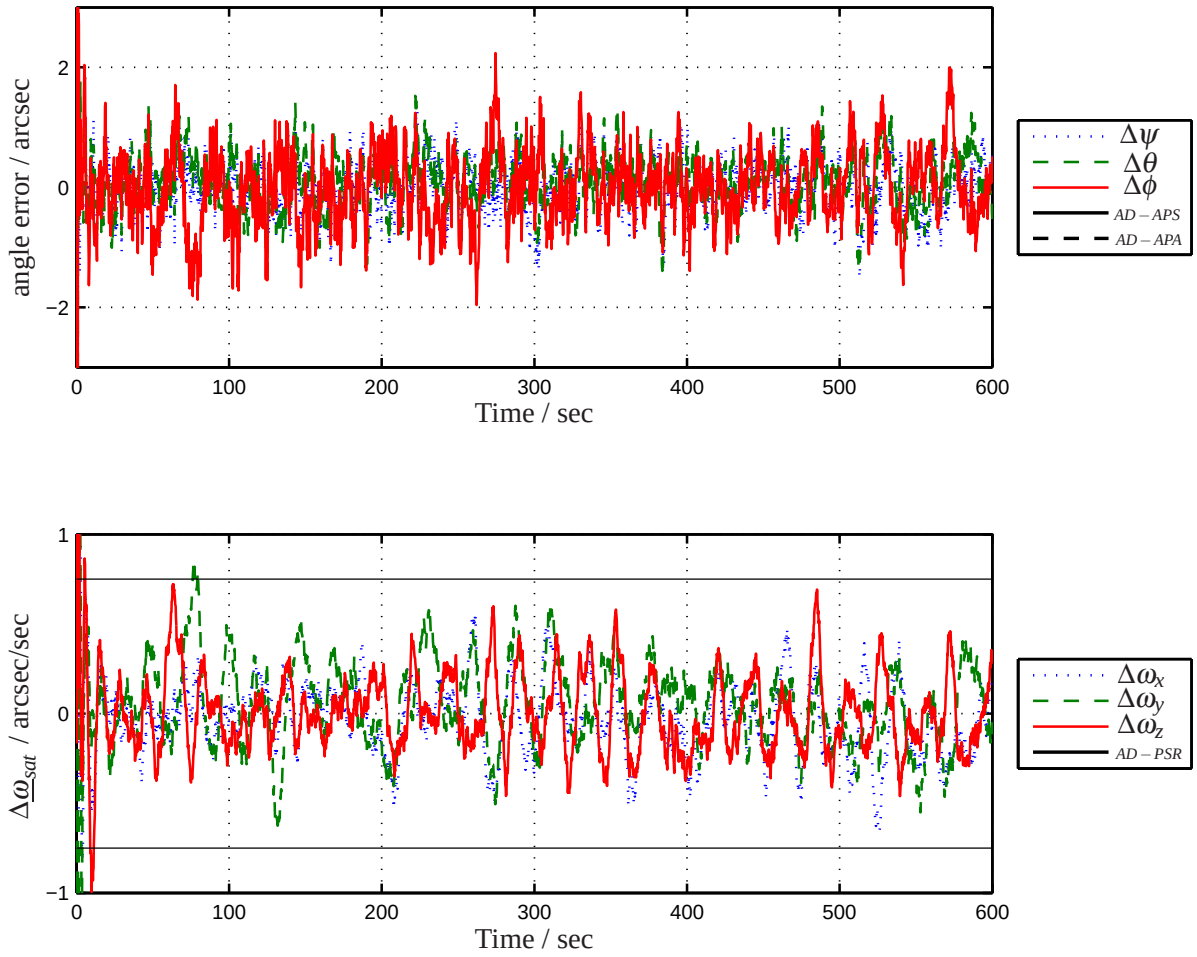

Figure 3.2: Performance of the tuned extended KALMAN filter

To be able to reach the angular rate requirement the filter has to be tuned. This tuning is done by adjusting the covariance matrices of the system and the measurement. After some simulation runs the system standard deviation

$$\sigma_{\delta q} = 1 \cdot 10^{-4} \tag{3.65}$$

$$\sigma_{\Delta\omega} = 1 \cdot 10^{-5} \tag{3.66}$$

$$\sigma_{\Delta T_d} = 1 \cdot 10^{-4} \tag{3.67}$$

and the measurement standard deviation

$$\sigma_{q_{st}} = 1 \cdot 10^{-3} \tag{3.68}$$

$$\sigma_{\omega_{st}} = 1 \cdot 10^{-3} \tag{3.69}$$

$$\sigma_{\omega_{gyro}} = 1 \cdot 10^{-2} \tag{3.70}$$

where chosen. The results of these tuning parameter set is shown in figure 3.2. Here it can be seen that the performance of the EKF is significantly improved. In the tuned case the EKF is

able to remove the white noise from the system state and the sensor measurements. Therefore it allows a precise attitude determination. The required error angle is reached which is not surprising but in addition to this the angular rate deviation is lowered significantly. The problem is still that it does not fulfill completely the requirement although it is tuned in a good way. During simulation there was no tuning configuration found that was able to fulfill the requirement without any violation. Therefore another attitude determination algorithm was investigated.

3.2 Unscented KALMAN Filter

The unscented KALMAN filter (UKF) is a relative new approach to overcome some of the disadvantages of the extended KALMAN filter. It was developed during the 1990s by Simon J. Julier and Jeffrey K. Uhlmann and is based on the unscented transformation (UT). The unscented transformation allows to calculated the mean and covariance of a variable which is connected to another variable through a nonlinear function. The idea behind unscented transformation is that it is easier to approximate a probability distribution than it is to approximate an arbitrary nonlinear function. The following section will summarize the framework which is needed to understand and to use an unscented KALMAN filter. For detailed mathematical proofs of the equations the reader is referred to [17], [18] and [19] which is the original work referred to UKF development. As secondary literature [38], [40], [39] and [10] gives some good introduction.

3.2.1 The Scaled Unscented Transformation

The basis for every UKF is the unscented transformation. The idea behind such a transformation is to propagate means and covariance matrices of a random variable $\underline{y}$ which is related to another random variable $\underline{x}$ with known mean and covariance through a nonlinear function $f(\underline{x})$.

$$\underline{y} = f(\underline{x}) \tag{3.71}$$

The standard procedure to calculate such a propagation is the Monte Carlo method [5]. With that method a certain amount of samples for $\underline{x}$ is chosen and propagated to get many distributed values for $\underline{y}$. In the literature each sample of $\underline{x}$ is called a particle or sigma point. If there are enough values for $\underline{y}$, its mean and covariance can be calculated. The disadvantage of the Monte Carlo method is the large amount of propagations that have to be performed to get adequate results for the statistics of $\underline{y}$.

The unscented transformation tries to reduce the amount of sigma points to a minimum without loosing any information of the nonlinear propagation. Right now there are existing three different unscented transformations which allow some freedom in tailoring the UT to an application. These three UTs are called Simplex UT, Symmetric UT and Scaled UT.

In the following the Scaled UT will be described in more detail because it leaves the most degree of freedom to adjust the UT to any application. The Simplex UT and Symmetric UT are simplified versions of the Scaled UT and will not be considered any more in this diploma thesis.

The Scaled UT begins with the choice of sigma points $\underline{\chi}$ that are related to the random variable $\underline{x}$ with respect to its mean $\underline{\bar{x}}$ and covariance $\underline{\underline{P}}_{xx}$.

$$\underline{\chi}_0 = \underline{x} \tag{3.72}$$

$$\underline{\chi}_i = \underline{x} + \sqrt{n+\lambda}\,\underline{c}_i \tag{3.73}$$

$$\underline{\chi}_{n+i} = \underline{x} - \sqrt{n+\lambda}\,\underline{c}_i \tag{3.74}$$

with

$$\begin{aligned} i &= 1 \ldots n \\ \underline{\underline{G}} &= \sqrt{\underline{\underline{P}}_{xx}} \end{aligned} \tag{3.75}$$

Where n is the dimension of $\underline{x}$, $\underline{c}_i$ is the ith column of $\underline{\underline{G}}$ and λ is a scaling parameter. The calculation of the matrix square root of $\underline{\underline{P}}_{xx}$ is done by a Cholesky decomposition [5] where $\underline{\underline{P}}_{xx} = \underline{\underline{G}}\,\underline{\underline{G}}^T$ and $\underline{\underline{G}}$ is a lower triangle matrix. The choice of such a sigma point set ensures that the covariance and the mean of $\underline{x}$ is identical to the mean and covariance of the sigma points.

In addition to the choice of a sigma point set the weights W for mean (^{m}) and covariance (^{c}) of the propagated random variable $\underline{y}$ have to be chosen. They are chosen as

$$W_0^m = \frac{\lambda}{n+\lambda} \tag{3.76}$$

$$W_0^c = \frac{\lambda}{n+\lambda} + 1 - \alpha^2 + \beta \tag{3.77}$$

$$W_i^m = W_i^c = \frac{1}{2(n+\lambda)} \tag{3.78}$$

$$W_{n+i}^m = W_{n+i}^c = \frac{1}{2(n+\lambda)} \tag{3.79}$$

with

$$\begin{aligned} i &= 1 \ldots n \\ \lambda &= \alpha^2(n+\kappa) - n \\ &= \alpha^2\kappa + (\alpha^2 - 1)n \end{aligned} \tag{3.80}$$

Here α,β and κ are scaling parameters which allow some adjustments in the transformation. Their effects will be described later. The next step of the UT is to propagate each sigma point $\underline{\chi}$ with the nonlinear function f.

$$\underline{y}_i = f(\underline{\chi}_i)$$

with

$$i = 0 \ldots 2n$$

After the propagation is performed the mean $\underline{\overline{y}}$ and covariance $\underline{\underline{\overline{P}}}_{yy}$ can be calculated and the UT is completed.

$$\underline{\overline{y}} = \sum_{i=0}^{2n} W_i^m \underline{y}_i \tag{3.81}$$

$$\underline{\underline{\overline{P}}}_{yy} = \sum_{i=0}^{2n} W_i^c \left(\underline{y}_i - \underline{\overline{y}}\right)\left(\underline{y}_i - \underline{\overline{y}}\right)^T \tag{3.82}$$

The Scaled UT incorporates three scaling parameters α,β and κ which allow some tailoring down to a specific application. Their different effects shall be explained in the following.

- α: It defines the spread of the sigma points regarding to the Symmetric UT ($\alpha = 1$). If $\alpha < 1$ the sigma points are moved toward the original values of $\underline{x}$ and the influence of nonlinearities beyond second order in $f(\underline{x})$ for the approximation of $\underline{\overline{y}}$ and $\underline{\underline{\overline{P}}}_{yy}$ is reduced. If $\alpha > 1$ the influence of nonlinearities is more covered. Nonlinearities up to the second order are covered for any α value by the unscented transformation. A negative value of α does not make any sense due to the fact that only the squared value is taken into account.
- β: This parameter is used to create two different weights W_0. One for the calculation of the mean $\underline{\overline{y}}$ and another for the calculation of the covariance $\underline{\underline{\overline{P}}}_{yy}$. If no prior knowledge of $f(\underline{x})$ is available choose $\beta = 2$. This will assume a Gaussian distribution of the transformed $\underline{y}$ values.
- κ: The last scaling parameter is used to apply a different weight on the zeroth point while calculating $\underline{\overline{y}}$ and $\underline{\underline{\overline{P}}}_{yy}$. When $\kappa = 0$ the sigma point $\underline{\chi}_0$ is effectively omitted otherwise it is taken into account.κ can be seen as a "fine tuning" value to incorporate a "trust" level for the original $\underline{x}$ value. For example if $\kappa = 0.5$ the zeroth point is weighted equal to the other sigma points and if $\kappa = 2$ the zeroth point gets twice the weight as the other sigma points. Negative values of κ are not advised due to the fact that the positive definiteness of the resulting covariance matrix $\underline{\underline{\overline{P}}}_{yy}$ cannot be guaranteed, which could lead to numerical problems during the UKF algorithm.

3.2.2 Algorithm

The combination of the unscented transformation with the KALMAN filter algorithm is known as the unscented KALMAN filter (UKF). The following section describes the procedure of applying the UT to the KALMAN filter.

The starting point is the same as it is for the EKF. There is the state vector $\underline{x}$, the nonlinear system model $f(\underline{x})$ and the measurement model equation $h(\underline{x})$.

For the initialisation of the filter an initial state estimate $\underline{\hat{x}}_0$, its initial covariance $\underline{\underline{P}}_0^{xx}$, the covariances of the model $\underline{\underline{Q}}$ and the measurements $\underline{\underline{R}}$ have to be chosen. This is fully identical with the EKF. The index $()^{xx}$ is moved to the top due to better readability and shall be equal to $()_{xx}$ which is used in the previous chapters.

In addition to the EKF the three scaling parameters α,β, and κ have to be chosen. As a starting point the choice of

$$\begin{aligned} \alpha &= 1 \\ \beta &= 2 \\ \kappa &= 0 \end{aligned}$$

is a good assumption.

After defining these initial conditions the sigma point set for the state vector can be calculated. Regarding to equation 3.72 till 3.73 these sigma points are:

$$\underline{\hat{\chi}}_{k,0}^{+} = \underline{\hat{x}}_k^{+} \tag{3.83}$$

$$\underline{\hat{\chi}}_{k,i}^{+} = \underline{\hat{x}}_k^{+} + \sqrt{n+\lambda}\, c_i \tag{3.84}$$

$$\underline{\hat{\chi}}_{k,n+i}^{+} = \underline{\hat{x}}_k^{+} - \sqrt{n+\lambda}\, c_i \tag{3.85}$$

with

$$i = 1 \ldots n \tag{3.86}$$

$$c = \sqrt{\underline{\underline{P}}_k^{+,xx}} \tag{3.87}$$

Where k is indicating the time steps and $k = 0$ would be the initial condition. The $()^{+}$ indicates the last updated state estimation.

In the next step of the UKF the weights for the propagated mean and covariance are calculated. This is done via the equations 3.76 to 3.79. It should be mentioned that the weight calculation just have to be performed once if there is no explicit knowledge of the functions f and h. Otherwise there should be two independent weight calculation to include as much knowledge as possible of the process and the measurement equation.

After the weights are calculated the sigma points can be propagated up to the next time step with the nonlinear process model function f.

$$\underline{\hat{\chi}}_{k+1,i}^{-} = f(\underline{\hat{\chi}}_{k,i}^{+}) \tag{3.88}$$

The $()^{-}$ indicates the estimated predicted values of the KALMAN filter without the correction update.

Regarding to equation 3.81 and 3.82 the mean and the covariance of the propagated state vector can be calculated.

$$\underline{\hat{x}}^{-}_{k+1} = \sum_{i=0}^{2L} W_i^m \underline{\hat{\chi}}^{-}_{k+1,i} \tag{3.89}$$

$$\underline{\underline{P}}^{-,xx}_{k+1} = \sum_{i=0}^{2L} W_i^c \left(\underline{\hat{\chi}}^{-}_{k+1,i} - \underline{\hat{x}}^{-}_{k+1}\right)\left(\underline{\hat{\chi}}^{-}_{k+1,i} - \underline{\hat{x}}^{-}_{k+1}\right)^T + \underline{\underline{Q}} \tag{3.90}$$

During this calculation the uncertainties of the model are included into the UKF by the addition of $\underline{\underline{Q}}$.

Now a set of predicted sigma points is available which have to be transformed to a set of measurement points $\underline{\hat{\zeta}}^{-}_{k+1,i}$ to be able to calculate the expected mean and covariance of the measurements. From the mathematical point of view this is the same procedure as above but with different functions and variables which leads to the measurements equation.

$$\underline{\hat{\zeta}}^{-}_{k+1,i} = h(\underline{\hat{\chi}}^{-}_{k+1,i}) \tag{3.91}$$

The predicted mean and and covariance of the expected measurements is calculated as

$$\underline{\hat{z}}^{-}_{k+1} = \sum_{i=0}^{2L} W_i^m \underline{\hat{\zeta}}^{-}_{k+1,i} \tag{3.92}$$

$$\underline{\underline{P}}^{-,zz}_{k+1} = \sum_{i=0}^{2L} W_i^c \left(\underline{\hat{\zeta}}^{-}_{k+1,i} - \underline{\hat{z}}^{-}_{k+1}\right)\left(\underline{\hat{\zeta}}^{-}_{k+1,i} - \underline{\hat{z}}^{-}_{k+1}\right)^T + \underline{\underline{R}} \tag{3.93}$$

where the uncertainties of the measurement model are included by the addition of $\underline{\underline{R}}$.

For the actual calculation of the KALMAN gain another covariance has to be known. This is the cross covariance between the predicted state and the expected measurements. This cross covariance an be easily calculated.

$$\underline{\underline{P}}^{-,xz}_{k+1} = \sum_{i=0}^{2L} W_i^c \left(\underline{\hat{\chi}}^{-}_{k+1,i} - \underline{\hat{x}}^{-}_{k+1}\right)\left(\underline{\hat{\zeta}}^{-}_{k+1,i} - \underline{\hat{z}}^{-}_{k+1}\right)^T \tag{3.94}$$

After the cross covariance is known the KALMAN gain can be obtained.

$$\underline{\underline{K}}_{k+1} = \underline{\underline{P}}^{-,xz}_{k+1}\left(\underline{\underline{P}}^{-,zz}_{k+1}\right)^{-1} \tag{3.95}$$

The next steps equals the procedure of the EKF. At first the innovation $\underline{\nu}_{k+1}$ is calculated which relates the real measurements $\underline{z}_{k+1}$ to the expected ones $\underline{\hat{z}}^{-}_{k+1}$.

$$\underline{\nu}_{k+1} = \underline{z}_{k+1} - \underline{\hat{z}}^{-}_{k+1} \tag{3.96}$$

In the last correction step the estimated state and its covariance is updated as it is done in the EKF.

$$\underline{\hat{x}}^{+}_{k+1} = \underline{\hat{x}}^{-}_{k+1} + \underline{\underline{K}}_{k+1}\underline{\nu}_{k+1} \tag{3.97}$$

$$\underline{\underline{P}}^{+,xx}_{k+1} = \underline{\underline{P}}^{-,xx}_{k+1} - \underline{\underline{K}}_{k+1}\underline{\underline{P}}^{-,zz}_{k+1}\underline{\underline{K}}^{T}_{k+1} \tag{3.98}$$

With the last updates the loop is closed and the calculation can start again.

3.2.3 Implementation

To implement an UKF it is important to chose a state vector which is suitable for the UKF algorithm. The desired state information regarding to attitude control is the same as it is used for the EKF algorithm. This results in the same full state vector for the UKF and EKF implementation which was defined in equation 3.12.

$$\underline{x} = [q_1\ q_2\ q_3\ q_4\ \omega_{sat,x}\ \omega_{sat,y}\ \omega_{sat,z}\ T_{d,x}\ T_{d,y}\ T_{d,z}]^T$$

Due to the properties of the UKF algorithm and quaternion algebra it is not possible to use this state vector directly. This can be show by a simple example. Consider two quaternions $\underline{q}_A$ and $\underline{q}_B$ which describe the same rotation.

$$\underline{q}_A = (0\ 0.5\ 0\ 0.5)^T$$
$$\underline{q}_B = (0\ -0.5\ 0\ -0.5)^T$$

A problem in the UKF formulation is that an "average" state vector is calculated (see equation 3.81). This average is calculated by getting the weighted summing of all different state vectors. Consider for the example a weight of $\frac{1}{2}$ due to two quaternions. The problem is that the quaternions can not be averaged in this way because it would lead to the following result off $\underline{q}_C$.

$$\underline{q}_C = \frac{\underline{q}_A + \underline{q}_B}{2}$$
$$= (0\ 0\ 0\ 0)^T$$

This calculation is obviously wrong cause the right solution would be either directly $\underline{q}_A$ or $\underline{q}_B$. The origin of this problem is the definition of quaternion algebra which can not be combined without a modification to the UKF algorithm.

To solve this problem the UKF algorithm will use as well as the EKF an reduced error state vector $\delta\underline{x}$ which is going to be estimated. In difference to the EKF the UKF does not require

any linearisation and can use equation 3.26 and 3.36 directly. With the disturbance dynamic the following three equations are relevant for the UKF.

$$\begin{aligned}
\Delta\dot{\underline{q}} &= \frac{1}{2}\left[\hat{\underline{\omega}}_{sat} \otimes \Delta\underline{q} + \Delta\underline{\omega}_{sat} \otimes \Delta\underline{q} - \Delta\underline{q} \otimes \hat{\underline{\omega}}_{sat}\right] \\
\Delta\dot{\underline{\omega}} &= \underline{\underline{I}}^{-1}\left[\Delta\underline{T}_d - \underline{\omega} \times \underline{\underline{I}}\,\Delta\underline{\omega} - \Delta\underline{\omega} \times \underline{\underline{I}}\underline{\omega} - \Delta\underline{\omega} \times \underline{\underline{I}}\Delta\underline{\omega} - \Delta\underline{\omega} \times \underline{L}_{rw}\right] \\
\Delta\dot{\underline{T}}_d &= 0
\end{aligned}$$

For the internal propagation scheme the full error quaternion is used while the mean is calculated with the reduced error quaternion $\delta\underline{q}$. The propagation of the system dynamics is solved by direct integration which is equal to equation 3.3 in the EKF formulation.

In addition to the system dynamic the measurement equation 3.44 can be used directly. Although the UKF is calculating an average for the measurements and therefore a quaternion average is calculated in the wrong way this measurement model was recognized to be sufficient enough.

$$h(\underline{x}) = \begin{bmatrix} \underline{q} \\ \underline{\omega} \\ \underline{\omega} \end{bmatrix}$$

3.2.4 Tests

For the UKF test the same parameters have to be chosen as it is done for the EKF. To compare them the values for the untuned were chosen equal to the untuned EKF parameters.

Figure 3.3 shows the performance of the untuned unscented KALMAN filter. The x-axis is indicating the time and while the upper diagram is the angle deviation and the lower diagramm the angular rate deviation. This diagram is prepared in the same way as it was done for the EKF.

It can be seen that the UKF is already able to fulfill the requirements for the angle error but not for the angular rate error. Therefor the UKF has to be tuned as well as the EKF. In the tuned case it was shown that the same tuning parameters for the EKF and the UKF are not interchangeable directly. Therefore a new tuning parameter set for the UKF was found by simulations and identified as

$$\sigma_{\delta q} = 1 \cdot 10^{-4} \tag{3.99}$$

$$\sigma_{\Delta\omega} = 1 \cdot 10^{-5} \tag{3.100}$$

$$\sigma_{\Delta T_d} = 1 \cdot 10^{-4} \tag{3.101}$$

for the system uncertainties and

$$\sigma_{q_{st}} = 1 \cdot 10^{-3} \tag{3.102}$$

$$\sigma_{\omega_{st}} = 1 \cdot 10^{-3} \tag{3.103}$$

$$\sigma_{\omega_{gyro}} = 1 \cdot 10^{-2} \tag{3.104}$$

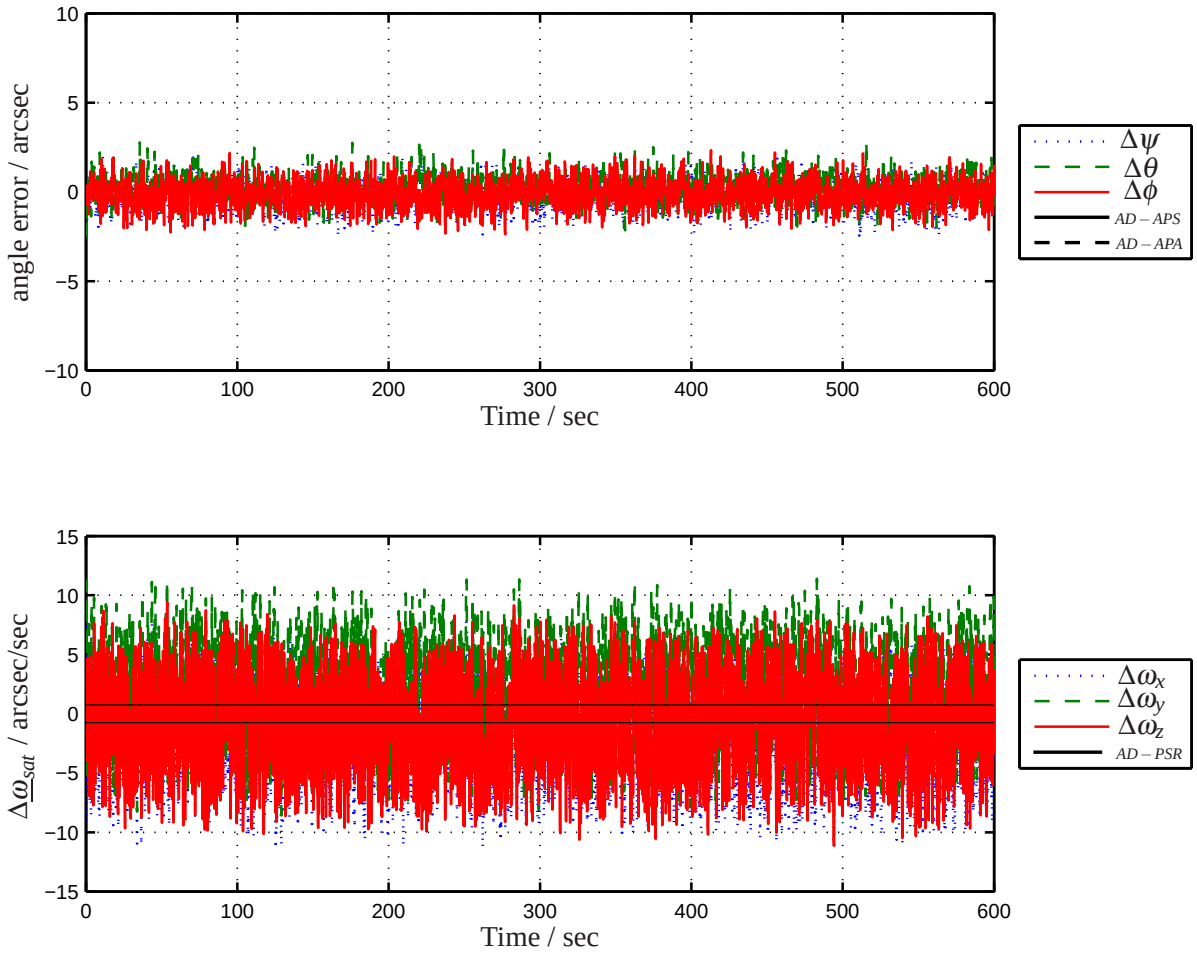

Figure 3.3: Performance of the untuned unscented KALMAN filter

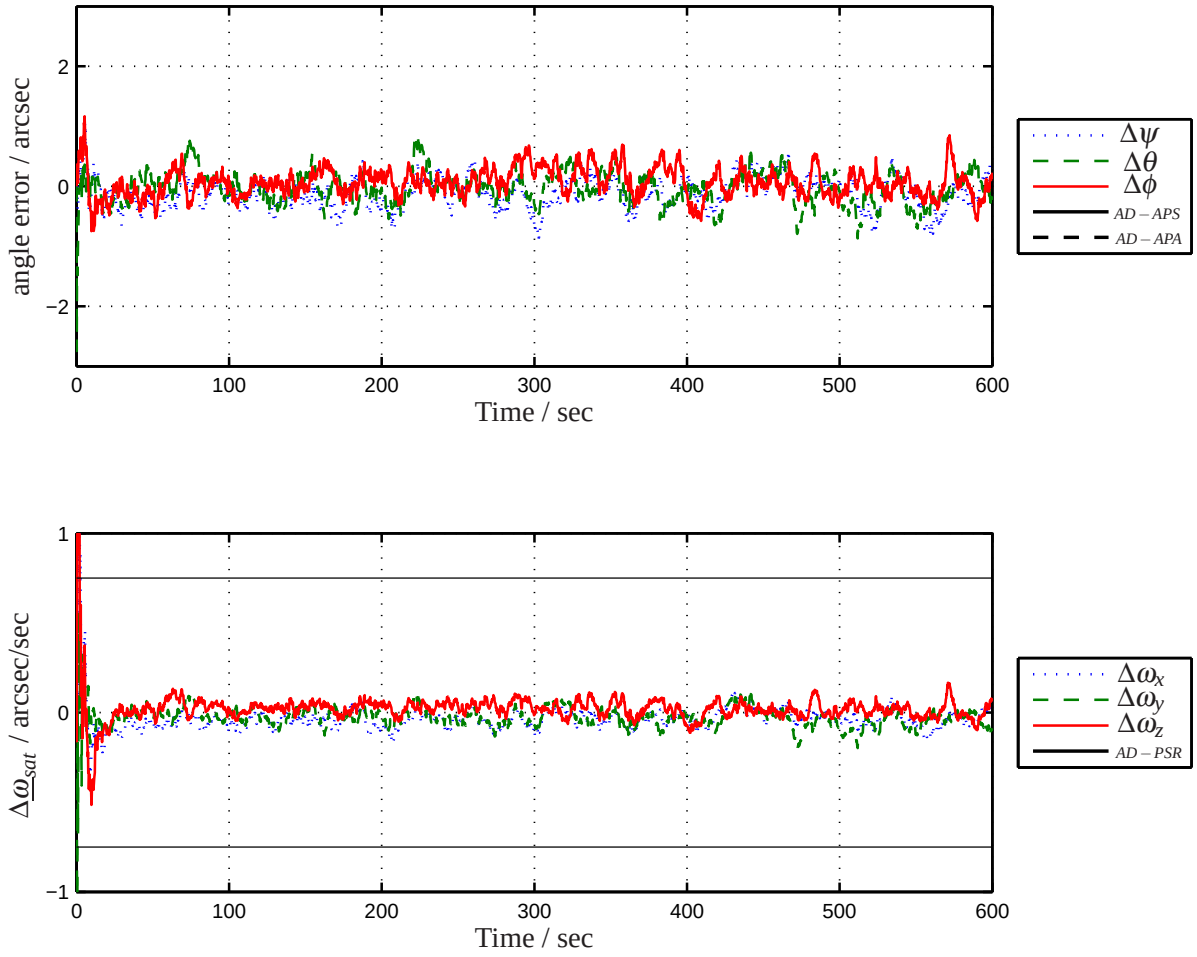

Figure 3.4: Performance of the tuned unscented KALMAN filter

for the measurements uncertainties. The covariance matrices were assumed in the same way as it was done for the EKF in equation 3.57 and 3.61.

Figure 3.4 shows that the tuned UKF is able to fulfill all requirements in a very good way. It determines the the actual attitude up to an error of an arcsecond and the angular rate error even far below an arcsecond per second. Of course this test was simulated without any attitude control interaction but it is still a better result as it could be reached with the EKF.

3.3 Comparison

The comparison between the EKF and the UKF can be done by a direct comparison of figure 3.2 and 3.4. Here it can be seen that the UKF is superior with respect to the EKF. To be able to get a better feeling for the estimated errors in both filters another error visualisation is performed. Therefore the EUKLIDIAN length of the errors are calculated and integrated over time.

$$e_q = \int |\delta \underline{q}| \, dt \tag{3.105}$$

$$e_\omega = \int |\Delta \underline{\omega}_{sat}| \, dt \tag{3.106}$$

$$e_{T_d} = \int |\Delta \underline{T}_d| dt \tag{3.107}$$

The delta values are referring here to the errors in the full state vector. The values of these integration are shown in figure 3.5. On the x-axis the time is plotted and on the y-axis the error integral is plotted. The upper diagram shows the error in the angle, the middle diagram the angular rate and the lowest diagram the disturbance torque error integral. All y-axis have a logarithmic scale to allow a good overview of the error integral.

It can be seen that in all three diagrams the UKF error is below the EKF error. In addition to this it can be seen that between the EKF and the UKF is a constant distance which shows that the steady state performance of the UKF is superior. The reasons for the better performance of the UKF can be found in the different algorithm strategies. At first the UKF is calculating the covariances by the usage of a sigma point set while the EKF is linearising around a set point. This sigma point set allows clearly to cover more uncertainties and nonlinearities than it is possible with the linearised approximation of the EKF. In addition to this the state vector was chosen to include a constant disturbing torque which as a rough assumption. Due to the fact that this only was a rough assumption the EKF is nearly not able to estimate it in a correct way. Instead the UKF can cover the nonlinearities of the disturbance in a superior way and therefore deliver a better attitude estimation.

In addition to the superior steady state performance of the UKF it was recognized that it has a better initialisation performance too. This is directly related to the sigma point concept which allows a much more rapid convergence than the EKF.

Although the UKF is superior to the EKF in the sense of accuracy it consumes more computing power than the EKF. This fact becomes clear due to the propagation of each sigma point. The more sigma points are there the more computing power is needed. One option to reduce the

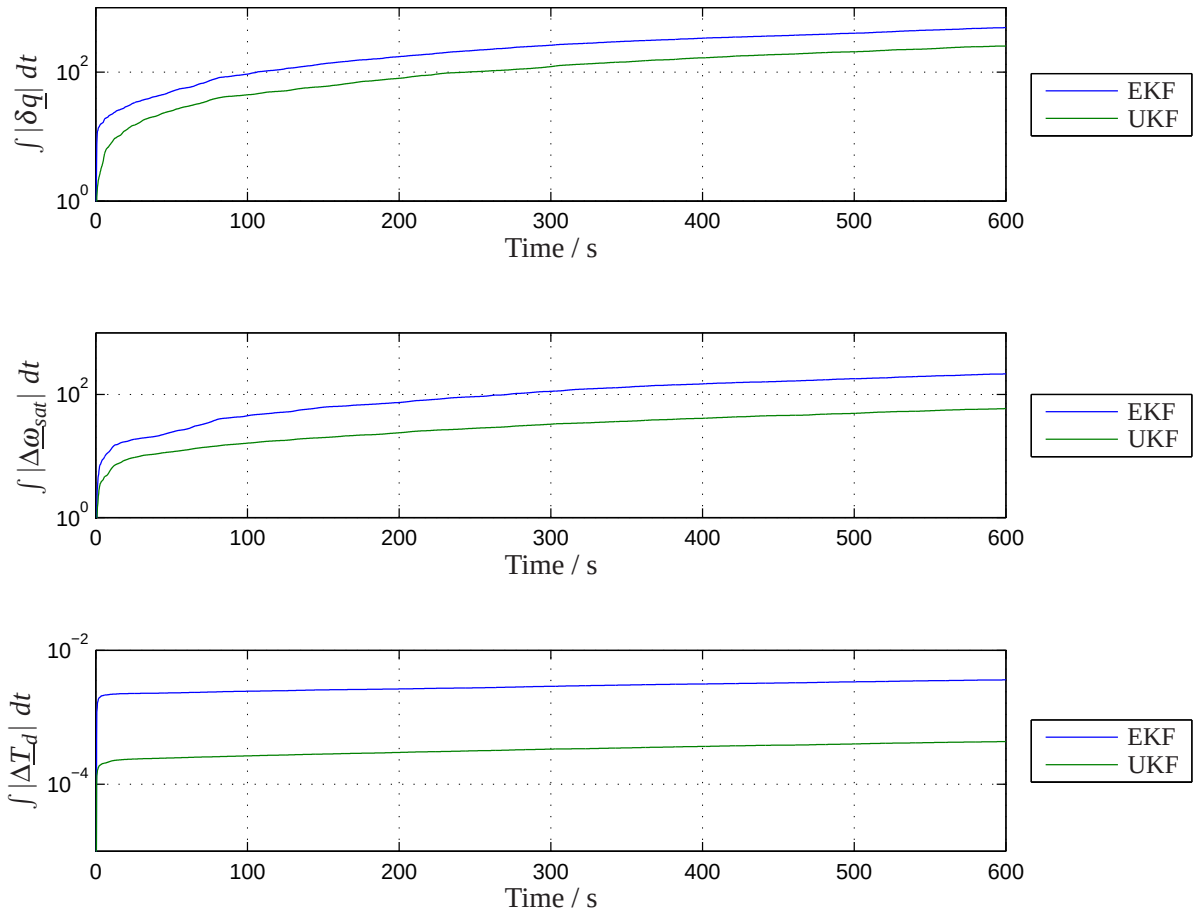

Figure 3.5: Error integral of EKF and UKF

computing power is to use the simplex UT [10] instead of the scaled UT. This is an option that could be addressed in further studies.

All in all in can be said that the AsteroidFinder/SSB is placing high attitude control requirements and therefore the best available attitude determination algorithm should be used. The logical choice is the unscented KALMAN filter with the scaled unscented transformation which will be used in the further development.

Chapter 4

Guidance and Attitude Control

This chapter describes algorithms for guidance and attitude control. It starts with the definition of the wording. In a next step different guidance algorithms are developed and linear system dynamics are derived. Afterwards a Linear Quadric Gaussian (LQG) controller design is applied to the system and the attitude control scheme is verified through a simulation.

4.1 Definition of Guidance, Navigation and Control

For the attitude control task of a satellite system there are three single tasks that have to be performed. Regarding to the AsteroidFinder mission the three terms navigation, guidance and control could be defined as follows.

- Navigation is the task to orient oneself in an environment. Therefore navigation includes the determination of position and velocity of an object with respect to a reference. Especially on a satellite systems navigation includes the attitude determination task. In the AsteroidFinder mission position and velocity will be determined by the On-Bord-Navigation-System (ONS) which includes a global positioning system receiver (GPS) while the attitude determination is done by the previous defined algorithm.
- Guidance is the task to determine the desired satellite state with respect to time. For the satellite especially the desired attitude quaternion, the angular rate and the needed torque should be determined. These values are compared with the actual state and delivered to the control algorithm.
- Control is the task to keep the satellite at a desired state. The control algorithm tries to minimize the deviation between the actual and the desired state.

4.2 Guidance

The task of the Guidance is to provide the desired attitude quaternion $\underline{q}_D$, the desired angular rate $\underline{\omega}_D$ and the desired torque $\underline{T}_D$ during the whole mission. It should be mentioned that the capital

index $_D$ indicates the desired values while $_d$ indicates a disturbance. For the AsteroidFinder/SSB mission there are four different guidance scenarios relevant.

1. Pointing the optical axis of the telescope towards an inertial target in space.
2. Move the optical axis of the telescope from one target to another target during a small time interval.
3. Point the high gain antenna or secondary payload of the satellite towards a target on the Earth surface.
4. Perform large angular maneuvers

These four scenarios are investigated in the next four sections.

4.2.1 Inertial Target Pointing

The inertial target pointing is a quite trivial problem for guidance. In this scenario only the desired quaternion has to be given. The attitude controller will minimize the deviation between the desired and the actual quaternion. The desired quaternion describes the rotation from the inertial frame to the body fixed frame and therefore it is constant during inertial target pointing.

$$\underline{q}_D = const. \tag{4.1}$$

$$\underline{\omega}_D = 0 \tag{4.2}$$

$$\underline{T}_D = 0 \tag{4.3}$$

This guidance mode is the basic mode for observation. During this mode the telescope is observing the sky and taking pictures.

4.2.2 Small Angular Maneuvers

The second scenario is a bit more complicated than the first one. In this scenario a small angular maneuver has to be performed to move from one target to another target in a fixed time step. The problem can be described as a change in the desired quaternion from the start time $t = 0$ to the end time $t = T$.

$$\underline{q}_D(t = 0) = \underline{q}_0 \tag{4.4}$$

$$\underline{q}_D(t = T) = \underline{q}_T \tag{4.5}$$

$\underline{q}_0$ is the quaternion at the beginning of the maneuver and $\underline{q}_T$ at its end. The rotation that has to be carried out between these two attitude quaternions can be described with a third quaternion q_{rot}. This third quaternion describes a single rotation about an eigenaxis of the rotation matrix.

$$\underline{q}_{rot} = \underline{q}_T \otimes \underline{q}_0^{-1} \tag{4.6}$$

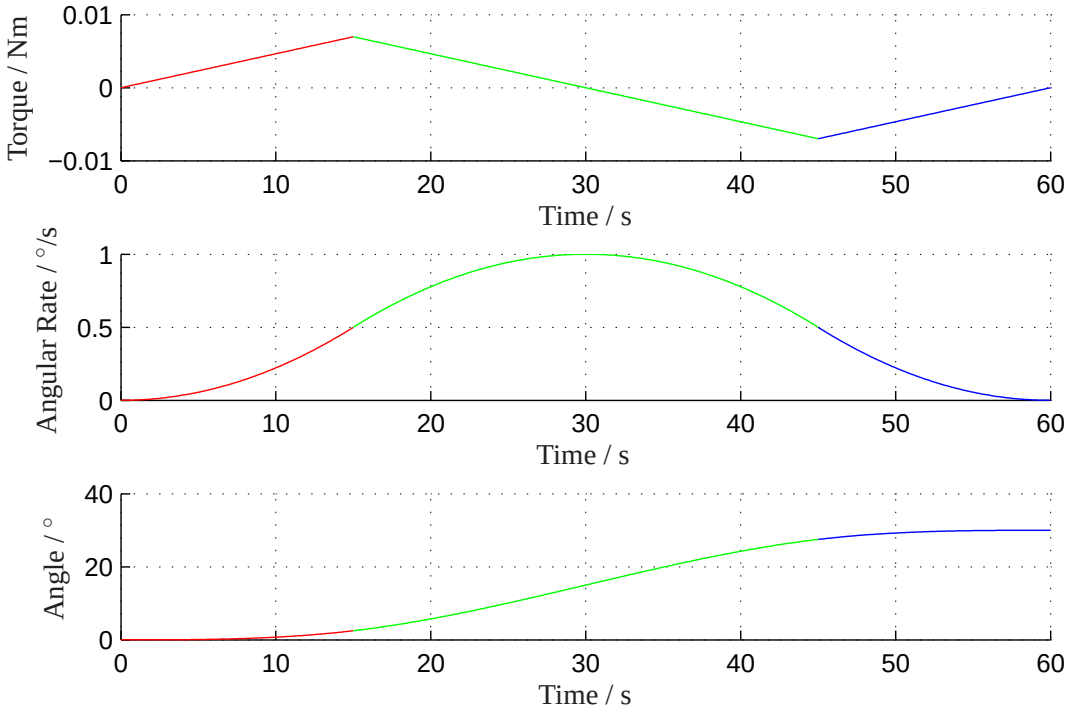

Figure 4.1: Guidance for a 30° eigenaxis rotation with a parabolic trajectory

The idea of the small angular maneuver is to define the trajectory of the rotation angle θ that is included inside the rotation quaternion $\underline{q}_{rot}$. To find such a trajectory several boundary conditions shall be considered.

- There shall be a “smooth” transfer between the two attitudes to reduce the settling time at the end of a maneuver as much as possible. This has to be taken into account because the telescope has to be stabilized up to a certain limit at the end of each maneuver.
- The maximum angular rate of the star camera shall not be exceeded. This avoids a reinitialization of the star tracker which would lead to an additional settling time of the whole attitude control system.
- The maximum torque is limited by the reaction wheel system.

The starting point of the trajectory design will be the angular rate ω. The idea is to apply three quadric equations to the angular rate and identify all variables in the resulting equation. The result of such a desired trajectory is shown in figure 4.1 and the following shall show how this result can be reached.

At first we define the three basic equation of each trajectory section (red, green, blue). Where the starting point is the equation for ω with the values of x and y which define the apex of each parabola.

$$\omega_n(t) = a_n(t-x_n)^2 + y_n \tag{4.7}$$

$$\dot{\omega}_n(t) = a_n(2t - 2x_n) \tag{4.8}$$

$$\theta_n(t) = \int \omega_n(t)\, dt = a_n\left(\frac{1}{3}t^3 - t^2 x_n + t x_n^2\right) + t y_n + c_n \tag{4.9}$$

Here n identifies the three different parabola sections. This set of equations has to be applied to all three sections of the whole trajectory which leads to a set of nine equations with twenty two unknown variables. To solve this equation system thirteen additional equations have to be identified to get a unique solution to every unknown variable. Finding the missing equations is the next task.

Due to the symmetry characteristic of the problem and the zero angular rate condition at the end of the maneuver seven additional equations can be found.

$$x_1 = y_1 = 0 \tag{4.10}$$

$$x_2 = \frac{T}{2} \tag{4.11}$$

$$x_3 = T \tag{4.12}$$

$$y_3 = 0 \tag{4.13}$$

$$a_1 = -a_2 = a_3 \tag{4.14}$$

Two additional equations can be identified due to the fact that the starting angle θ is zero and the desired angle θ_{end} shall be reached at the end.

$$\theta_1(t = 0) = 0 \tag{4.15}$$

$$\theta_3(t = T) = \theta_{end} \tag{4.16}$$

The remaining four equations can be found at the intersection of two neighbouring parabola sections. Where the angular acceleration and the angle have to be the same.

$$\dot{\omega}_1(t = \frac{T}{4}) = \dot{\omega}_2(t = \frac{T}{4}) \tag{4.17}$$

$$\dot{\omega}_2(t = \frac{3T}{4}) = \dot{\omega}_3(t = \frac{3T}{4}) \tag{4.18}$$

$$\theta_1(t = \frac{T}{4}) = \theta_2(t = \frac{T}{4}) \tag{4.19}$$

$$\theta_2(t = \frac{3T}{4}) = \theta_3(t = \frac{3T}{4}) \tag{4.20}$$

After some algebraic rearrangement all unknown variables can be identified.

$$a_1 = 16\frac{\theta_{end}}{T^3} \tag{4.21}$$

$$c_1 = 0 \tag{4.22}$$

$$y_2 = 2a_1\left(\frac{T}{4}\right)^2 \tag{4.23}$$

$$c_2 = \frac{2}{192}a_1T^3 \tag{4.24}$$

$$c_3 = \theta_{end} - a_1\frac{T^3}{3} \tag{4.25}$$

The remaining unknown variables are only θ_{end}, which is defined by the rotation that has to be performed, and T the time of the maneuver.

With these the basic trajectory is designed but there are two more boundaries that have to be considered. The first one is the maximum allowed angular rate which shall not be exceeded. The problem can be addressed by rewriting equation 4.21 and 4.23 to:

$$\begin{aligned} y_2 &= 2\frac{\theta_{end}}{T} \\ T &\geq 2\frac{\theta_{end}}{y_{2,max}} \end{aligned} \tag{4.26}$$

Where $y_{2,max}$ is identifying the maximum allowed angular rate and has to be defined.

The second one is the maximum torque that could be applied to the system. This boundary condition can be formulated by:

$$\begin{aligned} T_{orque} &= J\dot{\omega}_1\left(t = \frac{T}{4}\right) \\ T_{orque} &= 8\,J\,\frac{\theta_{end}}{T^2} \\ T &\geq \sqrt{\frac{8\,J\,\theta_{end}}{T_{orque,max}}} \end{aligned} \tag{4.27}$$

Where J is identifying the moment of inertia around the eigenaxis and $T_{orque,max}$ defines the maximum torque that can be applied around this axis. If these conditions can be meet by the choice of rotation angle θ and execution time T the guidance trajectory can be calculated and is fully defined.

The moment of inertia that belongs to the rotational eigenaxis is depending on the angular rate and the moment of inertia tensor.

$$\omega \cdot J \cdot \omega = \underline{\omega}^T \cdot \underline{\underline{I}} \cdot \underline{\omega} \tag{4.28}$$

$$J = \frac{1}{\omega^2}\underline{\omega}^T \cdot \underline{\underline{I}} \cdot \underline{\omega} \tag{4.29}$$

The last step to apply the trajectory is to transform it to the rotation quaternion $\underline{q}_{rot}$ that has to be multiplied with the starting quaternion $\underline{q}_0$.

At first the eigenaxis $\underline{e}$ of the rotation has to be identified. This is done by the direct extraction out of the full rotation quaternion

$$\underline{e} = \frac{(q_{rot,1}, q_{rot,2}, q_{rot,3})^T}{\left|\sqrt{q_{rot,1}^2 + q_{rot,2}^2 + q_{rot,3}^2}\right|} \tag{4.30}$$

Now the rotational quaternion trajectory can be calculated.

$$\underline{q}_{rot}(\theta(t)) = \left(\sin\frac{\theta}{2}e_x, \sin\frac{\theta}{2}e_y, \sin\frac{\theta}{2}e_z, \cos\frac{\theta}{2}\right)^T \tag{4.31}$$

The actual desired guidance quaternion is therefore defined.

$$\underline{q}_D(t) = \underline{q}_{rot}(\theta(t)) \otimes \underline{q}_0 \tag{4.32}$$

The desired angular rate trajectory is simply defined by the projection of the angular rate to the system axis.

$$\underline{\omega}_D(t) = \omega(t)\underline{e} \tag{4.33}$$

And at last the torque that has to be applied on every spacecraft axis is calculated out of the eigenaxis, the moment of inertia and the angular acceleration.

$$T_D(t) = \underline{\underline{I}}_{sat} \cdot \dot{\omega} \cdot \underline{e} \tag{4.34}$$

Now the trajectory for a small angular maneuver is fully defined and can be applied to the satellite system.

As an example the resulting trajectory out of figure 4.1 for a random starting quaternion is shown in figure 4.2.

4.2.3 Large Angular Maneuver

In many spacecrafts there is a difference between small and large angular maneuvers. Mainly this results out of different control algorithms and guidance strategies. Especially if the attitude is represented by EULER angles the avoidance of singularities [23] has to be taken into account which is often addressed by different guidance algorithms. Another reason could be an energy or fuel optimal maneuver that is not necessarily equal to an eigenaxis maneuver [33], [43].

For the AsteroidFinder mission there will be no basic difference in the guidance module for small and large angular maneuvers. This results out of the high pointing stability requirements that should be achieved as soon as the payload is working. Due to the fact that the AsteroidFinder has to be able to move from one observation area to another observation area during

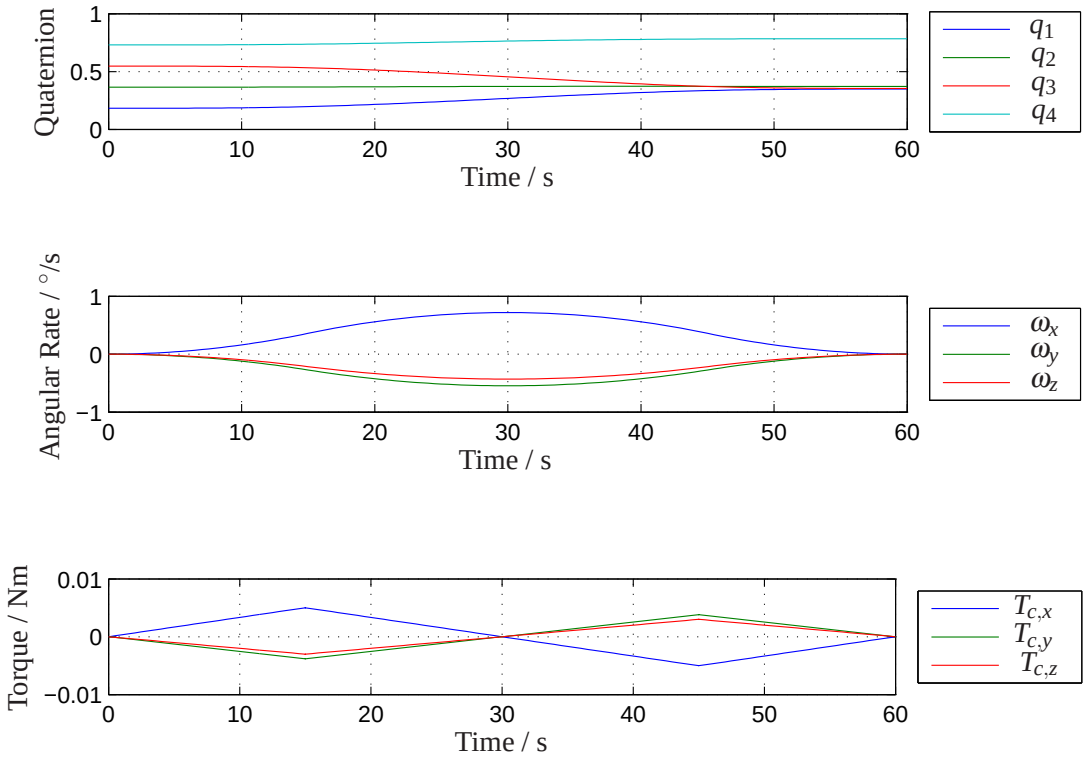

Figure 4.2: Resulting trajectory for a 30° angular maneuver

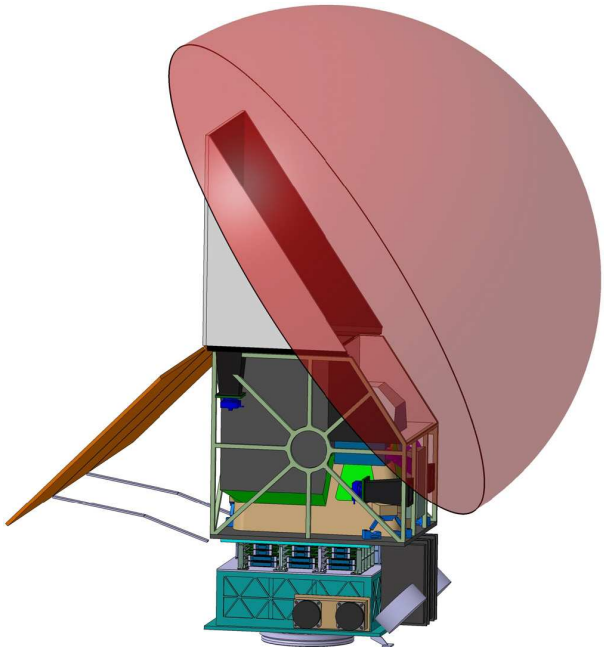

Figure 4.3: Forbidden hemisphere of AsteroidFinder/SSB

payload activity it is not useful to define a new guidance algorithm for such a scenario. In addition to this the attitude is globally described by quaternions which do not have the singularity problem.

Therefor the guidance can use the same algorithm for small and large angular maneuvers with one slight modification. The modification addresses the forbidden attitudes. For the AsteroidFinder/SSB a forbidden hemisphere (figure 4.3) was defined that is never allowed to be exposed to the sun. The algorithm for large angular maneuver checks if the angle α between the normal forbidden hemisphere vector $\underline{N}$ and the sun vector $\underline{S}$ is reducing to a value lower than 90°. This can be checked by the calculation of the dot product.

$$\cos\alpha = \frac{\underline{S}\cdot\underline{N}}{|\underline{S}|\cdot|\underline{N}|} \tag{4.35}$$

If $\cos\alpha \geq 0$ the angle between sun vector $\underline{S}$ and forbidden hemisphere vector $\underline{N}$ is below 90° and therefore forbidden. If such a forbidden attitude is identified during the precalculation of a guidance maneuver the algorithm is rejecting this maneuver and tries to carry out the opposition rotation around the same rotation axis. If this rotation is rejected as well it goes to the next maneuver point.

It should be mentioned that if the start and end point of a maneuver are allowed there exists an allowed eigenaxis rotation to perform this maneuver but it is not always the shortest rotation. This is the logical interpretation of the forbidden hemisphere concept which can be understood with figure 4.4. This figure shows the unit sphere where the spacecraft is located in the center.

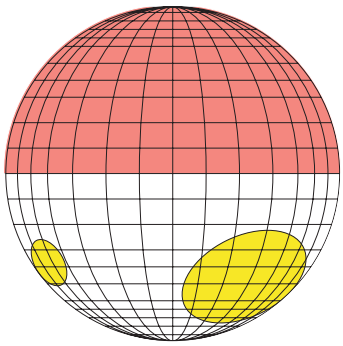

Figure 4.4: Forbidden hemisphere concept

The red region indicates the forbidden hemisphere which is never allowed to enter the yellow areas. The yellow areas are indicating the angular regions of the Sun and the Earth under which they would appear on the unit sphere. An allowed maneuver can be seen now as the movement of the red area around the unit sphere while the yellow areas are fixed. But the same maneuver could be seen from another perspective as a movement of the yellow ares with a fixed red area. Therefore every allowed maneuver is only defining a movement of the yellow areas inside the lower hemisphere.

From this logical interpretation it became clear that there is existing always an eigenaxis rotation that moves from one allowed point to another allowed point.

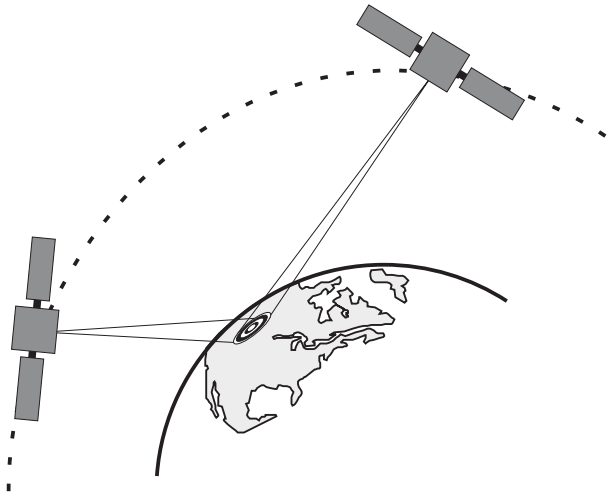

Figure 4.5: Ground station pointing

4.2.4 Ground Station Pointing

The guidance for a ground station pointing (figure 4.5) is another guidance mode that will be addressed in the following section. The reason for the ground station pointing is the telemetry. To achieve a high data rate the maximum antenna beam should be pointed towards the ground station. Another reason is the optional secondary payload which requires a ground station pointing. Therefore such a guidance has to be implemented on the satellite.

The task is now to identify the guidance quaternion. The starting point of the whole guidance are the coordinates of the ground station. It is assumed that these coordinates are given in the World Geodetic System of 1984 (WGS84) and they are expressed as latitude ϕ, longitude λ and altitude h.

As a first step these coordinate set λ,ϕ has to be expressed as Cartesian coordinates u^{wgs},v^{wgs} and w^{wgs} which is achieved by applying the transformation [14]

$$u^{wgs} = (N+h)\cos\phi\cos\lambda \tag{4.36}$$

$$v^{wgs} = (N+h)\cos\phi\sin\lambda \tag{4.37}$$

$$w^{wgs} = ((1-e^2)N+h)\sin\phi \tag{4.38}$$

with

$$e = \frac{R_{earth}}{\sqrt{1-e(2-e)\sin^2\phi}} \tag{4.39}$$

$$R_{earth} = 6378137m \tag{4.40}$$

$$f = \frac{1}{298.257223563} \tag{4.41}$$

The parameters of the Earth radius R_{earth} and the deformation f are defined by the used coordinate system [12].

At a next step this position information has to be transformed into an inertial frame. This frame has to be the same that is used for the satellite position and attitude control information. For the AsteroidFinder mission this will be the "True Of Date" (TOD) frame and the transformation is done by multiplying the vector $\underline{u}^{wgs}$ with a defined direct cosine matrix.

$$\begin{aligned} \underline{u}^{wgs} &= (u^{wgs}, v^{wgs}, w^{wgs})^T \\ \underline{u}^{tod} &= \underline{\underline{M}}^{tod}_{wgs}(t)\underline{u}^{wgs} \end{aligned} \tag{4.42}$$

The direct cosine matrix $\underline{\underline{M}}^{tod}_{wgs}$ depends on the actual time. Its calculation is quite complicated due to rotational effects of the earth and the pertuberation of other extraterestical bodys. Its derivation is described in detail in [28] and shall not be addressed any further at this point.

If the vector $\underline{u}^{tod}$ is known in an inertial frame it is clear that this vector has to be aligned with the antenna beam which is described in a body fixed system. The problem is that this single vector can not define the allowed rotation around this vector. Therefor a second information has to be known to identify the full desired attitude. For the first analysis this second vector will be the solar panel vector which should be pointed as good as possible towards the sun.

Now there are four independent informations to be able to determine a guidance.

- Pointing direction of the antenna known in body fixed coordinates $\underline{u}^{bf}$.
- Desired pointing direction of the antenna known in inertial coordinates $\underline{u}^{tod}$
- Pointing direction of the main solar panel known in body fixed coordinates $\underline{v}^{bf}$
- Desired pointing direction of the main solar panel known in inertial coordinates $\underline{v}^{tod}$

These informations can be used to identify the desired attitude. Therefore the algebraic method which is described in [42] is used. If there are two non parallel vectors $\underline{u}$ and $\underline{v}$ they define a coordinate system with the basis vectors $\underline{u}$,$\underline{r}$ and $\underline{s}$.

$$\underline{r} = \frac{\underline{u} \times \underline{v}}{|\underline{u} \times \underline{v}|} \tag{4.43}$$

$$\underline{s} = \underline{u} \times \underline{r} \tag{4.44}$$

$$|\underline{u} \cdot \underline{v}| < 1 \tag{4.45}$$

Due to the knowledge of two non parallel vectors in two different coordinate systems the two basis $\underline{\underline{M}}$ of both coordinate systems are known.

$$\underline{\underline{M}}^{bf} = \left[\underline{u}^{bf}, \underline{r}^{bf}, \underline{s}^{bf}\right] \tag{4.46}$$

$$\underline{\underline{M}}^{tod} = \left[\underline{u}^{tod}, \underline{r}^{tod}, \underline{s}^{tod}\right] \tag{4.47}$$

The transformation between these to coordinate frames can be described through the matrix $\underline{\underline{M}}^{bf}_{tod}$.

$$\underline{\underline{M}}^{bf}_{tod}\,\underline{\underline{M}}^{tod} = \underline{\underline{M}}^{bf} \tag{4.48}$$

$$\underline{\underline{M}}^{bf}_{tod} = \underline{\underline{M}}^{bf}\,\underline{\underline{M}}^{tod^T} \tag{4.49}$$

$\underline{\underline{M}}^{bf}_{tod}$ is representing the desired direct cosine matrix that can be rewritten to a desired guidance quaternion $\underline{q}_D$.

Due to the fact that the satellite position will be determined on orbit and the guidance quaternion is related to this on board position determination it is not useful to recalculated a complete trajectory as it is done for the small angular maneuver. Therefore it is much more efficient to determine the angular rate by using the quaternion derivatives.

$$\lim_{\Delta t\to 0}\frac{\underline{q}(t+\Delta t)-\underline{q}(t)}{\Delta t} = \frac{1}{2}\underline{\underline{\Xi}}(\underline{q})\underline{\omega} \tag{4.50}$$

By reformulating this equation the angular rate can be calculated from two following quaternions.

$$\underline{\omega}_D = 2\underline{\underline{\Xi}}^{-1}(\underline{q}(t_1))\,\frac{\underline{q}(t_1)-\underline{q}(t_0)}{\Delta t} \tag{4.51}$$

According to the angular rate the guidance torque can be calculated as a derivative of it.

$$\dot{\underline{\omega}}_D = \frac{\underline{\omega}_D(t_1)-\underline{\omega}_D(t_0)}{\Delta t} \tag{4.52}$$

$$\underline{T}_D = \underline{\underline{I}}\dot{\underline{\omega}}_D \tag{4.53}$$

With the knowledge of the quaternion $\underline{q}_D$, the angular rate $\underline{\omega}_D$ and the torque $\underline{T}_D$ the guidance is fully defined and can be applied to the satellite system.

It should be mentioned that this approach leads to a delay of the desired angular rate and torque. This is the result of taking the derivatives of the quaternion at each sample time. Another option would be to calculate the angular rate and torque directly through the angular momentum vector of the satellite. The single guidance for the ground station could be calculated in this way quite easily but to incorporate a secondary information (like the sun) would lead to a more complicated formulation. Therefore the procedure above will be used for the further thesis to simplify the calculation.

4.2.5 Example Guidance Profile

The following sections are often referring to a guidance profile which is applied during tests. The test case guidance profile which will be used is shown in figure 4.6. The three diagrams show the desired quaternion, the desired angular rate in arcseconds per second and the desired torque. The x-axis shows the time of one orbit period.

The profile itself was derived from an ideal payload observation profile an shall reflect a possible guidance scenario. If the satellite system is able to follow these guidance it is able to fulfill the mission requirements.

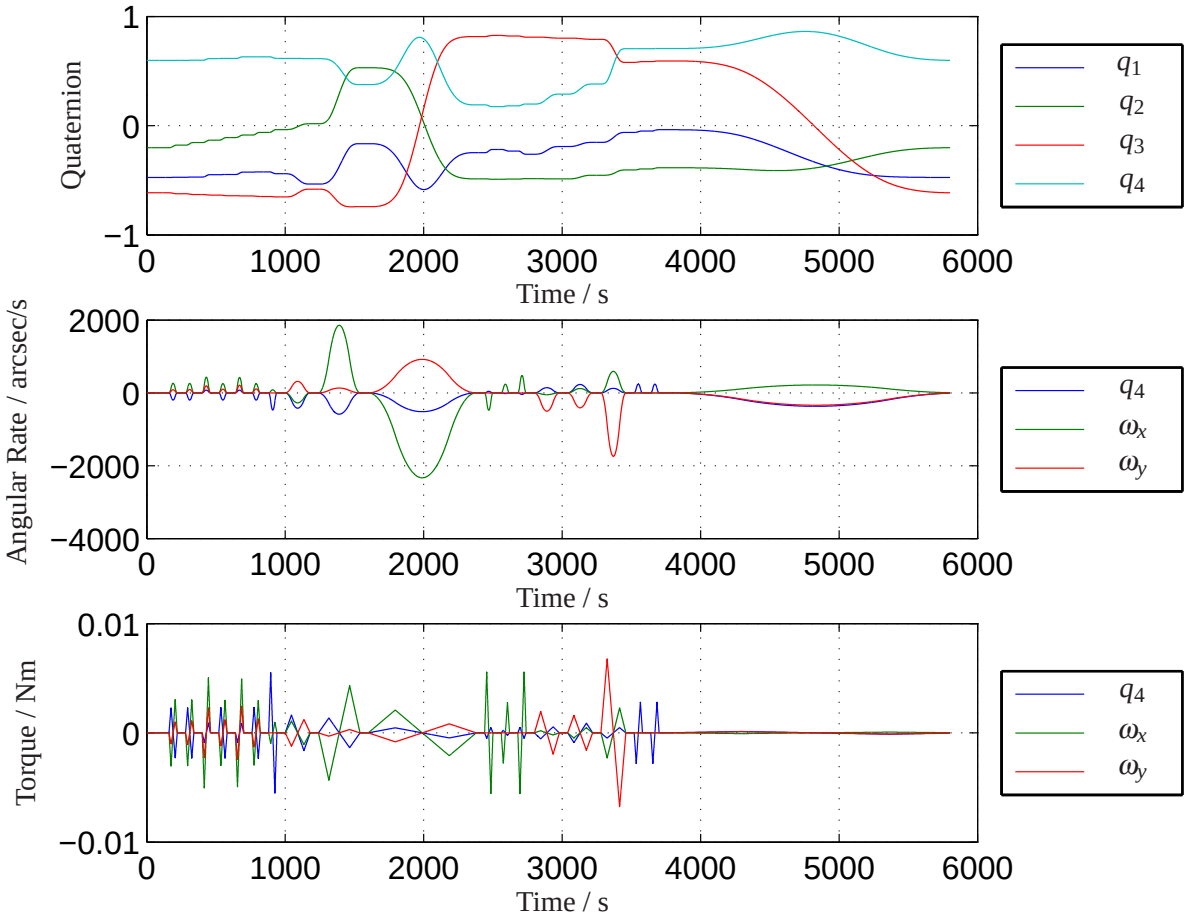

Figure 4.6: Guidance profile for controller tests

4.3 Attitude Control

Beside guidance attitude control is another essential task to fulfill the AsteroidFinder/SSB mission. While guidance is delivering the desired state information attitude control cancel out the disturbances at the desired attitude.

It is important to keep the satellite exactly at a desired state. Therefore an active attitude control has to be implemented on board of the satellite. In the AsteroidFinder/SSB design an active

attitude control without orbit control is foreseen [11]. This boundary condition is fixed due to the fact that the only actuators on board are reaction wheels and magnetic torquers, which can only produce torques and no forces. With this condition the satellite is able to turn around its Center of Gravity (CoG). It is not possible to control the position of the CoG without the possibility to apply forces directly. The task is now to identify a control scheme that is suitable for the attitude control task.

Current control theory can be divided into two big sections linear and nonlinear control. Basically both systems starts with the mathematical description of the plant. Such a description is derived from the physical properties and its interaction which each other. The more values are interacting with each other the more complicated the system description is. Often this results in a nonlinear differential function that describes the system behavior.

Nonlinear control tries to use the nonlinear function directly and apply control theories that are reasonable to the system (e.g. neural networks, fuzzy logic etc.). It became more and more popular with increasing computing power and is under continues development.

Linear control strategies find its origin the fact that a system can be described with a linear function. There are existing a lot of approaches to derive linear control strategies and proof their stability and robustness. One development of linear control strategy is the optimal control. Which became popular in the 1970s [6]. The closed theory for linear systems is the main reason why it shall be applied to the AsteroidFinder/SSB although it is a nonlinear system. The reason for the linear approach is that it is more easy to understand and to verify it, than it is for a pure nonlinear control strategy. Additionally attitude control will be performed around a set point which is delivered by the guidance algorithm. The deviations around this set point are changing nearly linear and therefore a linear control scheme will be used.

4.3.1 Restriction to Linear System Dynamic

Due to the choice of a linear control design there are two restrictions which should be take into account for the further design. These two restrictions are the choice of an operating point and the uncoupled dynamic of all three axis at that point. The following point out two strategies to solve these problems to get a more detailed representation of the satellite system.

4.3.1.1 Feedforward Control

Due to a linearisation there will be two terms of the systems dynamics equations $\underline{\dot{\omega}}_{sat}$ 2.22 ignored. These terms are describing the coupling torque between the three axis of the satellite and the coupling between the satellite and the reaction wheels.

$$\underline{T}_{C,sat} = \underline{\omega}_{sat} \times \underline{L}_{sat} \tag{4.54}$$

$$\underline{T}_{C,sat,rw} = \underline{\omega}_{sat} \times \underline{L}_{rw} \tag{4.55}$$

The problem of the linearisation is that these two terms will not be noticed during the controller design due to the choice of the operating point. From the physical point of view the satellite will be described as a nonrotating mass without any rotating mass inside. This is a problem

because at least the reaction wheels will rotate inside the satellite and especially for ground station pointing the satellite will have a defined angular rate.

The problem is that these two terms will act as an unknown disturbance torque although they are well known. Too get a more precise control algorithm it is important to address theses two terms.

One possible way to do this is to use a feedforward control [25], [37] which is able to cancel known disturbances.

Such a feedforward control leads to a canceling of the coupling torques and the linearised dynamics will reflect the satellite system in a better way as it is done without canceling. The feedforward control is implemented inside the control loop an is supporting the actual attitude control. During the controller design it was realized that without feedforward control the induced disturbances are to big to ensure a precise attitude control system.

4.3.1.2 Operating Point Control

The linearisation itself will be performed at an operating point. To ensure that the mathematical description is valid for all desired states the control should work all the time around this operating point. To achieve this only the errors of the state will be given to the control law which is equal to an operation around zero.

$$\Delta\underline{q} = \underline{q}_D \otimes \hat{\underline{q}}^{-1} \tag{4.56}$$

$$\Delta\underline{\omega}_{sat} = \underline{\omega}_D - \hat{\underline{\omega}}_{sat} \tag{4.57}$$

Here $_D$ identifies the desired values while $\hat{}$ are the measured values that were processed by the attitude determination. If the guidance is changing the desired $_D$ values slowly the error is increasing and therefor the attitude control is activated. The formulation of this error allows the controller to work all the time around the zeroth point.

4.3.2 Linear System Dynamic

To be able to apply a linear control strategy on the satellite system. The system itself has to have a linearised form. The linearised model shall fit into the standard form of a linear state space system which can be found in many textbooks [6],[37], [24], [25].

$$\dot{\underline{x}}(t) = \underline{\underline{A}}(t)\,\underline{x}(t) + \underline{\underline{B}}(t)\,\underline{u}(t) + \underline{\underline{E}}(t)\,\underline{z}(t) \tag{4.58}$$

$$\underline{y}(t) = \underline{\underline{C}}(t)\,\underline{x}(t) + \underline{\underline{D}}(t)\,\underline{u}(t) \tag{4.59}$$

Where $\underline{x}(t) \in \Re^{n_x}$ is the state of the system, $\underline{u}(t) \in \Re^{n_u}$ is the control signal, $\underline{z}(t) \in \Re^{n_z}$ are the disturbances and $\underline{y}(t) \in \Re^{n_y}$ is the output of the system. The matrix $\underline{\underline{A}}(t) \in \Re^{n_x \times n_x}$ is the state matrix, $\underline{\underline{B}}(t) \in \Re^{n_x \times n_u}$ is the input matrix, $\underline{\underline{C}}(t) \in \Re^{n_y \times n_x}$ the output matrix, $\underline{\underline{D}}(t) \in \Re^{n_y \times n_u}$ the

input to output coupling matrix and $\underline{\underline{E}}(t) \in \Re^{n_x \times n_z}$ the disturbance matrix. The variable t is the time while n indicates the dimension of each matrix and vector.

It is already known that the dynamics of the satellite system are a nonlinear function. The system dynamic equations where identified in the previous chapters and shall be recalled here.

$$\begin{aligned} \dot{\underline{q}}(t) &= \frac{1}{2}\,\underline{\underline{\Omega}}(\underline{\omega}_{sat}(t))\,\underline{q}(t) \\ \dot{\underline{\omega}}_{sat}(t) &= \underline{\underline{I}}_{sat}^{-1}\left(\underline{T}_D(t) - \underline{\omega}_{sat}(t) \times \underline{L}_{sat}(t) - \underline{\omega}_{sat}(t) \times \underline{L}_{rw}(t) - \dot{\underline{L}}_{rw}(t)\right) \end{aligned}$$

Where the quaternion and the angular rate specifies the full satellite state. To be able to use a linear control strategy this system dynamics have to be linearised around an operating point $()_0$. The choice of the operating point is done in such a way that the dynamics became quite simple.

$$\underline{q}_0 = (0,0,0,1)^T \tag{4.60}$$

$$\underline{\omega}_{sat,0} = (0,0,0)^T \tag{4.61}$$

With the help of the two restrictions of the operating point and a decoupled behavior of all satellite axis the linearised system matrices can be determined.

$$\underline{\underline{A}} = \begin{bmatrix} \frac{\partial \dot{\underline{q}}}{\partial \underline{q}} & \frac{\partial \dot{\underline{q}}}{\partial \underline{\omega}_{sat}} \\ \frac{\partial \dot{\underline{\omega}}_{sat}}{\partial \underline{q}} & \frac{\partial \dot{\underline{\omega}}_{sat}}{\partial \underline{\omega}_{sat}} \end{bmatrix}_{\underline{q}_0, \underline{\omega}_{sat,0}} \tag{4.62}$$

$$\underline{\underline{B}} = \begin{bmatrix} \frac{\partial \dot{\underline{q}}}{\partial \underline{T}_c} \\ \frac{\partial \dot{\underline{\omega}}_{sat}}{\partial \underline{T}_c} \end{bmatrix}_{\underline{q}_0, \underline{\omega}_{sat,0}} \tag{4.63}$$

$$\underline{\underline{C}} = \begin{bmatrix} 1 & 0 & \dots \\ 0 & 1 & \\ \vdots & & \ddots \end{bmatrix} \tag{4.64}$$

$$\underline{\underline{D}} = \underline{\underline{0}} \tag{4.65}$$

Where $\underline{T}_c = \dot{\underline{L}}_{rw}$ is the control torque. The calculation of the Jacobian matrices can be done in straight forward manner. In addition to this the state vector can be reduced by one value due to the choice of $q_{0,4} = 1$. The reduction of the quaternion was already shown during the EKF and UKF development and is used here one more time. With the characteristics of the new operating point the linearized dynamics can be defined.

$$\underline{\underline{A}} = \begin{bmatrix} 0 & 0 & 0 & 0.5 & 0 & 0 \\ 0 & 0 & 0 & 0 & 0.5 & 0 \\ 0 & 0 & 0 & 0 & 0 & 0.5 \\ 0 & 0 & 0 & 0 & 0 & 0 \\ 0 & 0 & 0 & 0 & 0 & 0 \\ 0 & 0 & 0 & 0 & 0 & 0 \end{bmatrix} \tag{4.66}$$

$$\underline{\underline{B}} = \begin{bmatrix} \underline{\underline{0}} \\ \underline{\underline{I}}_{sat}^{-1} \end{bmatrix} \tag{4.67}$$

These are the dynamics of a continues linearised system that represents the continues nonlinear satellite dynamics. The design of a continues control gain can be done with the help of these continues linear system.

If the controller is discrete (as it will be for the real satellite system) the previous continues system dynamics should be discretised. A discrete Version of the system equations can be found by the standard state transition [25], [24].

$$\underline{\underline{\Phi}} = \exp\left(\underline{\underline{A}}\,\Delta t\right) \tag{4.68}$$

$$\underline{\underline{\Gamma}} = \int_0^T \exp\left(\underline{\underline{A}}\,\Delta t\right)\underline{\underline{B}}\,dt \tag{4.69}$$

Where $\underline{\underline{\Phi}}$ is the discrete state dynamic and $\underline{\underline{\Gamma}}$ the discrete input matrix. The time between two samples is specified by Δt.

4.3.3 Linear Quadric Gaussian Control

The basic idea behind the Linear Quadric Gaussian Control (LQG) is to transfer a system optimal from an initial state $\underline{x}_0$ to the final state $\underline{x}_f = \underline{0}$. To do this LQG calculates a control gain $\underline{\underline{K}}(t)$ and multiply this with the state to derive a control command $\underline{u}(t)$.

$$\underline{u}(t) = -\underline{\underline{K}}(t)\,\underline{x}(t) \tag{4.70}$$

To find the control gain LQG is minimizing a quadric cost function J, which relates the system state $\underline{x}$ and the control input $\underline{u}$ to each other [6], [24].

$$J\left(\underline{x}(t),\underline{u}(t)\right) = \frac{1}{2}\int_0^\infty \underline{x}^T(t)\,\underline{\underline{Q}}\,\underline{x}(t) + \underline{u}^T(t)\,\underline{\underline{R}}\,\underline{u}(t)dt \tag{4.71}$$

The matrices $\underline{\underline{Q}}$ and $\underline{\underline{R}}$ are weighting matrices that define the term “optimal”. The matrix $\underline{\underline{K}}(t)$ which minimize this cost function is the optimal control gain for the system.

If the optimization horizon is set to infinity ($t = \infty$) the control gain reaches a steady state. Due to that fact the calculation of the optimal control gain simplifies to the solution of

$$\underline{\underline{K}} = \underline{\underline{R}}^{-1}\,\underline{\underline{B}}^T\,\underline{\underline{P}}(t) \tag{4.72}$$

where $\underline{\underline{P}}$ is the solution of the following matrix RICCATI equation.

$$\dot{\underline{\underline{P}}}(t) = \underline{\underline{A}}^T\,\underline{\underline{P}}(t) + \underline{\underline{P}}(t)\,\underline{\underline{A}} - \underline{\underline{P}}(t)\,\underline{\underline{B}}\,\underline{\underline{R}}^{-1}\,\underline{\underline{B}}^T\,\underline{\underline{P}}(t) + \underline{\underline{Q}} \tag{4.73}$$

$$\dot{\underline{\underline{P}}}(t_\infty) = \underline{\underline{0}} \tag{4.74}$$

This equation can be solved through numerical integration [24], [6] and allows the computation of the optimal control gain. This design procedure of the control gain is very useful for a multiply input multiply output system (MIMO), which is the fact for the satellite system. The design is able to treat all system values at the same time which allow a much better representation of the system dynamics than it would be possible for a reduced single input single output (SISO) system. Especially if the moment of inertia of the satellite is not diagonal in the controlled frame there exist a coupling between the axis which can be covered by the system dynamics and the LQG control approach.

In addition to the MIMO capabilities, a characteristic of the LQG design is to derive a control gain that ensures a stable control loop [24]. This can be shown with the help of a LJAPUNOW equation of the form.

$$\underline{\underline{A}}^T \underline{\underline{P}} + \underline{\underline{P}}\,\underline{\underline{A}} = -\underline{\underline{Q}} \tag{4.75}$$

If $\underline{\underline{Q}}$ is positive, symmetric and definite this equation has only a positive, symmetric and definite solution for $\underline{\underline{P}}$ if $\underline{\underline{A}}$ is asymptotic stable.

If the control system loop is closed the system dynamic matrix changes to its closed loop description $\underline{\underline{A}}_{cl}$.

$$\underline{\underline{A}}_{cl} = \underline{\underline{A}} - \underline{\underline{B}} \cdot \underline{\underline{K}} \tag{4.76}$$

Through the combination of equation 4.76, 4.73 and 4.74 the matrix RICCATI equation can be reformulated to a LIAPUNOW equation.

$$\underline{\underline{A}}_{cl}^T \underline{\underline{P}} + \underline{\underline{P}}\,\underline{\underline{A}}_{cl} = -\underline{\underline{P}}\,\underline{\underline{B}}\,\underline{\underline{R}}^{-1}\,\underline{\underline{B}}^T\,\underline{\underline{P}} - \underline{\underline{Q}} \tag{4.77}$$

Which has a positive, symmetric and definite solution of $\underline{\underline{P}}$. Therefore the closed loop system is stable [24].

By the previous definition of the attitude control to work around a zero operation point the LQG design methodology can be applied to the satellite system. To be able to identify the optimal control gain the remaining task is to select appropriate weighting matrices.

4.3.3.1 Selecting Weighting Matrices

The design of the optimal control gain can be influenced by the two weighting matrices $\underline{\underline{Q}}$ and $\underline{\underline{R}}$ which allow to incorporate some desired behavior of the control loop into the control gain design. While the matrix $\underline{\underline{Q}}$ is weighting the system state the matrix $\underline{\underline{R}}$ is weighting the control commands.

In the most general way every single element of the two matrices can be used to influence the control gain design. In the case of the simple linearized system dynamics for the satellite this

would lead to $6 \cdot 6 = 36$ parameters for $\underline{\underline{Q}}$ and $3 \cdot 6 = 18$ parameters for $\underline{\underline{R}}$. It is obvious that such an amount of parameters is not very useful therefore it should be reduced to a set of some key parameters.

One suggestions is the choice of the weighting matrices as diagonal matrices. With such an approach each state and each control command is decoupled from the other variables. It is shown in many textbooks [24], [6] that such a choice does not have much disadvantages. Especially if the overall system is modeled as a decoupled system. Although this is can not be said completely for the satellite system a choice of diagonal matrices shall be applied in the further chapters.

In addition to the diagonal choice of the matrices each value which weights the equal states or control inputs should be chosen as the same value. E.g. it does not make sense to choose different weightings for the three error angular velocities of the satellite due to the fact that they should be treated equally.

4.3.4 Controller Design

With the help of the LQG approach different state controllers are designed which are all stable due to their design procedure.

4.3.4.1 Proportional Derivative Control

The simplest controller that can be derived form the satellite system dynamics is a proportional derivative controller (PD). Therefore the LQG approach is directly applied to the system dynamics derived in chapter 4.3.2. The weighing matrices are chosen to be diagonal

$$\underline{\underline{Q}} = \begin{bmatrix} I_{[3\times3]} \cdot \sigma_{\delta q} & 0 \\ 0 & I_{[3\times3]} \cdot \sigma_{\omega} \end{bmatrix} \tag{4.78}$$

$$\underline{\underline{R}} = I_{[3\times3]} \cdot \sigma_{T_c} \tag{4.79}$$

therefore only the weighting factors have to be chosen. For the final PD controller the following weighting factors where chosen.

$$\sigma_{\delta q} = 1 \tag{4.80}$$

$$\sigma_{\omega} = 10 \tag{4.81}$$

$$\sigma_{T_c} = 100 \tag{4.82}$$

The weighting factors are chosen according to relevance for the control loop. $\sigma_{\delta q}$ is the smallest value due to the fact that the exact control of the angle is not so important. σ_{ω} is bigger than the angle weight due to the fact that the angular rate is more relevant to be controlled. The control

weight σ_{T_c} is the biggest to allow a good robustness of the closed loop system and to lower the actuator activity. With these preconditions the steady state control gains become

$$\underline{\underline{K}}_{PD,c} = \begin{pmatrix} 0.1 & 0 & 0 & 0.8367 & 0 & 0 \\ 0 & 0.1 & 0 & 0 & 0.8367 & 0 \\ 0 & 0 & 0.1 & 0 & 0 & 0.8367 \end{pmatrix} \tag{4.83}$$

$$\underline{\underline{K}}_{PD,d} = \begin{pmatrix} 0.0966 & 0 & 0 & 0.8202 & 0 & 0 \\ 0 & 0.0966 & 0 & 0 & 0.8202 & 0 \\ 0 & 0 & 0.0966 & 0 & 0 & 0.8202 \end{pmatrix} \tag{4.84}$$

Here both control gains are shown. The first one is the solution for a continues systems $\underline{\underline{K}}_{PD,c}$ while the second one is the discrete control gain for a continues system with a sample time of $\Delta t = 0.5$ seconds. The discrete control gain will be used in the simulation due to the fact that the real controller will be executed as a discrete system. The duty cycle of 2 Hz was the specification of the BIRD and TET satellites and therefore it is the starting point.

The reason for the diagonal form of the control gain is the diagonal form of the moment of inertia tensor. Although the moment of inertia tensor is assumed to be diagonal it can take other values due to the fact that the design procedure of the control gain would stay the same. For the further studies the non diagonal form of the Moment of Inertia shall not be taken into account, but for a real control gain derivation it should be taken into account.

With the knowledge of a control gain the control loop can be closed and tested. As a proof of concept the ideal system behavior including the PD-controller toward a step function is shown in figure 4.7. It shows the step response of all system states with respect to a step in the control input. Here it can be seen that the controller itself is stable and can control the attitude and the angular rate under ideal conditions. After proofing the ideal stability of the PD-controller it is implemented inside the whole system simulator which includes the full system dynamics, disturbance torques and feedforward control. To ensure that only the attitude control behavior is investigated the attitude determination is skip temporary and ideal measurements are assumed.

The first test of the PD-controller is how it is reacting to a constant disturbing torque. Therefore a step function with a constant disturbing torque of

$$\underline{T_d} = [1\ 2\ 3]^T \cdot 10^{-4}\ \text{Nm} \tag{4.85}$$

was designed and executed at $t = 250$ seconds. The choice of the disturbances is far above the realistic estimates that were made in the second chapter. Therefore they can be seen as a worst case scenario. The reaction toward this step function can be seen in figure 4.8. It shows that the PD-controller is able to stabilize the system in about 50 seconds but at the same time an error steady state error in the angle can be see. This clearly shows the disadvantage of the PD-controller for high pointing accuracy which is necessary for payload activity. The PD controller is not able to drive the deviation angle to zero.

The next test shall show the ability to follow a guidance profile. Figure 4.9 shows the system reaction with a PD-controller towards a guidance profile. The applied guidance profile can be seen in figure 4.6. It can be seen that the PD-controller is able to follow the previous defined

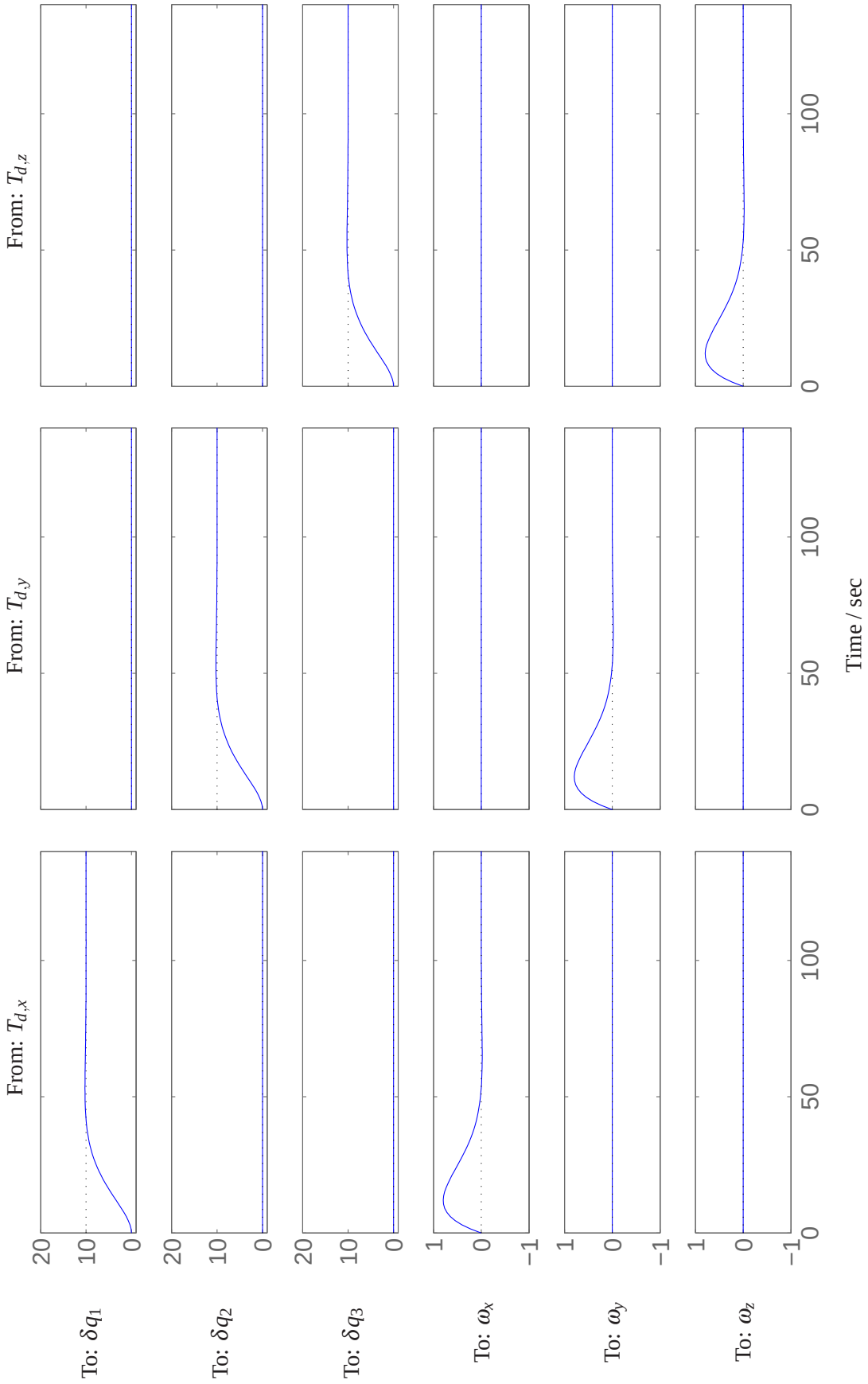

Figure 4.7: Step response of the ideal system with a PD-controller

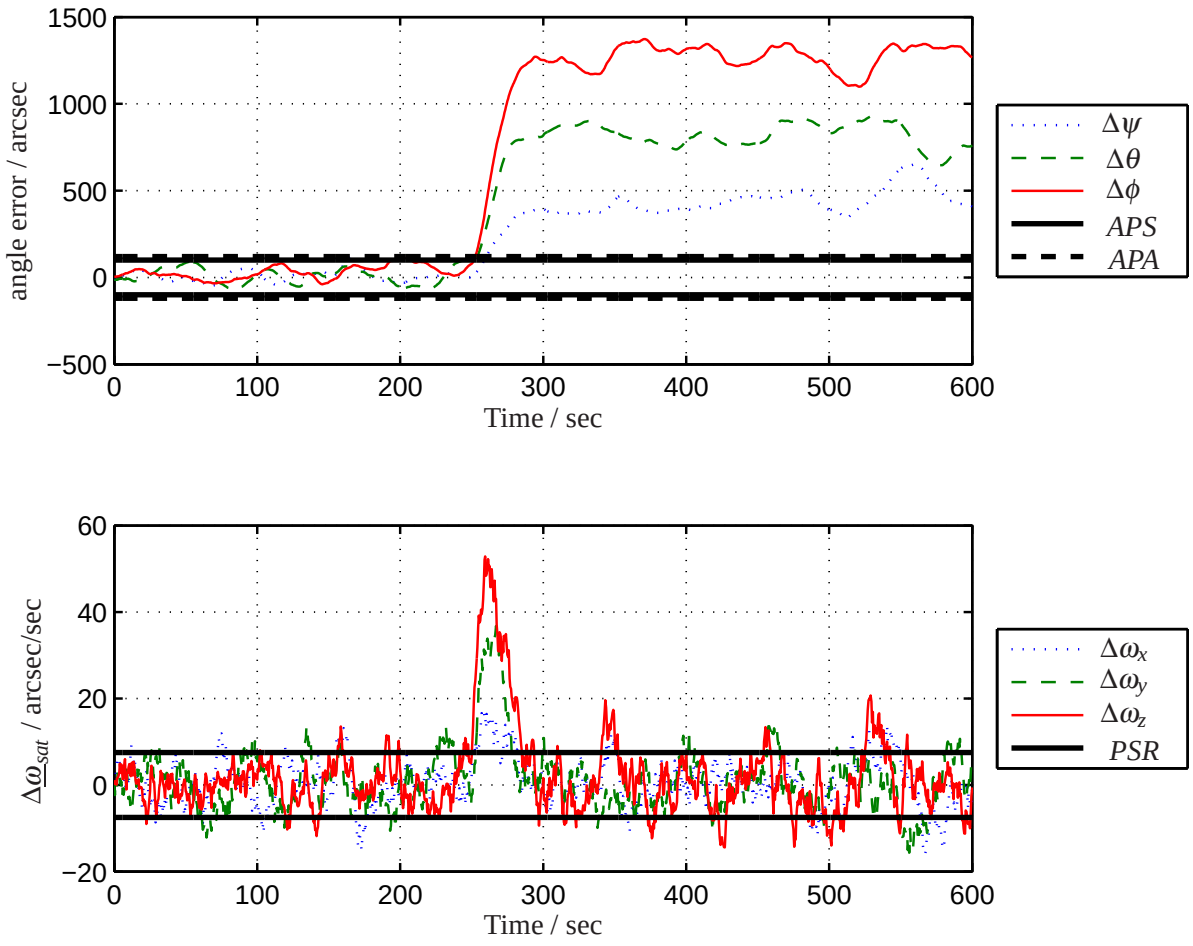

Figure 4.8: Response of the real system with a 2 Hz PD-controller toward a constant disturbance torque

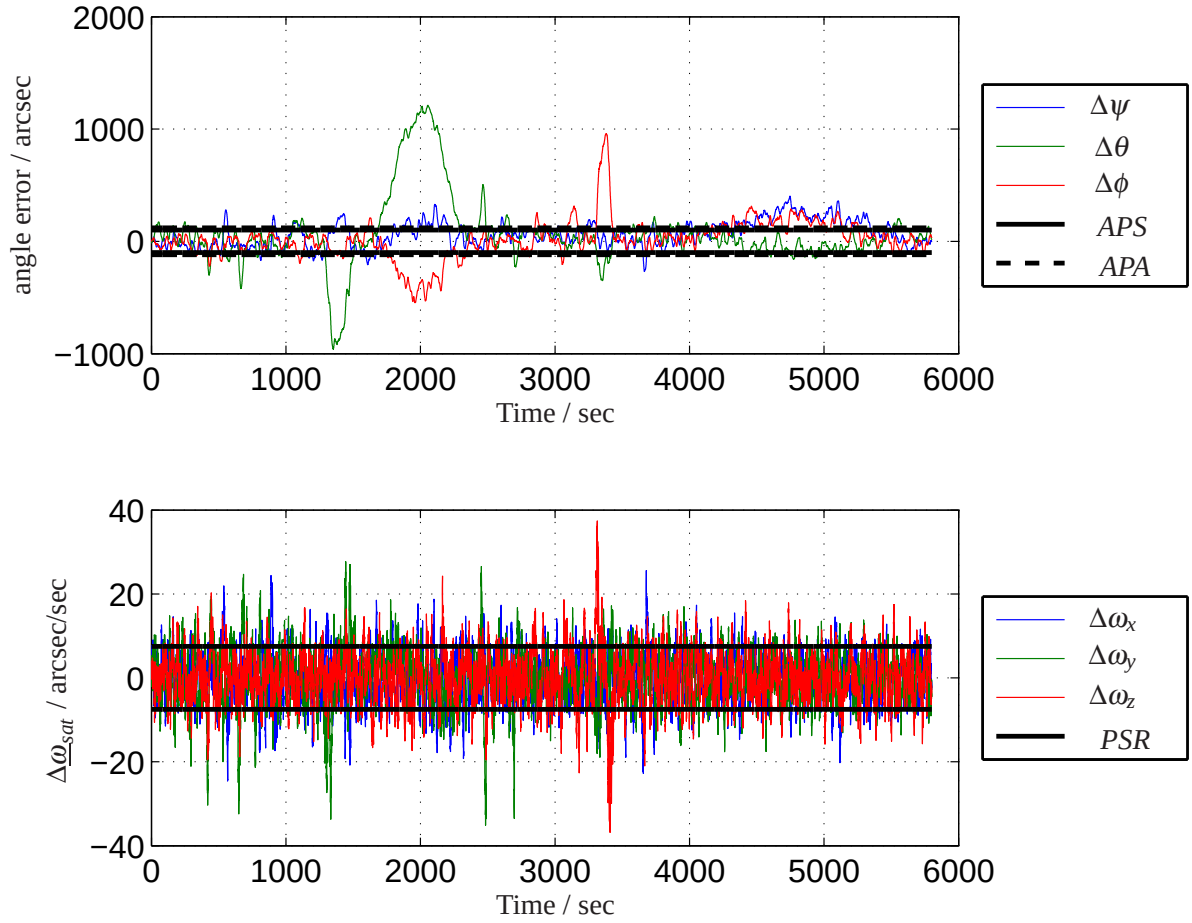

Figure 4.9: Ability of 2 Hz PD-controller to follow a guidance profile

guidance profile and keep the satellite in a stable state. The disadvantage is that the controller is not able to follow the profile good enough to fulfill the requirements.

Regarding to this the PD-controller is a robust controller that allows good control of the satellite but can not be used for the observation mode. Therefore another controller has to be investigated.

4.3.4.2 Proportional Integral Derivative Control

The biggest disadvantage of the PD-controller is the inability to fully compensate a constant disturbing torque. The solution to this problem is an integrating gain which leads to a proportional integral derivative controller (PID) that should be able to overcome this disadvantage of the PD-controller.

To be able to use the LQG approach the system dynamics have to be extended by an integrating state $\underline{e}$. This state should include the integral of the error quaternion. The system state is therefore defined as

$$\underline{x} = \begin{pmatrix} \Delta\underline{\delta q} \\ \Delta\underline{\omega} \\ \underline{e} \end{pmatrix} \tag{4.86}$$

With this new state the linearised system dynamics have to be extended in the following way.

$$\underline{\underline{A}} = \begin{bmatrix} 0 & 0 & 0 & 0.5 & 0 & 0 & 0 & 0 & 0 \\ 0 & 0 & 0 & 0 & 0.5 & 0 & 0 & 0 & 0 \\ 0 & 0 & 0 & 0 & 0 & 0.5 & 0 & 0 & 0 \\ 0 & 0 & 0 & 0 & 0 & 0 & 0 & 0 & 0 \\ 0 & 0 & 0 & 0 & 0 & 0 & 0 & 0 & 0 \\ 0 & 0 & 0 & 0 & 0 & 0 & 0 & 0 & 0 \\ 1 & 0 & 0 & 0 & 0 & 0 & 0 & 0 & 0 \\ 0 & 1 & 0 & 0 & 0 & 0 & 0 & 0 & 0 \\ 0 & 0 & 1 & 0 & 0 & 0 & 0 & 0 & 0 \end{bmatrix} \tag{4.87}$$

$$\underline{\underline{B}} = \begin{bmatrix} \underline{\underline{0}} \\ \underline{\underline{I}}_{sat}^{-1} \\ \underline{\underline{0}} \end{bmatrix} \tag{4.88}$$

It should be mentioned that for the control gain design only the first equation of the linear system dynamics (equation 4.58) has to be adapted. The upper left part of $\underline{\underline{A}}$ and the upper part of $\underline{\underline{B}}$ still stay the same as they are defined in the linearised system dynamics but they are extended about the integral part for $\Delta\underline{\delta q}$

The next step is the choice of two sufficient weighting matrices. For the PID-controller they are defined in the following way.

$$\underline{\underline{Q}} = \begin{bmatrix} I_{[3\times3]} \cdot \sigma_{\delta q} & 0 & 0 \\ 0 & I_{[3\times3]} \cdot \sigma_{\omega} & 0 \\ 0 & 0 & I_{[3\times3]} \cdot \sigma_{e} \end{bmatrix} \tag{4.89}$$

$$\underline{\underline{R}} = I_{[3\times3]} \cdot \sigma_{T_c} \tag{4.90}$$

The single σ values are defined as.

$$\sigma_{\delta q} = 1 \tag{4.91}$$
$$\sigma_{\omega} = 1000 \tag{4.92}$$
$$\sigma_{e} = 10 \tag{4.93}$$
$$\sigma_{T_c} = 10 \tag{4.94}$$

The choice of these values is addressing the fact that the angular rate error has highest priority. The angle itself is treated as less important and while the error integral of the error and the controller input are weighted in the same way. The control gains that were designed for this case are

$$\underline{\underline{K}}_{PID,c} = \begin{pmatrix} 6.9043 & 0 & 0 & 11.8923 & 0 & 0 & 1 & 0 & 0 \\ 0 & 6.9043 & 0 & 0 & 11.8923 & 0 & 0 & 1 & 0 \\ 0 & 0 & 6.9043 & 0 & 0 & 11.8923 & 0 & 0 & 1 \end{pmatrix} \tag{4.95}$$

$$\underline{\underline{K}}_{PID,2Hz} = \begin{pmatrix} 4.5902 & 0 & 0 & 8.2211 & 0 & 0 & 0.6395 & 0 & 0 \\ 0 & 4.5902 & 0 & 0 & 8.2211 & 0 & 0 & 0.6395 & 0 \\ 0 & 0 & 4.5902 & 0 & 0 & 8.2211 & 0 & 0 & 0.6395 \end{pmatrix} \tag{4.96}$$

where the discrete gain is for a sampling time of $\Delta t = 0.5$ s.

Figure 4.10 shows the ideal system response toward a step in the control inputs. This figure shows that a constant disturbance which is applied to the input is compensated completely and does not lead to any remaining error in the angel or angular rate. The expected results of this controller should therefore be better than for the simple PD-controller.

After implementing this controller inside the simulation environment it is tested with the same tests as it is done for the PD-controller. Figure 4.11 shows the step response of the real system towards the step at 250 seconds. The figure shows clearly that the PID controller compensates completely the constant disturbance and only a small peak in the angle deviation can be seen at 250 seconds. In addition to this the overall performance is much better than with the PD-controller. For completeness a possible guidance profile was simulated and it is shown in figure 4.12 that the 2 Hz PID-controller is able to follow this profile.

Although the 2 Hz PID-controller is better than the PD-controller it is not sufficient enough to guarantee the angular rate requirement. To solve this problem the duty cycle frequency is increased from 2 Hz to 5 Hz and a new discrete control gain is designed. The weighting matrices were not changed and the resulting gain is obtained.

$$\underline{\underline{K}}_{PID,5Hz} = \begin{pmatrix} 5.7975 & 0 & 0 & 10.1367 & 0 & 0 & 0.8273 & 0 & 0 \\ 0 & 5.7975 & 0 & 0 & 10.1367 & 0 & 0 & 0.8273 & 0 \\ 0 & 0 & 5.7975 & 0 & 0 & 10.1367 & 0 & 0 & 0.8273 \end{pmatrix} \tag{4.97}$$

Now the same tests are performed and it is shown that the angular rate deviation fulfill the requirements. Figure 4.13 shows the step response and figure 4.14 the guidance profile. In both figures it can be recognized that the requirements can be fulfilled. Although the angular rate deviation is sometimes penetrating the requirement values. These penetrating points are directly related to maneuvers which are not relevant for the observation mode.

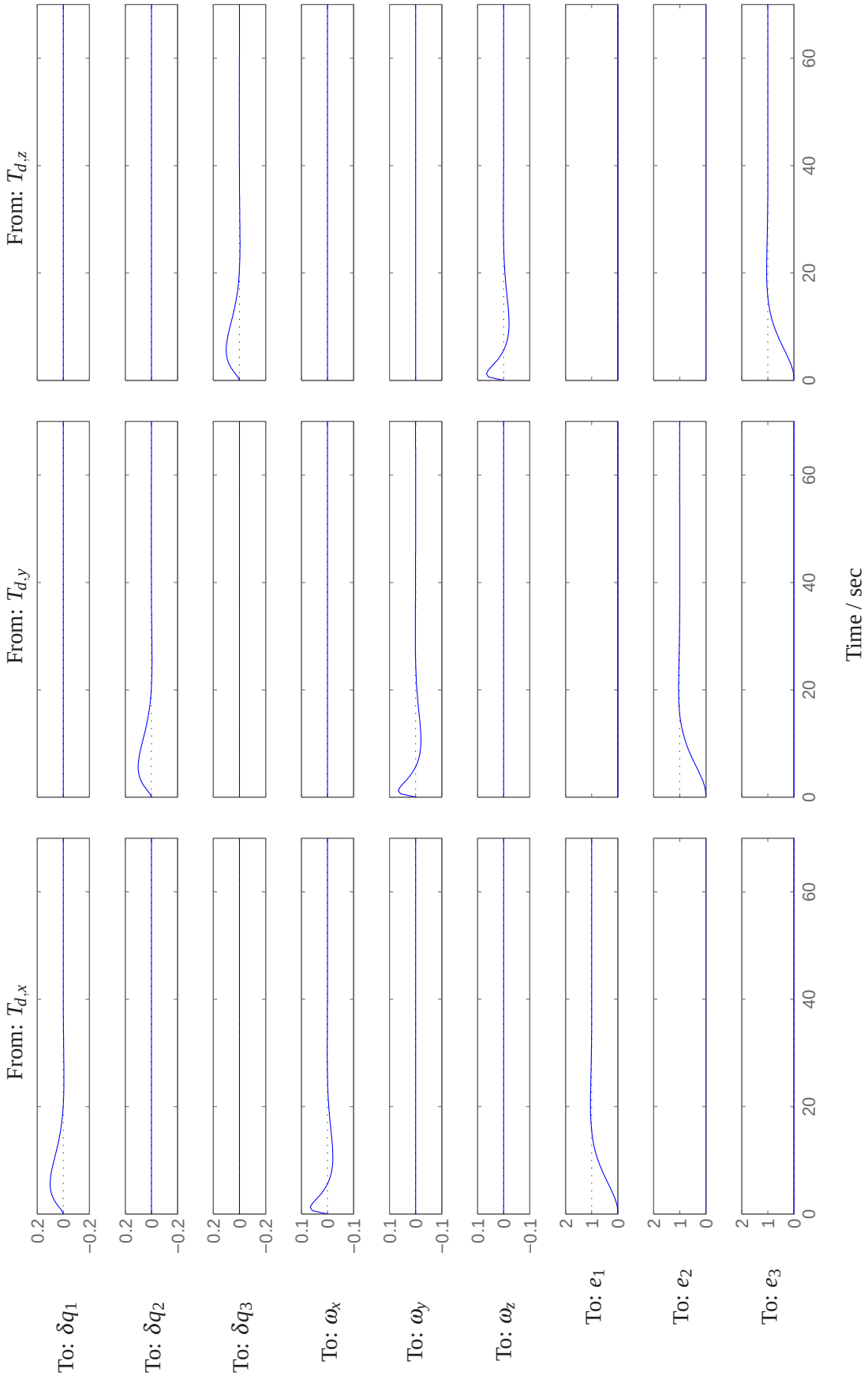

Figure 4.10: Step response of the ideal system with PID-controller

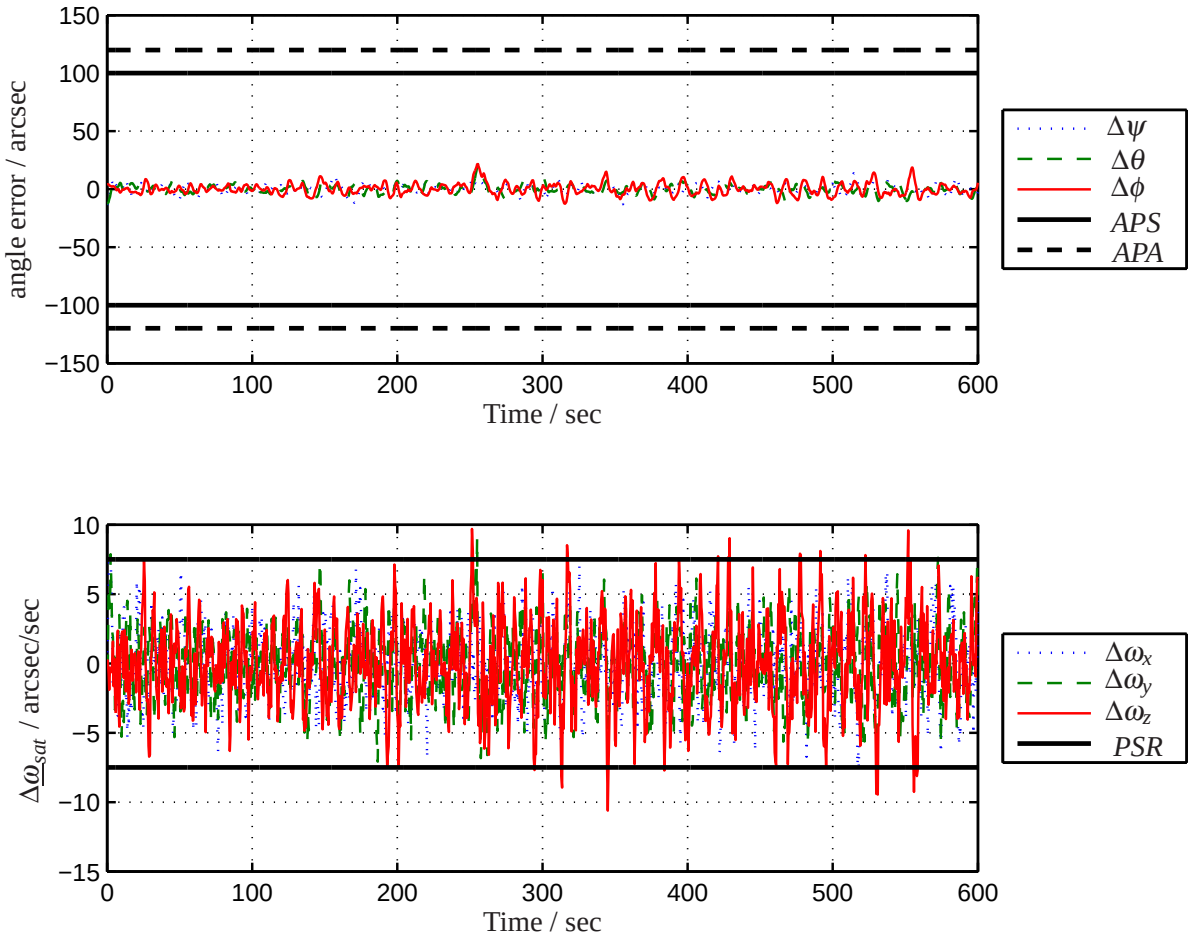

Figure 4.11: Response of the real system with a 2 Hz PID-controller toward a constant disturbance torque

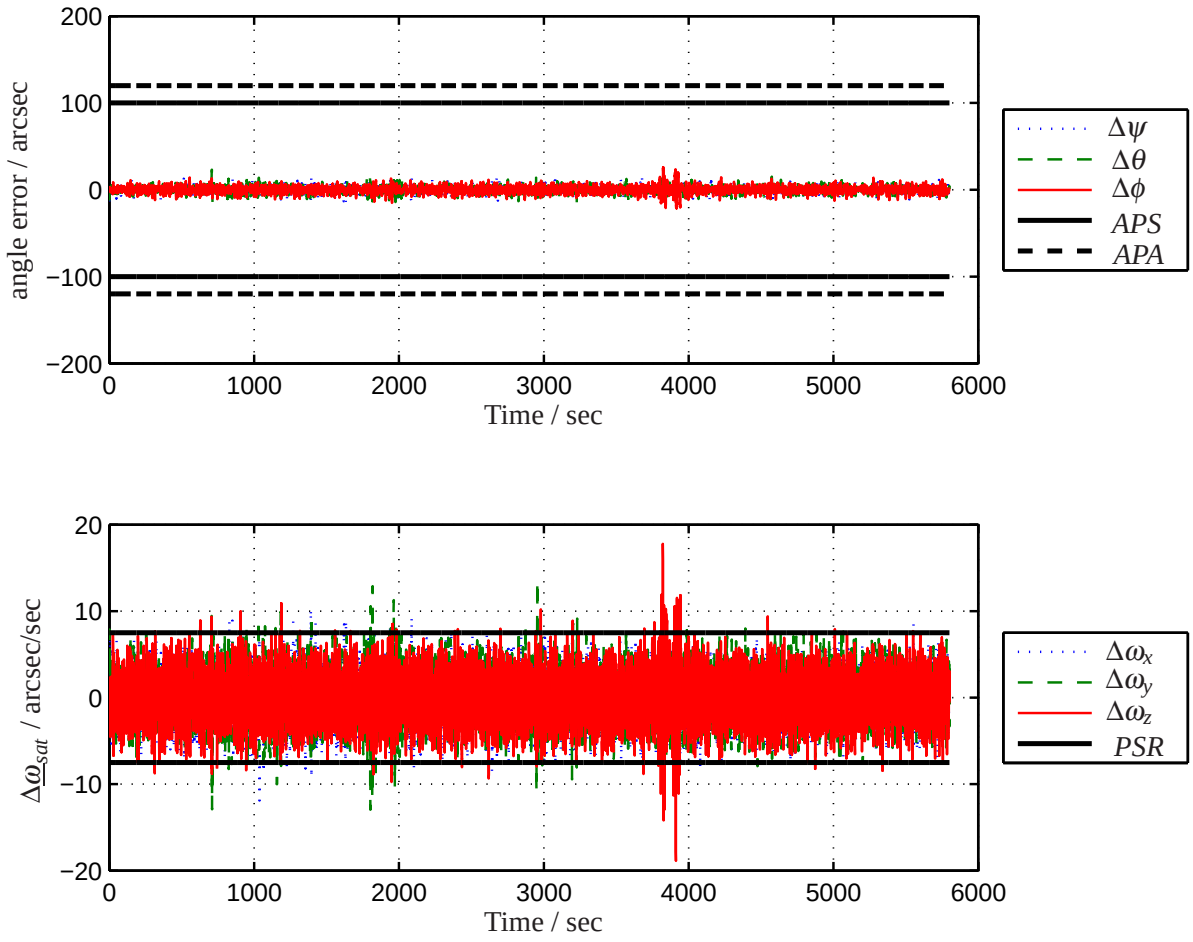

Figure 4.12: Ability of 2 Hz PID-controller to follow a guidance profile

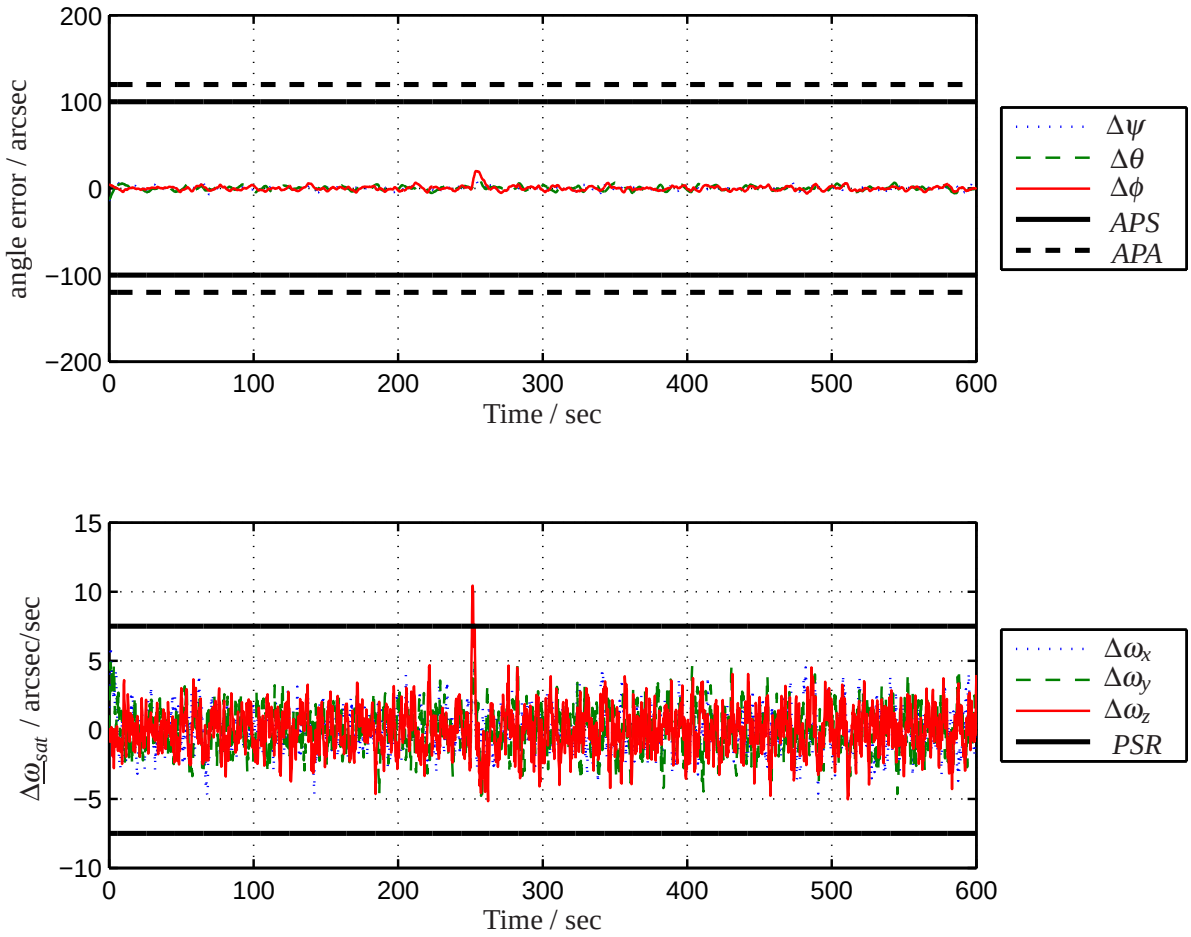

Figure 4.13: Response of the real system with a 5 Hz PID-controller toward a constant disturbance torque

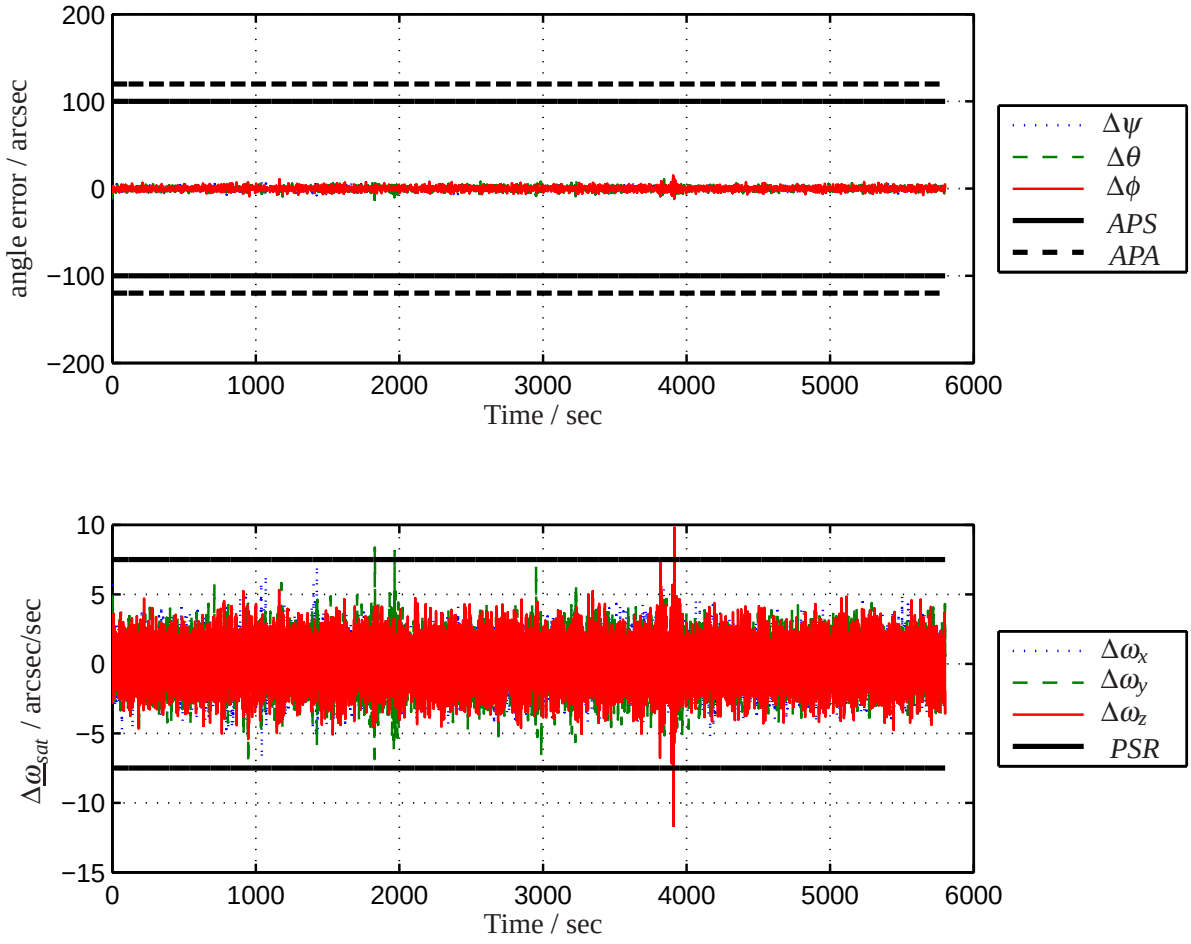

Figure 4.14: Ability of 5 Hz PID-controller to follow a guidance profile

4.3.5 Conclusion

The comparison of the three controllers can be achieved by the comparision of figuer4.9, 4.12 and 4.14. All figures show the attitude control errors during a guidance maneuver. It can be seen that from the three controllers PD-2Hz, PID-2Hz and PID-5Hz only the 5Hz PID-controller is able to fulfill the high pointing requirements. Therefore the logical choice it to use this controller to reach the primary mission goals. The stability of this controller is ensured by it design principal and it is implemented inside the control loop.

Chapter 5

Algorithm Tests

The following chapter is focused on the whole system tests. It describes the different test cases and its results.

The previous chapters were addressed to single aspects of the attitude control system for the AsteroidFinder/SSB mission. The remaining task is now to verify the functionality of the full attitude control system regarding to the combination of all single aspects.

To achieve the best possible results the attitude determination and attitude control should use the best algorithms that are available. Therefore the attitude control uses a proportional integral derivative state controller which was developed in chapter 4.3 and the attitude determination uses the unscented KALMAN filter from chapter 3.2. For all following tests the control loop is executed with a sampling time of 5 Hz and is equal to the attitude determination frequency.

The disturbances of the sensors and actuators are always taken into account. They are simulated as it is described in chapter 2. For the simulation only the reaction wheels, the star camera and the gyroscopes are used. This is equal to the best available sensor suite and should therefore give representative results.

5.1 Disturbance Cancellation

The worst case of a disturbance is a torque that appears as a step function therefore the system is simulated under this condition. To investigate the system behavior it is first simulated without any external disturbances. When the unscented KALMAN filter and the controller are in steady state a constant external disturbing torque of

$$\underline{\underline{T}}_d = [1 \cdot 10^{-4}, 2 \cdot 10^{-4}, 3 \cdot 10^{-4}]^T \text{Nm} \tag{5.1}$$

is applied at $t = 50$ seconds. This torque is above the maximum expected disturbing torque [16] and is therefore a valid test case. Figure 5.1 shows the resulting attitude control error. It can be seen that the system is reacting toward the disturbance with a deviation but it can be seen that it returns to the desired stable state after about 50 seconds. This result is longer than

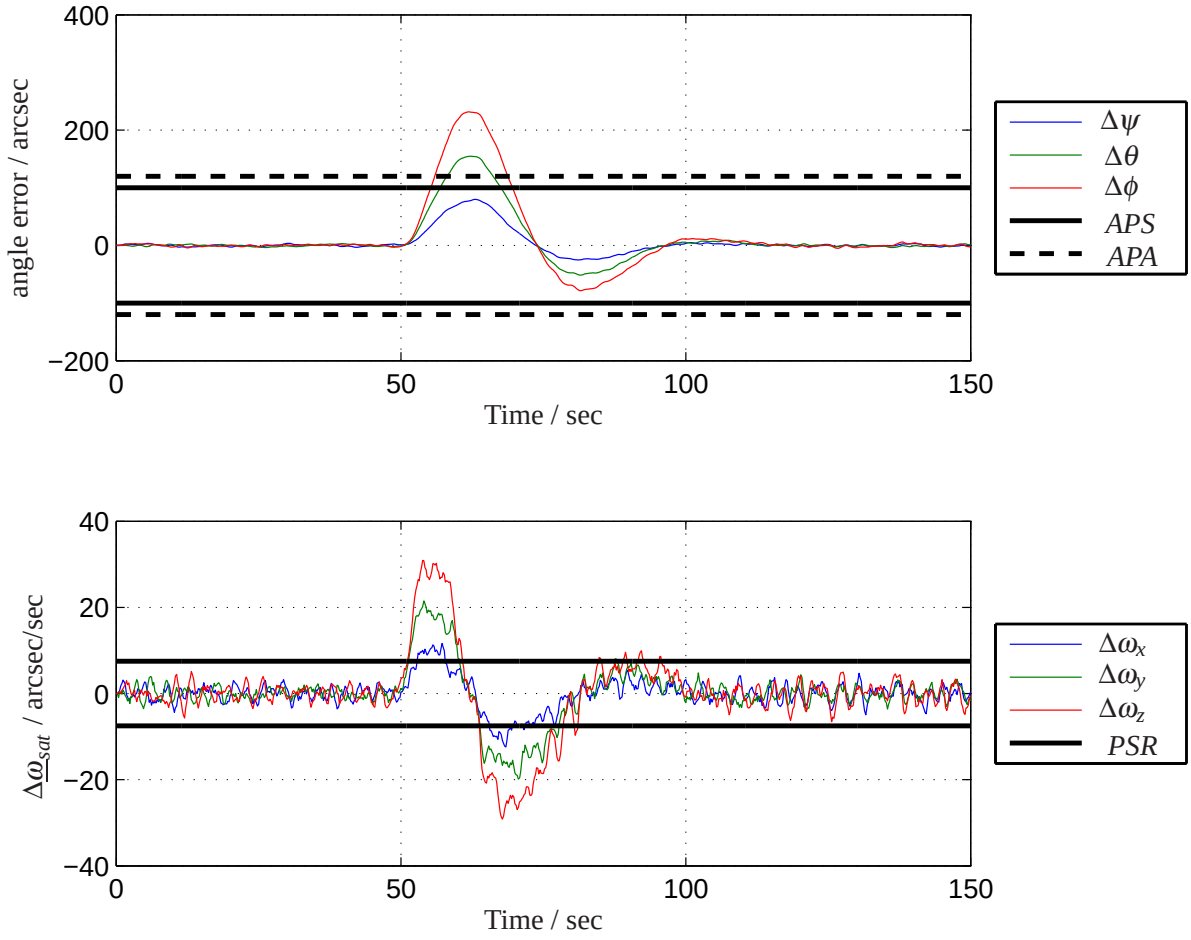

Figure 5.1: Control error for a step function

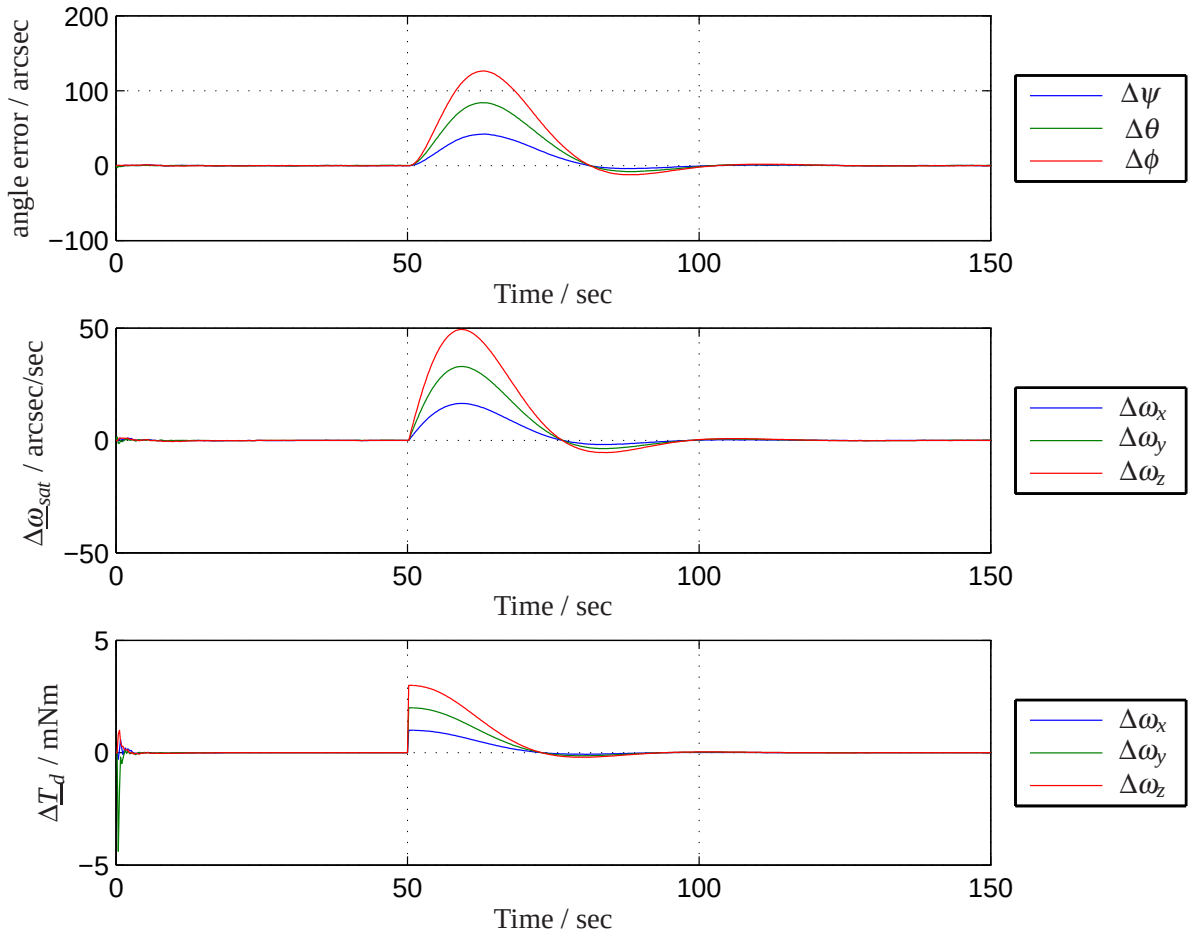

Figure 5.2: UKF response to a step function

it would be with an optimal attitude determination and attitude control. One reason is that the disturbance has to be realized by the attitude estimation algorithm, which has its own dynamic. The dynamic of the unscented KALMAN filter can be seen in figure 5.2. Here the deviation between the real and the estimated angle, the angular rate and the disturbance torque is shown. It can be seen that the UKF is not able to estimate the correct attitude directly after the step is applied. Further it can be seen that it takes about 50 seconds to return to steady state. This shows that the dynamic of the UKF is responsible for the attitude control deviation that is visible in figure 5.1.

If the dynamic of the UKF could be made faster it should be possible to reduce the attitude control error even more. Nevertheless this test shows that the designed system is able to withstand a disturbance and return to steady state.

5.2 Observation Mode

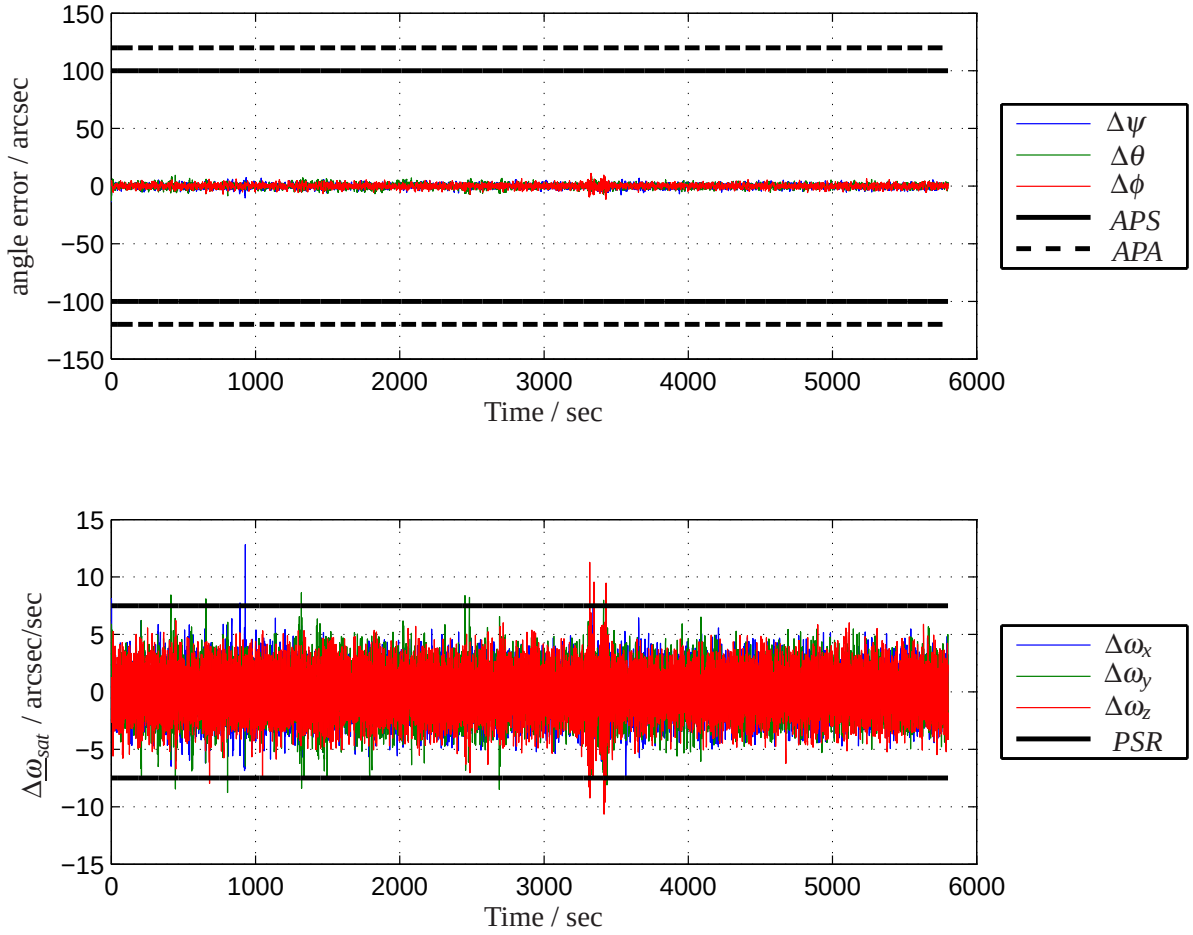

Figure 5.3: Attitude control error for a 5 Hz control loop with a PID control and UKF attitude determination

The observation mode is the main mode for the AsteroidFinder/SSB. During this mode the telescope payload is activated. To test this mode the desired observation profile of figure 4.6

was loaded while the simulated disturbances are acting on the satellite. The simulation was run for a whole orbit period and the resulting attitude deviation is shown in figure 5.3. Here it can be seen that the whole system is able to fulfill the requirements which are indicated as the 3σ boundaries. The angle deviation (upper diagram) is seen as no problem due to the fact that there is enough margin to the requirements. The challenge is still the pointing stability requirement which is shown in the lower diagram. It shows that the attitude controller in combination with the attitude estimator is able to reach the requirement nearly all the time. The times were the angular rate deviation is penetrating the 3σ boundary is directly related to a maneuver and is therefore not relevant for the actual observation. Nevertheless the pointing stability does not have that much margin. The main disturbances which are contributing to this pointing stability error are the disturbing torques of the reaction wheels. Therefore the behavior of the reaction wheels should be investigated in a precise way. The reaction wheels should operate at an angular rate where they produce as less disturbance as possible. Only on such it point it will be possible to reach the requirements. Nevertheless this simulation shows that it is a challenging but not impossible task to reach the requirements.

5.3 Ground Station Mode

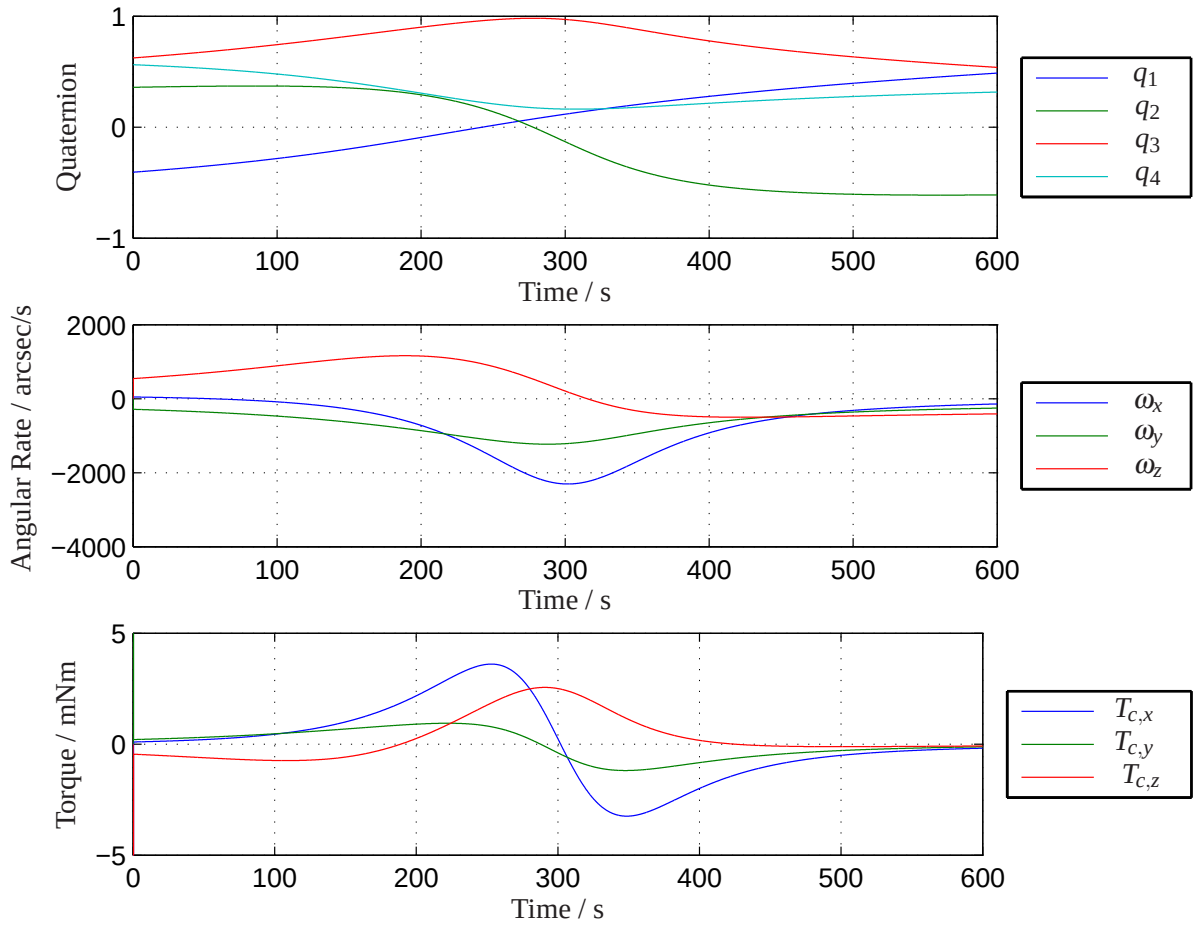

Figure 5.4: Guidance profile for a worst case ground station pointing

The last test is performed for a ten minute ground station pointing which is required for the high gain antenna and the secondary payload OSIRIS. The worst case ground station pointing is a direct pass over the ground station. During such a maneuver the angular rate is increasing during approaching to the ground station while it is decreasing when the satellite drifts away from it. The guidance for such a worst case scenario is shown in figure 5.4. This figure shows the desired quaternion, angular rate and angle. It was calculated following the procedure described in chapter 4.2.4. The maximum angular rate is reached at 300 seconds which indicates a direct pass over the ground station. At 300 seconds the ground station lies exactly on the sub satellite track which is the worst case ground station pointing scenario.

The resulting error of this maneuver is shown in figure 5.5. It can be seen that the deviation are nearly in the same range as they were for the other test cases. The high gain antenna requires only an absolute pointing of about 2° (3σ) which is easily meet by the control system. In fact the maximum pointing error is not bigger than 20 arc seconds, which is the requirement of the secondary payload OSIRIS. The ability to fulfill the requirements of the secondary payload

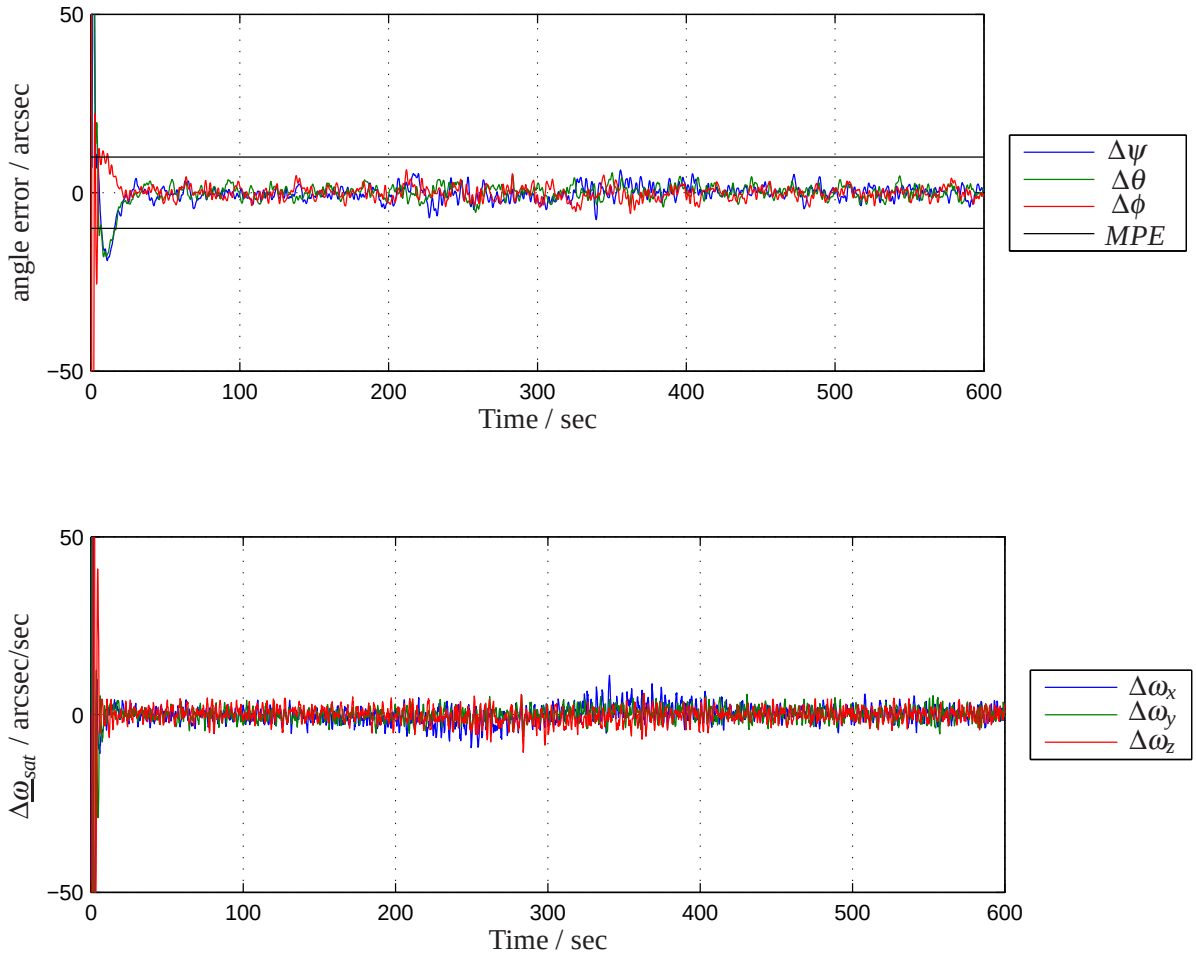

Figure 5.5: Attitude control error for a 5 Hz control loop with PID control and UKF attitude determination during ground station pointing

is an unexpected result. It was not expected that the ACS is able to follow a ground station pointing in such a good way. In a further study this fact should be investigated in more detail but from today's point of view it is possible to fulfill the requirements for all ground station

pointing scenarios.

5.4 Identified Issues

During the tests it was recognized that the system is able to fulfill all requirements in a sufficient way. Nevertheless there are a few issues that should be mentioned. At first the internal dynamic of the UKF algorithm is to slow to compensate a step function in a direct way. Out of this the attitude control error is drifting for a few seconds. It should be investigated if it is possible to ensure the same performance of the UKF but with a better internal dynamic.

The system was simulated with a 5 Hz control loop. The design should be investigated if it is possible to lower this frequency in some controller modes (e.g. during ground station pointing). If this is possible it would decrease the computing power and therefore it would consume less energy.

The whole simulation was performed with data that was accessible through the company fact sheets of the sensors and actuators producers. Regarding to this the simulation should be carried out with more detailed sensor and actuator data as soon as they are available.

The system itself is getting instable as soon as the resulting disturbing angular momentum is bigger than the angular momentum capacity of the reaction wheels. At this point the reaction wheels are going to saturation and they are no more able to compensate the disturbances. The solution to this issue is a desaturation strategy which will be applied by the magnetic torquers. Right now there is no magnetic attitude control system developed that will be combined with the previous defined control strategy. This has to be one of the next tasks.

The pointing stability is still the driving requirement. It was shown that it is in principal possible to reach this requirements but therefore a lot of single issues has to be addressed. The most important one is the detailed investigation of the reaction wheels. Their disturbance torques at different angular rates have to be investigated. The goal has to be to find an operating point where the disturbances of the reaction wheels are as low as possible.

Although these tasks should be addressed in further study the previous tests could show that the system is able to fulfill the requirements and its feasibility is shown.

Chapter 6

Summary

This diploma thesis is related to the Attitude Control System (ACS) the AsteroidFinder/SSB project. AsteroidFiner/SSB is a compact satellite with a mass of 130 kg. It is based on the Bi-Spectral-InfraRed-Detection (BIRD) satellite and the Technologieerprobungsträger (TET) that were build with contribution of the DLR.

The standard satellite bus (SSB) follows BIRD and TET and shall establish necessary capabilities and facilities for small satellite development. AsteroidFinder is the primary payload of the first SSB mission and will characterize the population of asteroids. Especially objects with an orbit completely inside the Earth's orbit are of interest. The detection will be done by an optical telescope. The task of detecting light weak objects places challenging requirements toward the attitude control system. Therefore a three axis stabilisation with four reaction wheels and a set of sensors for attitude determination was chosen during a Phase 0/A study.

Based on the results of this study this diploma thesis establishes a simulation environment to develop attitude determination and control algorithms. The simulation environment is realised with the help of Matlab/Simulink and includes attitude dynamics, sensor and actuator models and models for space environment.

Due to the fact that the attitude determination and control requirements are challenging two high precisions attitude determination algorithms are developed. The first one is an extended KALMAN filter (EKF) that estimates the state vector of the satellite. The second one is an unscented KALMAN filter (UKF) which is able to solve some of the EKF problems. Especially problems of nonlinearity can be covered in a more precise way by the UKF. Both filters are implemented inside the simulation and compared with each other. In the comparison it can be shown that the UKF outperform the EKF.

In a next task the guidance and attitude control problem is addressed. At first four different guidance strategies are derived. These are inertial target pointing, small angular maneuver, large angular maneuver and ground station pointing. Afterwards a controller is designed with the help of linear quadric GAUSSIAN (LQG) control. Due to the heritage of BIRD and TET the development of the control loop starts with a 2 Hz duty cycle. At first a simple PD-controller is developed and tested. It is shown that this controller does not fulfill the requirements. The next step is a PID-controller which gives a better accuracy but is still not sufficient enough. Therefor the duty cycle is raised to 5 Hz and tested with the PID controller. The combination of a 5 Hz duty cycle with a PID-controller is able to fulfill the requirements.

At the end the best algorithms of attitude determination and attitude control are combined and simulated. Here it is shown that the UKF in combination with the PID-controller is able to fulfill all requirements. Even the secondary payload requirement can be reached which is an unexpected result.

Therefore the functionality of the ACS toward the primary mission goal could be shown in this diploma thesis. All requirements can be fulfilled although it still will be a challenging task. This task can only be managed when there is detailed investigation of the components that are belonging to the ACS.

The further development of the AsteroidFinder/SSBs ACS should include a detailed test of the reaction wheels which where identified as the main disturbance driver. In addition to this the momentum management of the reaction wheels in combination with a magnetic attitude control should be investigated. In addition to this a save mode configuration and error management have to developed.

Nevertheless it can be said that the primary mission goal can be reached from the ACS point of view.

Bibliography

[1] Astro- und Feinwerktechnik Adlershof GmbH, Reaction Wheel RW90: For Small and Micro Satellites, Berlin, 2009.

[2] T. Bak, "Spacecraft Attitude Determination, a Magnetometer Approach," Ph.D. dissertation, Aalborg University, Department of Control Engineering, 1999.

[3] J. Bendisch, Raumfahrttechnik 2: Raumfahrtmissionen: Umdruck zur Vorlesung, Technische Universtität Braunschweig, Institut für Luft- und Raumfahrtsysteme, Braunschweig, SS 2005.

[4] ——, Raumfahrttechnik 1: Raumfahrttechnische Grundlagen: Umdruck zur Vorlesung, Technische Universtität Braunschweig, Institut für Luft- und Raumfahrtsysteme, Braunschweig, WS 2004/05.

[5] I. Bronstein and K. Semendjajew, Taschenbuch der Mathematik, 6th ed. Frankfurt am Main: Deutsch, 2006.

[6] J. Burl, Linear optimal control: H 2 and H ∞ methods. Menlo Park, Calif.: Addison-Wesley, 1999.

[7] J. Crassidis and F. Markley, "Unscented Filtering for Spacecraft Attitude Estimation," Journal of Guidance, Control, and Dynamics, vol. 26, no. 4, pp. 536–542, 2003.

[8] P. Fortescue and P. J. Stark, Spacecraft systems engineering, 3rd ed. Chichester: Wiley, 2003.

[9] S. Gerené and J. Behrens, Kompaktsatellit AsteroidFinder/SSB Delta Phase A: System Requirements, Deutsches Zentrum für Luft- und Raumfahrt e.V., Institut für Raumfahrtsysteme (Bremen), March 3rd, 2009.

[10] M. Grewal and A. Andrews, Kalman filtering: Theory and practice using MATLAB, 3rd ed. Hoboken, NJ: Wiley, 2008.

[11] T. Grundmann, B. Kazeminejad, P. Spietz, and S. Montenegro, Projekt Kompaktsatellit AsteroidFinder/SSB: Phase 0 Studie, Deutsches Zentrum für Luft- und Raumfahrt e.V., Institut für Raumfahrtsysteme (Bremen), 21.12.2007.

[12] M. Hallmann, Kompaktsatellit AsteroidFinder/SSB Delta Phase A: Coordinate Systems, Deutsches Zentrum für Luft- und Raumfahrt e.V., Institut für Raumfahrtsysteme (Bremen), January 1st, 2009.

[13] J. Hartmann and M. Lieder, Kompaktsatellit AsteroidFinder/SSB Delta Phase A: Structure and Accomodation, Deutsches Zentrum für Luft- und Raumfahrt e.V., Institut für Raumfahrtsysteme (Bremen), March 3rd, 2009.

[14] P. Hecker, Satellitennavigation: Technologien und Anwendungen: Umdruck zur Vorlesung, Technische Universtität Braunschweig, Institut für Flugführung, Braunschweig, WS 2007/08.

[15] A. Heidecker, M. Schlotterer, M. Hallmann, and T. Terzibaschian, Kompaktsatellit AsteroidFinder/SSB Delta Phase A: Attitude Control System: Temporary Specification, Deutsches Zentrum für Luft- und Raumfahrt e.V., Institut für Raumfahrtsysteme (Bremen), August 10th, 2008.

[16] ——, Kompaktsatellit AsteroidFinder/SSB Delta Phase A: Attitude Control System: Preliminary Design Report, Deutsches Zentrum für Luft- und Raumfahrt e.V., Institut für Raumfahrtsysteme (Bremen), March 5th, 2009.

[17] S. Julier, J. Uhlmann, and H. Durrant-Whyte, "A New Approach for Filtering Nonlinear Systems," Proceedings of the American Control Conference, pp. 1628–1623, 1995.

[18] S. Julier, "The Scaled Unscented Transformation," in Proceedings of the 2002 American Control Conference, ACC: May 8 - 10, 2002, Hilton Anchorage and Egan Convention Center, Anchorage, Alaska, USA. IEEE Service Center, 2002, pp. 4555–4559.

[19] S. Julier and U. Jeffrey, "Unscented filtering and nonlinear estimation," PROCEEDINGS OF THE IEEE, 2004.

[20] R. Kálmán, "A New Approach to Linear Filtering and Prediction Problems," Transactions of the ASME-Journal of Basic Engineering, vol. 82, pp. 35–54, 1960.

[21] E. Kührt, S. Mottola, N. Schmitz, H. Michaelis, and K. Scheibe, Kompaktsatellit AsteroidFinder/SSB Delta Phase A: AsteroidFinder Payload, Deutsches Zentrum für Luft- und Raumfahrt e.V., March 3rd, 2009.

[22] LITEF GmbH, μFORS-6U: Upgraded Fiber Optic Rate Sensor, Freiburg, Germany, 17.02.2006.

[23] B. Lübke-Ossenbeck, "Lageregelung für Mikrosatelliten," Ph.D. dissertation, Technische Universität Berlin, Berlin, 1996.

[24] J. Lunze, Mehrgrößensysteme, digitale Regelung: Mit 53 Beispielen, 91 Übungsaufgaben sowie einer Einführung in das Programmsystem MATLAB, 4th ed., ser. Springer-Lehrbuch. Berlin: Springer, 2006, vol. 2.

[25] H. Lutz and W. Wendt, Taschenbuch der Regelungstechnik: Mit MATLAB und Simulink, 7th ed. Frankfurt am Main: Deutsch, 2007.

[26] O. Matthews and P. Graven, Magnetic Torquers: for Spacecraft Attitude Control, ZARM Technik AG and Microcosm Inc., Bremen.

[27] ——, Magnetometers: for Spacecraft Attitude Determination, ZARM Technik AG and Microcosm Inc., Bremen.

[28] O. Montenbruck and E. Gill, Satellite orbits: Models, methods, and applications, 3rd ed. Berlin: Springer, 2005.

[29] M. Mortensen and J. Jorgensen, μ-Advanced Stellar Compass: General Information, Technical University of Denmark, Alborg, 01.04.2005.

[30] P. G. Ostermeyer, Stabilität, Kinematik und Kinetik, Schwingungen, Stoß, 1st ed., ser. Braunschweiger Schriften zum Maschinenbau. Braunschweig: Fachbereich Maschinenbau der TU Braunschweig, 2002, vol. 2.

[31] M. Schlotterer, Robuste Schätzung und Sensorfusion zur Navigation von wiederverwendbaren Raumtransportern, 1st ed. Göttingen: Cuvillier, 2008.

[32] L.-I. SDA, Configuration of 4Pi Sun Sensor Systems: OOV - TET - 1, Berlin, 20.08.2008.

[33] J. M. Sidi, Spacecraft dynamics and control: A practical engineering approach, ser. Cambridge aerospace series. Cambridge: Cambridge Univ. Press, 1997, vol. 7.

[34] P. Spietz and J. Behrens, Kompaktsatellit AsteroidFinder/SSB Delta Phase A: Mission Requirements, Deutsches Zentrum für Luft- und Raumfahrt e.V., Institut für Raumfahrtsysteme (Bremen), March 4th 2009.

[35] S. Theil and M. Wiegand, "High Accuracy Attitude Determination and Control of the DIVA Mission," in Spaceflight mechanics 1999: Proceedings of the AAS/AIAA Space Flight Mechanics Meeting held February 7 - 10, 1999, Breckenridge, Colorado, ser. Advances in the astronautical sciences, R. Bishop, Ed., vol. 102. Univelt, 1999, pp. 943–960.

[36] TNO Science and Industry, Commercial Off The Shelf sensors: Mini-FSS, Delft, The Netherlands, 25.06.2008.

[37] P. Vörsmann, Regelungstechnik 1: Umdruck zur Vorlesung, Technische Universtität Braunschweig, Institut für Luft- und Raumfahrtsysteme, Braunschweig, WS 2004/05.

[38] A. E. Wan and R. van der Merwe, "The Unscented Kalman Filter for nonlinear estimation," PROCEEDINGS OF SYMPOSIUM 2000 ON ADAPTIVE SYSTEMS FOR SIGNAL PROCESSING, COMMUNICATION AND CONTROL, pp. 153–158, 2000.

[39] ——, "Chapter 7: The unscented Kalman filter," KALMAN FILTERING AND NEURAL NETWORKS, pp. 221–280, 2001.

[40] A. E. Wan, R. van der Merwe, and T. A. Nelson, "Dual Estimation and the Unscented Transformation," IN NEURAL INFORMATION PROCESSING SYSTEMS, vol. 12, pp. 666–672, 2000.

[41] R. J. Wertz, Space mission analysis and design: [SMAD III], 3rd ed., ser. Space technology library. Torrance, Calif.: Microcosm Press [u.a.], 1999, vol. 8.

[42] ——, Spacecraft attitude determination and control, reprint ed., ser. Astrophysics an. Dordrecht: Kluver Acad. Publ, 2002, vol. 73.

[43] B. Wie, Space vehicle dynamics and control, ser. AIAA education series. Reston, Va.: American Institute of Aeronautics and Astronautics, 1998.

List of Figures

List of Tables

Appendix A

Zusammenfassung

Die vorliegende Diplomarbeit wurde im Rahmen des AsteroidFinder/SSB Projektes des Deutschen Zentrums für Luft- und Raumfahrt e.V. (DLR) erstellt. Sie bezieht sich dabei auf das Lageregelungssystem des Satelliten AsteroidFinder/SSB.

Der AsteroidFinder/SSB ist ein Kompaktsatellit mit einer Gesamtmasse von 130 kg. Er basiert auf den Entwicklungen und Erkenntnissen die bereits mit dem Bi-Spectral-InfraRed-Detection (BIRD) und dem Technologierprobungsträger (TET) Satelliten gesammelt wurden. Beide Satelliten wurden bzw. werden in Zusammenarbeit mit dem DLR entwickelt. BIRD wurde bereits im Oktober 2001 gestartet während sich TET derzeit in Phase C befindet.

Aufbauend auf diesen beiden Satelliten entstand die Idee einen Standard Satelliten Buss (SSB) zu entwickeln. Dieser soll dazu dienen DLR Instituten einen möglichst leichten Zugang zum Weltraum zu verschaffen und aus diesem Grund eine möglichst breite Palette an Anforderung erfüllen.

Anfang 2007 wurde die von der Programmdirektion des DLR ein interner “Call for Papers” durchgeführt in welchem eine Nutzlast für den ersten SSB gesucht wurde. Als Gewinner ging daraus der AsteroidFinder/SSB hervor.

AsteroidFinder soll dazu eingesetzt werden Asteroiden zu detektieren, die sich vollständig innerhalb des Erdorbits befinden. Dies geschieht mit Hilfe eines sehr empfindlichen Teleskops, welches als Nutzlast auf dem SSB untergebracht ist. Das Aufspüren lichtschwacher Objekte, wie z.B. Asteroiden, erfordert ein sehr genaues ausrichten und stabilisieren des Teleskops. Aus diesem Grund werden für die AsteroidFinder/SSB Mission sehr hohe Anforderungen an das Lageregelungssystem des Satelliten gestellt. Wobei der treibende Faktor die sogenannte Pointing Stabilität von < 7,5 ”/s ist.

Neben der Primärnutzlast wird in dieser Arbeit auch die Anforderung der potentiellen sekundär Nutzlast OSIRIS (Optical high speed infra red link system for low earth orbit satellites) berücksichtig. OSIRIS ist ein Technologiedemonstrator und soll eine optische Datenverbindung zwischen Bodenstation und Satellit herstellen. Dazu sollte das Lageregelungssystem eine maximale Abweichung von 20” zur geforderten Lage nicht überschreiten.

Durch eine vorangegangen Phase 0/A Studie wurde ein erstes Design für den AsteroidFinder/SSB festgelegt. Aufbauend auf diesen Ergebnissen wird in dieser Diplomarbeit die Entwicklung der Algorithmen vorangetrieben, welche für das Erfüllen der primären Mission benötigt werden.

Dazu wird zunächst eine neue Simulationsumgebung entwickelt, welche mit Hilfe von Matlab/Simulink realisiert wird. In dieser Umgebung wird zunächst die Lagedynamik des Satelliten realisiert. Gleichzeitig werden typische Lagebestimmungssensoren und Lageregelungsaktuatoren erläutert und deren mathematische Modelle entwickelt. Weiterhin werden erste Störmomente simuliert und integriert. Die Simulation der Störmomente nutzt dabei bereits entwickelte Modelle und schließt vorhandene Lücken. Bei der Umsetzung dieser Modelle wird darauf geachtet, sie möglichst allgemein zu halten, so dass sie in eine Simulationsbibliothek einfliesen können.

Nachdem die Simulationsumgebung entwickelt ist, wird sich auf das Gebiet der Lagebestimmung konzentriert. Hierbei wird sich auf sogenannte KALMAN Filter konzentriert. Da der Satellit ein nichtlineares System ist, wird zunächst ein Extended KALMAN Filter (EKF) entwickelt. Dieser EKF schätzt den eigentlichen Zustandsvektor des Satelliten mit Hilfe eines Fehlerzustandsvektors, wodurch eine präzise Lagebestimmung ermöglicht wird. Als Vergleich zum EKF wird eine relativ neu Erweiterung innerhalb der KALMAN Filter betrachtet. Dieser Unscented KALMAN Filter (UKF) ist in der Lage Nichtlinearitäten eines Systems besser abzubilden und somit eine höhere Genauigkeit zu erreicht. Sowohl der EKF wie auch der UKF werden theoretisch erläutert und anschließend in die Simulationsumgebung integriert. Die abschließenden Vergleichstests beider Filter zeigen, dass der UKF den EKF übertrifft und tatsächlich bessere Ergebnisse liefert.

Der nächste Bereich dieser Arbeit bezieht sich auf die Flugführung des Satelliten. Ihre Aufgabe ist das Bereitstellen eines gewünschten Zustandsvektors für die Lageregelung. Es werden hierzu inertiales Ausrichten, inertiale Manöver so wie der Kontakt zur Bodenstation behandelt. Für jedes dieser Szenarien werden Führungstrajektorien entwickelt und ebenfalls implementiert.

Nach der Entwicklung der Lagebestimmung und Flugführung erfolgt die Auslegung der Lageregelung. Diese stützt sich dabei ausschließlich auf vier Reaktionsräder, welche als Aktuatoren vorgesehen sind. Die Lageregelung selbst wird als Zustandsregelung entworfen, wobei sich auf Methoden der Linear Quadratischen Regelung bezogen wird. Hierzu wird zunächst das Satelliten System um einen Arbeitspunk linearisiert und die nichtlinearen Terme durch eine Vorsteuerung kompensiert. Auf dem linearisierten System werden ein Proportional Derivative Regler (PD) und Proportional Integral Derivative Regler (PID) untersucht. Zunächst wird ein Regeltakt von 2 Hz vorgeschlagen, wobei sich allerdings zeigt das sowohl PD wie auch PID nicht in der Lage sind die Anforderungen zu erfüllen. Aus diesem Grund wird der Regeltakt auf 5 Hz erhöht. Wodurch der PID Regler in der Lage ist den Anforderungen gerecht zu werden.

Das letzte Kapitel widmet sich der gesamt Simulation. Hier werden die beiden besten Algorithmen für Lagebestimmung (UKF) und Lageregelung (5Hz PID) miteinander kombiniert und verschiedenen Tests unterzogen. Es zeigt sich das diese Kombination in der Lage ist sämtliche Anforderungen zu erfüllen. Erstaunlicherweise kann sogar die Anforderung der Sekundärnutzlast OSIRIS als machbar eingestuft werden. Allerdings muss für das Erreichen dieser Anforderungen das Verhalten der einzelnen Aktuatoren und Sensoren möglichst genau bekannt sein.

Abschließen lässt sich sagen das mit dem Ende dieser Diplomarbeit eine Simulationsumgebung geschaffen wurde die eine weitere Entwicklung des AsteroidFinder/SSB Lageregelungssystems ermöglicht und seine Machbarkeit im Bezug auf die Anforderungen nachweißt.

Appendix B

Software

The following describes the main files that are responsible for the Attitude Control System Simulator. A more detailed documentation is found inside the Simulator itself.

File	Description
start.m	Main script to load the Attitude Control System Simulator.
start_path.m	Adds all needed path definitions to Matlab (not permanent)
start_parameter.m	Definition of the general parameters (e.g. mass, orbit, controller)
KALMAN_filter_parameter.m	Definition of the tuning parameter for the EKF and UKF
\..\mdl _files\ACS _simulator.mdl	Main simulink file of the Attitude Control System Simulator
\..\SpaceLib	Simulink library that is needed to execute the Simulator
\..\Subproject _ControllerDesign	m-files for different controller designs
\..\Subproject _Guidance	m-files for guidance development
\..\Subproject _Movie	m-files to create a short movie of the satellite from the simulator data
\..\Subproject _Raytrace	m-files to create the lookup tables for aerodynamic and solar radiation
\..\Subproject _UKF	Development folder of the EKF and UKF algorithm

Appendix C

Coordinate Systems

The following chapter describes the coordinate systems that are used inside the simulation environment. It is based on the coordinate systems document [12] of the AsteroifFinder/SSB project.

C.1 Mechanical Coordinate Frame (MCF)

The Mechanical Coordinate Frame (MCF) is a right hand oriented spacecraft body fixed system and directly related to the Structural Coordinate Frame (SCF) which is defined in [12]. SCF and MCF are only having another origin. The MCF is defined by:

- Origin - Satellite center of mass
- $+X_{MCF}$ - building a right handed orthogonal system
- $-Y_{MCF}$ - is perpendicular to the body fixed solar panel and is pointing “outwards”, i.e. from the geometric center of the satellite through the undeployed solar panel;
- $+Z_{MCF}$ - is perpendicular to the launcher adapter and is pointing from the geometric center into the direction of the payload segment (i.e., in launch configuration pointing away from the launcher adapter);

Center of Mass will change during design and maybe also during mission life time (deployable parts or consumables).

C.2 Principal Axes Body Fixed Frame (BF)

Because the moment of inertia tensor is a real-symmetric matrix, it has always three orthogonal eigenvectors and eigenvalues. The three eigenvalues are the principal moments of inertia. It can be shown that the principal MOIs include always the maximum and the minimum inertia. The corresponding three eigenvectors are building the new reference frame. At that point only three axes are defined, but it is not clear which one is X_{BF}. X_{BF} shall be the one which has the smallest angle to X_{SCF}. Y_{BF} and Z_{BF} building a right handed system.

- Origin - Satellites center of mass
- $+X_{BF}$ - Principal axis closest to X_{SCF}
- $+Y_{BF}$ - Principal axis building a right handed system
- $+Z_{BF}$ - Principal axis building a right handed system

For solving the dynamic equations the principal axes frame will be used. Center of mass and principal axes will change during design and maybe also during mission life time (deployable parts or consumables). Therefore ACS has to know the deployment status. It will be indicated in the ACS satellite configuration by a suitable set of deployment flags.

C.3 Earth Centered Fixed Frame (ECF)(WGS)

As Earth centered frame the WGS 84 frame will be used.

- Origin - Earths center of mass.
- $+X_{WGS}$ - It is located in the IERS Reference Meridian (IRM) and is normal to $+Z_{WGS}$, also called Greenwich
- $+Y_{WGS}$ - Building a right handed orthogonal system
- $+Z_{WGS}$ - The direction of the IERS Reference Pole (IRP), also called earth rotation axis

C.4 True Equinox and Equator of Date (TOD)

The TOD system is an Earth centered inertial reference frame, which is aligned with the true equator and equinox at the time of consideration.

- Origin - Earth Center of Mass
- $+X_{TOD}$ - Points into the direction of true vernal equinox at the concerned time
- $+Y_{TOD}$ - Building a right handed orthogonal system
- $+Z_{TOD}$ - Parallel to the instantaneous rotation axis of the Earth

Appendix D

Work Breakdown Structure

Development of algorithms for attitude determination and control of the AsteroidFinder satellite

WP 1	WP 2	WP 3	WP 4	WP 5	WP 6	WP 7
Orientation to the actual project state	**Development of a simulation in Matlab/Simulink for attitude control**	**Development of an attitude determination algorithm**	**Test of the attitude determination algorithm with the simulation**	**Development of an attitude control algorithm**	**Performance analysis of the attitude control in the closed loop simulation**	**Documentation**
Creating project schedule, WPD, WBS	Importing useful models to the simulation	Investigating existing KALMAN-Filters	Test functionality of the algorithm	Investigation of existing attitude control algorithms	Investigate performance of the developed control algorithm w.r.t. the requirements	Creating a LaTeX template
Reading Phase 0/A documentation	Creating simulated space environment	Preparing dynamics equation to be used in such a KALMAN-Filter	Investigate accuracy of the attitude determination	Developing of a control algorithm for inertial pointing w.r.t. an optical payload	Investigate the behaviour of the algorithm under irregular conditions	Creating a bibliography database
Literature research	Creating sensor models	Implementing dynamics equation in the algorithm	Analyse performance w.r.t. other attitude determination technologies	Developing of a guidance algorithm for target pointing	Compare performance to the performance of other satellite systems	Writhing thesis report
Investigation of existing Matlab/Simulink models	Creating actuator models	Implementing attitude determination algorithm to the simulation		Create and implementing of a control algorithm for target pointing		Preparing final presentation

Appendix E

Work Package Description

Development of algorithms for attitude determination and control of the AsteroidFinder satellite		**WP 1**
Title	**Orientation to the actual project state**	**Page:** 1 of 1
Responsible	Ansgar Heidecker	**version:** 1.0
		Date: 23.03.2009
Start	T0	
End	T0 + 4 days	**Duration:** 4 days
Working person	Ansgar Heidecker	

Goals:

- Gain knowledge of the project

Input

- Phase 0/A Documentation

Interfaces to other work packages

- Basis for all work packages

Tasks

- Creating project schedule, WPD, WBS
- Reading Phase 0/A documentation
- Literature research
- Investigation of existing Matlab/Simulink models

Results

- Understanding of the project and actual state of it
- Literature database
- Information for the technical report

Development of algorithms for attitude determination and control of the AsteroidFinder satellite		**WP 2**
Title	**Development of a simulation in Matlab/Simulink for attitude control**	**Page:** 2 of 1
Responsible	Ansgar Heidecker	**version:** 1.0
		Date: 23.03.2009
Start	T0 + 4 days	
End	T0 + 21 days	**Duration:** 17 days
Working person	Ansgar Heidecker	

Goals:

- Setup a basic simulation environment
- Setup a basic semolina library

Input

- Phase 0/A Documentation
- Literature form WP_1
- Models from WP_1

Interfaces to other work packages

- WP_1

Tasks

- Importing useful models to the simulation
- Creating simulated space environment
- Creating sensor models
- Creating actuator models

Results

- Basic simulation environment
- Basic semolina library
- Information for the technical report

Development of algorithms for attitude determination and control of the AsteroidFinder satellite		**WP 3**
Title	**Development of an attitude determination algorithm**	**Page:** 3 of 1
Responsible	Ansgar Heidecker	**version:** 1.0
		Date: 23.03.2009
Start	T0 + 21 days	
End	T0 + 41 days	**Duration:** 20 days
Working person	Ansgar Heidecker	

Goals:

- Define a suitable attitude determination algorithm

Input

- Phase 0/A Documentation
- Basic simulation environment form WP_2

Interfaces to other work packages

- WP_2

Tasks

- Investigating existing KALMAN-Filters
- Preparing dynamics equation to be used in such a KALMAN-Filter
- Implementing dynamics equation in the algorithm
- Implementing attitude determination algorithm to the simulation

Results

- Mathematical description of an attitude determination algorithm
- Implementation of the algorithm in Simulink
- Information for the technical report

Development of algorithms for attitude determination and control of the AsteroidFinder satellite		**WP 4**
Title	**Test of the attitude determination algorithm with the simulation**	**Page:** 4 of 1
Responsible	Ansgar Heidecker	**version:** 1.0
		Date: 23.03.2009
Start	T0 + 41 days	
End	T0 + 56 days	**Duration:** 15 days
Working person	Ansgar Heidecker	

Goals:

- Evaluate performance and ensure functionality of the attitude determination

Input

- Phase 0/A Documentation
- Attitude determination algorithm from WP_3
- Simulation environment form WP_2

Interfaces to other work packages

- WP_2
- WP_3

Tasks

- Test functionality of the algorithm
- Investigate accuracy of the attitude determination
- Analyse performance w.r.t. other attitude determination technologies

Results

- Performance characteristic of the algorithm
- Defined test cases for attitude determination
- Information for the technical report

Development of algorithms for attitude determination and control of the AsteroidFinder satellite		**WP 5**
Title	**Development of an attitude control algorithm**	**Page:** 5 of 1
Responsible	Ansgar Heidecker	**version:** 1.0
		Date: 23.03.2009
Start	T0 + 56 days	
End	T0 + 81 days	**Duration:** 25 days
Working person	Ansgar Heidecker	

Goals:

- Define two suitable attitude control algorithms for payload activity

Input

- Phase 0/A Documentation
- Simulation environment
- Literature form WP_1

Interfaces to other work packages

- WP_1

Tasks

- Investigation of existing attitude control algorithms
- Developing of a control algorithm for inertial pointing w.r.t. an optical payload
- Developing of a guidance algorithm for target pointing
- Create and implementing of a control algorithm for target pointing

Results

- Mathematical description of two attitude control algorithms
- Mathematical description of the guidance algorithm
- Simulink implementation of all algorithms

Development of algorithms for attitude determination and control of the AsteroidFinder satellite		**WP 6**
Title	**Performance analysis of the attitude control in the closed loop simulation**	**Page:** 6 of 1
Responsible	Ansgar Heidecker	**version:** 1.0
		Date: 23.03.2009
Start	T0 + 81 days	
End	T0 + 96 days	**Duration:** 15 days
Working person	Ansgar Heidecker	

Goals:

- Evaluate performance and ensure functionality of the attitude control

Input

- Phase 0/A Documentation
- Attitude control algorithm form WP_5
- Simulation environment form WP_2

Interfaces to other work packages

- WP_2
- WP_5

Tasks

- Investigate performance of the developed control algorithm w.r.t. the requirements
- Investigate the behaviour of the algorithm under irregular conditions
- Compare performance to the performance of other satellite systems

Results

- Performance characteristic of the algorithms
- Defined test cases for attitude control
- Information for the technical report

Development of algorithms for attitude determination and control of the AsteroidFinder satellite		**WP 7**
Title	**Documentation**	**Page:** 7 of 1
Responsible	Ansgar Heidecker	**version:** 1.0
		Date: 23.03.2009
Start	T0	
End	T0 + 120 days	**Duration:** 120 days
Working person	Ansgar Heidecker	

Goals:

- Final thesis report
- Protocol of all data and results

Input

- Phase 0/A Documentation
- Data and results from all work packages

Interfaces to other work packages

Tasks

- Creating a LaTeX template
- Creating a bibliography database
- Writhing thesis report
- Preparing final presentation

Results

- Final report
- Final presentation
-

Appendix F

Project Plan

Nr.	Vorgangsname
1	Start
2	**Orientation to the actual project state**
3	Creating project schedule, WPD, WBS
4	Reading Phase 0/A documentation
5	Literature research
6	Investigation of existing Matlab/Simulink models
7	**Development of a simulation in Matlab/Simulink for attitude control**
8	Importing useful models to the simulation
9	Creating simulated space environment
10	Creating sensor models
11	Creating actuator models
12	**Development of an attitude determination algorithm**
13	Investigating existing KALMAN-Filters
14	Preparing dynamics equation to be used in such a KALMAN-Filter
15	Implementing dynamics equation in the algorithm
16	Implementing attitude determination algorithm to the simulation
17	**Test of the attitude determination algorithm with the simulation**
18	Test functionality of the algorithm
19	Investigate accuracy of the attitude determination
20	Analyse performance w.r.t. other attitude determination technologies
21	**Development of an attitude control algorithm**
22	Investigation of existing attitude control algorithms
23	Developing of a control algorithm for inertial pointing w.r.t. an optical payload
24	Developing of a guidance algorithm for target pointing
25	Creating and implementing of a control algorithm for target pointing
26	**Performance analysis of the attitude control in the closed loop simulation**
27	Investigate performance of the developed control algorithm w.r.t. requirements
28	Investigate the behaviour of the algorithm under irregular conditions
29	Compare performance to performance of other satellite systems
30	**Documentation**
31	Creating a LaTeX template
32	Creating a bibliography database
33	Writing thesis report
34	Preparing final presentation

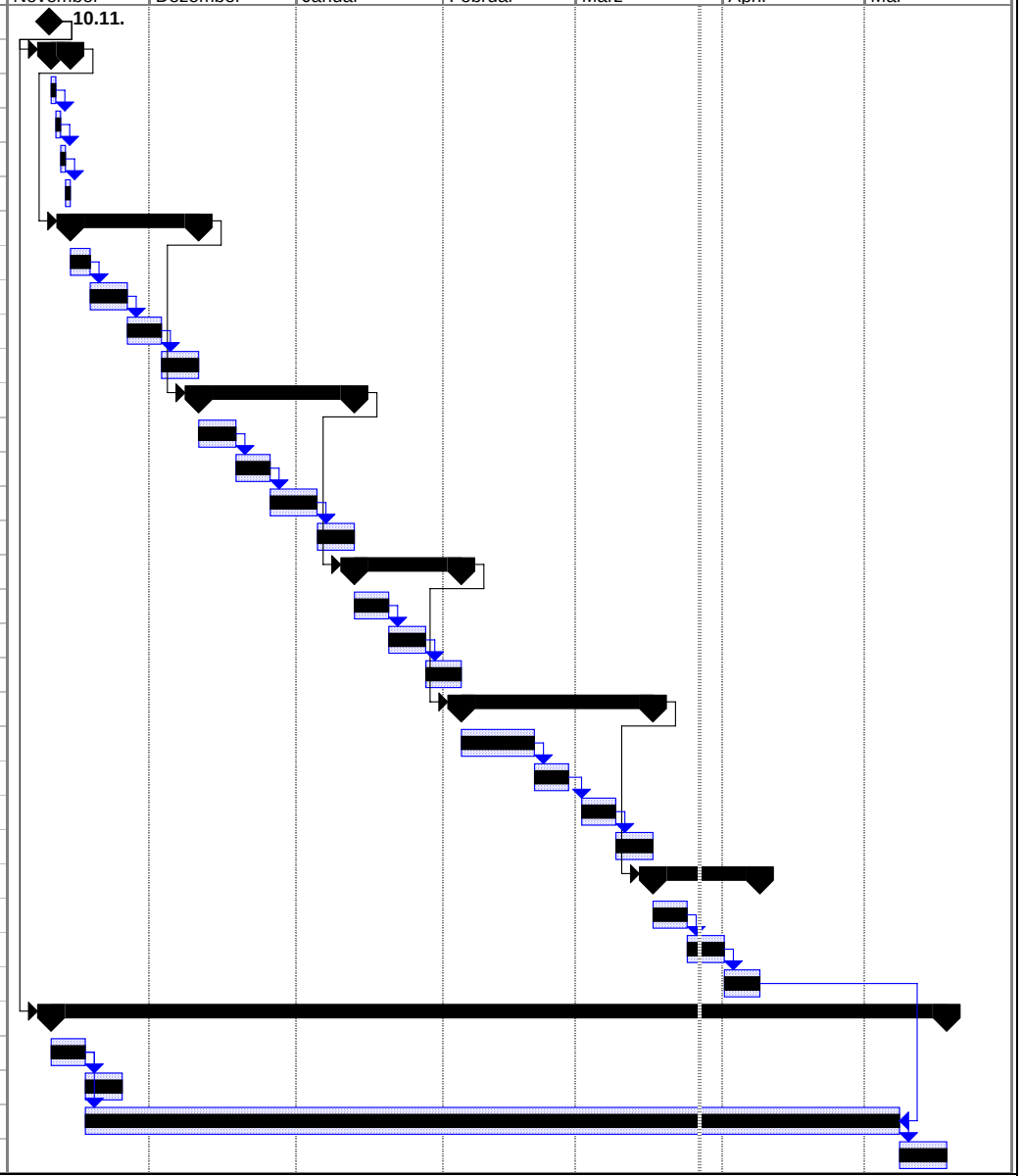

Project: DA_Project
Date: Fr 27.03.09
Ansgar Heidecker

Vorgang
Unterbrechung
In Arbeit
Meilenstein
Sammelvorgang
Projektsammelvorgang
Externe Vorgänge
Externer Meilenstein
Stichtag